Spring 12-4-2014

Historical Analysis of Arches and Modern Shells

Ryan Georg
University of Colorado at Boulder, ryan.georg@colorado.edu

Historical Analysis of Arches and Modern Shells

by

R. Georg

B.S., University of Wisconsin - Platteville, 2012

A thesis submitted to the

Faculty of the Graduate School of the

University of Colorado in partial fulfillment

of the requirements for the degree of

Master of Science

Department of Civil, Environmental and Architectural Engineering

2014

This thesis entitled:
Historical Analysis of Arches and Modern Shells
written by R. Georg
has been approved for the Department of Civil, Environmental and Architectural Engineering

_____

Prof. Victor Saouma

_____

Prof. George Hearn

_____

Prof. Abbie Liel

Date _____

The final copy of this thesis has been examined by the signatories, and we find that both the content and the form meet acceptable presentation standards of scholarly work in the above mentioned discipline.

Georg, R. (M.S. Civil Engineering)

Historical Analysis of Arches and Modern Shells

Thesis directed by Prof. Victor Saouma

Prior 20^{th} century, the study of masonry arches and domes consumed years of work with some of the greatest minds in history. However, with the advancements of materials, such as steel and concrete, and the use of computer analysis programs, the art of masonry arch and shell design has become stagnant. With various design methods seen throughout literature, an appreciation for the development of these methods, through basic hand calculations, must be understood to first, ensure correct design principles are applied and second, aid in the further development of these methods.

This thesis starts with an extensive literature review of historical analysis and design methodology, starting in the 16th century and continuing on through the mid-20th century and today's current practices. The review focuses first on masonry arch design, including principles of geometric design, wedge theory, line of thrust and the ultimate load theorem. The second part views the design and analysis of domes and vaults, concluding with a case study of St. Peter's Dome in Rome.

The thesis continues by reviewing the derivations of a beam and plate subjected to flexure, prior to the thin shell derivation. In all three cases, equilibrium, compatibility and stress-strain relationships are considered to develop the differential equation relating transverse displacement to the load. This methodology is chosen in order to introduce the shell gradually by building upon the initial derivations of the beam and plate.

Tying the historical design methods and derivation of the shell equation, the design and analysis of a circular cylindrical shell will be conducted. The derived shell equation will first be simplified to membrane theory, followed by the derivations of the governing equations for shells through the theory of shallow shells. The analysis of the cylindrical shell will hold similarity to the

analysis of statically indeterminate beams.

Finally, the methodology of shallow shells will be incorporated into the development of a reinforced concrete design and analysis program. The development of this program will simplify future analyses of circular cylindrical shells and improve design efficiency. The resulting design methodology will be recorded to aid in the future design of shells and the inspection of current structures. The thesis concludes by offering future studies to further develop the field of masonry arch and dome design.

Dedication

This thesis is dedicated to my parents Scott and Sherry Georg, who have continually pushed and instilled the passion to continue my education.

Acknowledgements

I would first like to thank Professor Saouma for selecting myself to perform this thesis and work under him. He has continually guided my efforts and offered aid and insight when necessary. Also, I would like to thank Prof. Hearn and Prof. Liel for agreeing to participate as members of the thesis committee and so graciously evaluating the work that I have performed.

Second, I would like to thank my thesis work group members Trupti Sonavane and Kyle Prusinski. We spent many meetings together collaborating and discussing our work. Both individuals have offered much aid and support in the development and finalization of my thesis.

Finally I would like to the University of Colorado and the administration, specifically Pamela Williams, and all her continuous help and guidance through the process of completing my master's thesis.

Contents

Chapter

Tables

Table

Figures

Figure

Chapter 1

Introduction

1.1 Motivation

The motivation for performing this thesis lies first with the interest of architecture and second with the necessity to understand the theory behind basic engineering principles. The beauty of basic structures that are utilized for daily use can often be overlooked. This thesis will re-enlighten the topic of architecture and its importance in the field of structural engineering.

In performing this particular thesis, one can mix the passion for architecture with structural design. Arches and shells have been some of the staples of architectural design due to the beauty of a curved structure that still exhibits great strength. Being able to study and analyze both the masonry arch and the shell allows for great insight into how many of the great cathedrals were constructed. These cathedrals are works of art architecturally, and yet structures that have stood the test of time due to key design features such as arches, flying buttresses and shells.

In addition to the passion of architecture and old age structures, this thesis allows for the study of the theory behind these structures. The arch and shell are both topics that are no longer discussed in today's concrete cities. Instead the focus lies in beams and columns of concrete and steel girders and joists. The theory of the arch and shell found in almost all historic structure now lay waste and are forgotten.

The theory of arches and shells requires no more than pen and paper and the patience to perform hand calculations. Rather than running to the computer, the design of these structures can be performed entirely with the use of basic equations derived years ago. Performing this analysis

and re-deriving the equations of the shell allows the designer to appreciate the work of past theorists and gain an understanding for the complex theory itself.

Ultimately this thesis will aid in the understanding of a forgotten theory and staple in architecture. Hopefully the following will bring an enlightenment to the structural and architectural field and remind those of the beauty and simplicity of these structures.

1.2 Evolution of Modern Era Shell Analysis

It was difficult to secure resources for the shell analytical study, especially current versions, since the topic has been neglected for many years. However, as of recent, a few authors have addressed the topic, Peerdeman (2008) and Krivoshapko and Hyeng (2014). Within their work a discussion of the evolution of shells in the modern era has been discussed and prepared by Prusinski (2015).

It was not until the early 20th century when German engineers Dischinger and Finsterwalder teamed up with Bauersfeld, an engineer of the Carl Zeiss Company, that the first thin-walled reinforced concrete shell structure was built. Bauersfeld wanted to build a planetarium and required a large hemisphere for the projection of the starry sky. Dischinger developed equations that would take into account the shearing forces and moments within a curved structure.

In 1923, Dischinger was the first to attempt the design of a shell that would cover a rectangular floor. The attempt failed as a consequence of the difficulties of the mathematical equations, but a successful second attempt was made the following year after implementing simplified equations. It was in 1925 that the Zeiss planetarium was built. At the same time, Finsterwalder was working in parallel to Dischinger to improve the design of concrete shells. Finsterwalder worked to improve Dischinger's equations and theories by including measurable displacements, which were later proved through experimentation. Finsterwalder eventually published this work in his doctoral thesis, dated 1930.

Over the course of the next six years, an American engineer by the name of Schorer worked to improve Finsterwalder's equations, publishing his findings 1936. It was at this time that the

material and physical demands of Second World War shifted the focus of study concerning modern technological advancements to studies that would benefit war-time necessities. This caused a brief interruption in shell development, but later resulted in the ideal conditions required for shell design and construction. With the advances of reinforcement within concrete, an opportunity presented itself in which shells could be redesigned to be thinner, resulting in a lower consumption of permanent materials compared to other structural designs of the time. Low labor cost in conjunction with a limited supply of steel paired perfectly with the low consumption of steel and high labor and formwork hours such shell designs called for.

With Schorer's equations in hand, shell structures could be designed with a measurable degree of confidence. Although Schorer's equations were proven sufficient for design, the actual computations called for by such equations were tedious and required an innumerable amount of man-hours to complete. With the demand for shell structures growing, The American Society of Civil Engineers appointed a committee to streamline the design process. The results of this committee included numerical tables and practical formulas for various cylindrical shell designs. This data was published in a manual titled "Design of Cylindrical Concrete Shells Roofs", dated 1952. For a span of 20 years, shell construction and design bloomed all across the globe. Shell construction and design became the flagship structural model for structural efficiency and architectural design.

It was not until the early 1970's that the blooming era of shells ended abruptly. The low permanent material consumption of the shell structure could no longer outweigh the rising cost of labor and formwork associated with such designs.

Within the context of this thesis, the books of Billington (1965) and ASCE design manual (Whitney, 1952) were used exclusively for the shell theories presented within the thesis. Even though books such as *Theory of Plates and Shells* by Timoshenko, and *Stresses in Shells* by Flugge were available, neither go into the length of detail seen within Billington (1965) and Whitney (1952).

The ASCE design manual was the inspirations for majority of the work found within Billington (1965). Both sources present the topic of membrane theory in great detail. However, the

theory of shallow shells is seen exclusively by Billington (1965) while the ASCE Manual no. 31 (Whitney, 1952) relies solely on the membrane theory along with an undefined correction method. Even though this corrective method is not mentioned specifically, the results of various examples within the manual are duplicated with the theory of shallow shells presented by Billington (1965).

Chapter two of the thesis presents a discussion of pre-modern era shell analysis focusing on the sources of Heyman (1997), Heyman (1998), Benvenuto (1991), and Kurrer (2012). Various other sources and papers have been cited within the thesis to aid in discussions and are presented within the context of the bibliography. Buckling was not considered for the context of this thesis as provided within multiple sources. Likewise, the focus on numerical methods is also neglected.

1.3 Thesis Organization

The first chapter of the thesis dives into a lengthy discussion of the historical theories of arch and shell design, and the founders of these theories. Topics presented within this discussion include geometry and art based design, wedge theory, line of thrust and stress analysis. Application of the theory is found within the case study at the end of the chapter.

Chapter three begins the discussion of shells and the modern age derivation of the design equations for a shell. The differential equations of a beam and plate in flexure are first derived, followed by the equation for thin shell.

Chapter four focuses on the analysis of a simply supported shell circular cylindrical shell with edge beams. The stress resultants, stress couples, and displacements are derived by membrane theory and the theory of shallow shells. A brief discussion is included comparing the results of the two theories.

Chapter five discusses the development of a design tool, utilizing the theory of shallow shells, along with a brief preliminary design. A discussion of the code and results follows.

The final chapter concludes the thesis and presents a discussion of future work to be conducted in connection with this thesis.

Chapter 2

Historical Review

2.1 Introduction

The architectural masterpieces of the arch and dome can be seen in various examples throughout historical landmarks. Structures like Notre-Dame, St. Peter's Basilica in Rome, and Hagia Sofia in Constantinople are only a few examples of such landmarks. These structures serve both the artistic sense along with the structural integrity required for stability.

This chapter dives into a lengthy discussion of the historical theories of arch and shell design, and the founders of these theories. This is not meant to be an exhaustive literature review. Rather, the historical review is meant to focus on important events related to arches and shells and the motivation of the shell theory development. As stated by Isaac Newton, "If I have seen further it is by standing on the shoulders of giants". Likewise, this chapter places the emphasis on the origination of the theory and how it progressed throughout history to our current methodologies. The topic of the masonry design is first explored in brief detail. The structural theory of masonry is discussed along with a brief discussion of modern design.

The chapter then shifts focus to the masonry arch beginning in the age of art with the likes of Da Vinci, Viviani and Derand. All three visionaries of the arch viewed the structure as art. Though all three methodologies differed, they all shared the same belief that the arch could be designed by geometry and trial and error. Often these structures were over designed to ensure stability.

Drifting slightly from the context of geometry and art, Hooke, Gregory, and Bernoulli brought about the idea of the catenary shape and the definition of the perfect arch. This would eventually

lead to the idea of thrust that is known and studied in all arches today.

The chapter continues with a new topic, being the wedge theory, and its counterpart collapse analysis. Designers such as La Hire, Belidor, and Coulumb spent many years developing the wedge theorem and the distribution of forces throughout the arch. With a concept of force distribution discovered, collapse analysis presented itself and opened the door for the ultimate load theorem.

Improving upon these methodologies, Gerstner, Moseley, and Scheffler brought about the idea of the line of thrust within the structure. This line of thrust would be the line of force transfer discovered by the wedge theorem. Though little improvement to the wedge theory came about from this new analysis theory it did enlighten the next step of arch analysis.

Stress analysis was soon introduced by Young, Huerta and Navier. Rather than having a single line of force distribution within the structure, the forces are distributed throughout its entire area and the stresses can then be analyzed at any point. Eventually the modern methodologies of elastic theorem and ultimate load theorem were created and used exclusively till the creation of finite element aided computer programming.

The chapter finishes by discussing the shell. Before discussing the theorists, once again the basic structural theory and analysis is discussed. This section concludes by discussing the work of Bossut, Mascheroni, and Salimbeni and their contributions to the field of shell design and analysis.

The chapter concludes with the case study of St. Peter's Basilica in Rome. In this case study, we review the historical task of confirming the safety of a structure prior to the use of computers. In this case, Poleni is assigned the task of determining the risk of collapse of the St. Peter's dome. Utilizing the historical methodology of the catenary and Hooke's hanging chain, Poleni successfully provides an analysis and confirmation of safety.

2.2 The Origin of Masonry Design

Masonry design often brings to mind words such as beautiful, or historical, or even strong. The Gothic and Renaissance eras used masonry exclusively due to the lack of better materials and ease of availability. Even with such a simple structural component, masonry structures were

designed with a strong focus of art and beauty. Key components, like the flying buttresses and towering spires of Notre-Dame, represented the essence of Gothic architecture. While the Renaissance showcased historical structures such as St. Peter's Basilica in Rome and Hagia Sofia in Constantinople, displaying the focus of both beauty and art.

Yet, the fundamental structure that undergirds such masonry design is the arch. The invention of the arch is impossible to date. Some of the earliest arches can be seen in the Mesopotamian burial chambers, and throughout the Etruscan civilization, about 3000 years ago. The stability and strength of these ancient structures fueled the advancement of masonry arch design well into the 20th century.

2.2.1 Structural Theory of Masonry

Strength, stiffness, and stability are required for the design of any structure. Even though strength and stability control the design for the majority of all structural materials, stability is the only focus of masonry design. Strength can be ignored due to masonry's high crushing capacity. The compressive stress experienced by masonry is often less than 1/10 of the crushing capacity. Also stiffness is ignored due to the low mean stresses and negligible deflection.

The majority of the focus of stability is placed on the compressive stresses formed through compaction under gravity. This compaction accounts for the three assumptions required for stability: masonry has no tensile strength, masonry has effectively unlimited compression strength, and sliding failure does not occur. Even though an individual masonry stone has the ability to transfer tensile stresses, the structure as a whole has no tensile strength capacity. The compressive stresses create friction forces between the stone wedges (voussoirs) and prevent the development of tensile stresses and sliding failure. Even though compressive stresses are important to stability, the location of these stresses and the resulting collapse mechanisms are the two main points of interest in stability design.

The thrust line is the line of force (compressive stresses) or load transfer line found within the structure. When the line of thrust remains entirely within the structure, the structure is considered

to be in a state of equilibrium. "The safe theorem states that if any one such position can be found for the line of thrust, then this is an absolute proof that the structure is stable, and indeed that collapse can never occur under the given loading" (Heyman, 1997, pg. 22). Thrust lines occurring at the edge of a structure indicate the development of a hinge. When a hinge develops, the thrust must be transferred through the point of contact between the two resulting bodies.

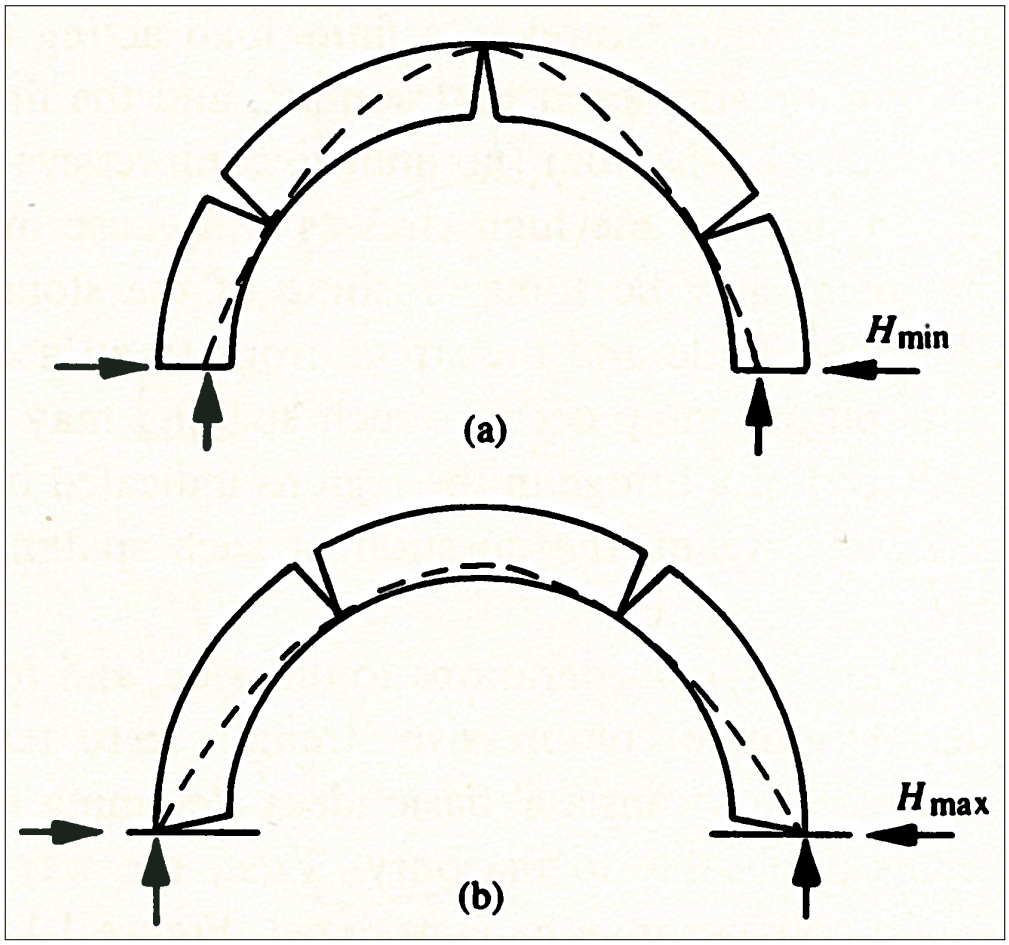

Figure 2.1: The semicircular arch under its own weight a) minimum abutment thrust; b) Maximum abutment thrust, (Heyman, 1997)

Hinges are found in the form of cracks. Cracking is inevitable due to shifting of the external environment and the necessity of the structure to respond. Cracks are often developed through settlement, leading to changes in the geometry of the structure. Most structures are designed to allow for some settlement and cracking. However, differential settlement is a major concern that

develops over time and causes hinging and often collapse mechanisms.

Collapse mechanisms develop only when a sufficient number of hinges form. A common collapse mechanism is the four-bar chain. This occurs when four hinges develop transforming "the stable arch into a mechanism of collapse" (Heyman, 1997, pg. 18) as seen in Fig. 2.2 (Heyman, 1997, pg. 19). However, hinging is not an indication of collapse until the load reaches a failure state. In fact, a three hinge arch is statically determinate as the thrust line is fixed by the hinges. Eventually, the load applied reaches the failure state, and the thrust line can no longer be contained within the structure. In turn, a collapse mechanism develops resulting in failure.

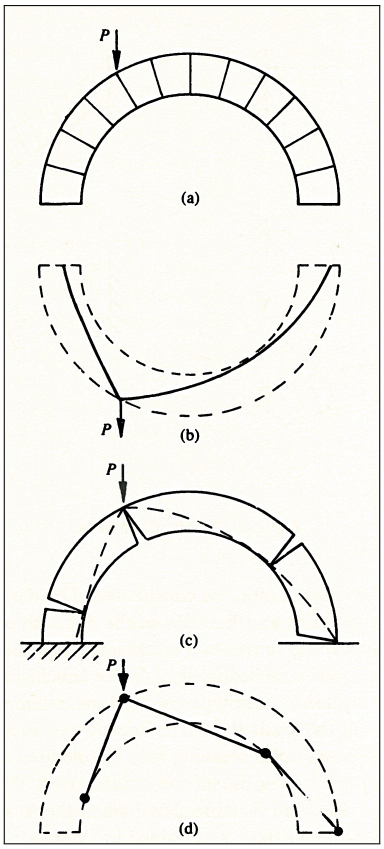

Figure 2.2: Collapse of a circular arch under a point load, (Heyman, 1997)

Since collapse mechanisms are dependent on the thrust line location and the resulting hinge formation, proper proportioning of the thickness of masonry will dictate the design and behavior. From this proportioning a geometric factor of safety can be developed. The factor of safety considers

the shape and size of the structure being analyzed. A "load bearing structure will not collapse when an equilibrium condition can be found that does not infringe the hinge condition" (Kurrer, 2012, pg. 236). The value of safety is the ratio of the actual size of the structure compared to the minimum size able to hold the thrust line without the development of a failure mechanism. In order to contain the line of thrust within the inner third of the structure, a geometric factor of safety of three must be implemented. Even though the computation of the true line of thrust is impossible to know, it is "also not important because the safety of the loadbearing structure can be calculated without having to make assumptions regarding its actual state" (Kurrer, 2012, pg. 236).

2.2.2 Modern Design

The development of modern age masonry design consumed many years and various theories to get to its finalized state. The earliest theories based design on the geometry and proportioning of the masonry structure, which was eventually determined to be outdated. Galileo found that "if the dimensions...were doubled, the strength was very much more than doubled" (Heyman, 1997, pg. 6). This discovery led to the emergence of mechanics and stresses in the determination of design. Modern engineering began to move from the idea of proportioning, focusing rather on internal stress and thrust lines within the structure. Eventually the elastic theory followed for the analysis of the arch and thrust line. However, ideal conditions required for the elastic method do not occur, jeopardizing the solution. This brought about the creation of the plastic theory, also utilized for masonry by finding an equilibrium state where forces remain within the boundary of the material.

2.3 Masonry Arch

2.3.1 Geometric Theory

2.3.1.1 Geometry and Art - Da Vinci

Leonardo da Vinci once said, "An arch is nothing but a strength caused by two weaknesses; that is why an arch in buildings is composed of two quarter-circles; these quarter-circles, each very weak in itself, wish to fall, and opposing each other's ruin, convert weakness into a single strength" (Benvenuto, 1991, pg. 309). Da Vinci envisioned the arch as man's artistry trying to overcome nature. He found interest in the arch not only as a beautiful work of art but also as a useful tool for structural applications. With no predecessors, he hinted at ideas that would be developed some three centuries later, such as the concepts of internal arch thrust, horizontal pier thrust, and his self-created wedge theorem.

Leonardo da Vinci envisioned the arch as a system made up of machines, including wedges, ropes and pulleys. He divided the arch into wedge-shaped, discrete elements matching the voussoirs. His wedge theorem became the first idealized approach to arch equilibrium and static analysis via simple machines. However, he "did not contradict the common conviction that geometry, not statics, could provide the simplest, most harmonious, and safest proportions for making arches" (Benvenuto, 1991, pg. 311).

2.3.1.2 Geometry and Art - Viviani

Da Vinci was not alone in the belief of geometry controlled design. In 1692, Vincenzo Viviani published a transcript on the formation and size of any regular arch. The work was intended to "teach the 'expert turner geometricians' how to use 'chisels, drills, and gimlets' to make any sort of vault or to bore out certain solids 'with highly usable rules'" (Benvenuto, 1991, pg. 311). Viviani's main focus dealt with the Florentine rib-and-panel vault and the Roman haul shaped vault. Though it strayed from the masonry arch, the sole basis of geometry and tracing design continued to be exhibited. Viviani attributes the shape of the domed vault to the observation of an eggshell placed

upside down and its immense strength. Once again the focus is not on the material properties but rather the shape of the structure.

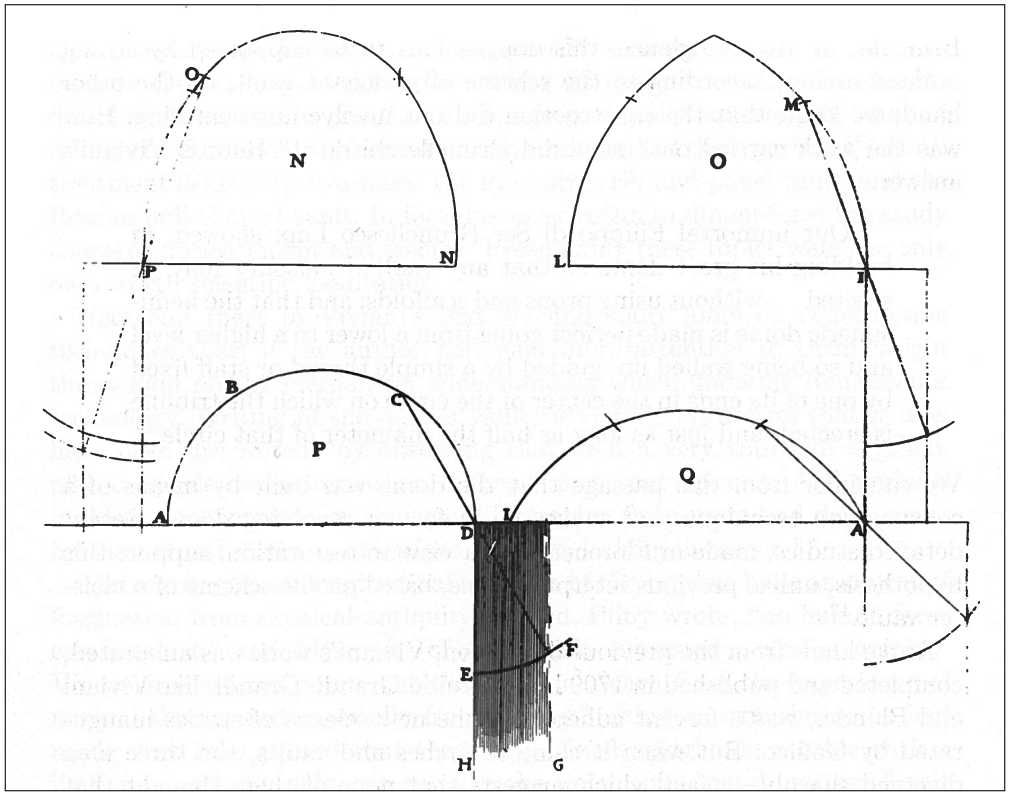

Figure 2.3: Fr. Derands's rule, (Derand, 1743) (Adapted by (Benvenuto, 1991))

2.3.1.3 Geometry and Art - Derand

Jesuit François Derand was one of the last visionaries of the 17th century to base arch design solely off of geometric tracing. In 1643, he transcribed his work entitled *L'Architecture des voûtes, ou l'art des traits et coupes des voûtes* which was not published until Derand (1743). The book detailed answers for various problems requiring expert geometric tracing, nearly neglecting all structural dimensions. In fact, only one chapter of the book dealt with thrusts and dimensioning. Within this chapter he developed Derand's Rule for determining abutment thickness, becoming the first theory developed not utilizing statics. Instead, he relied extensively on geometry and tracing.

The method can be seen in Fig. 2.3. The circular arch P can be broken into thirds $ABCD$.

Between points C and D a line is drawn and extended beyond D. A compass is then opened to the distance of chord CD with D at the center. A vertical line may be drawn where the new traced arc strikes the extended line CDF. This represents the outside wall of the abutment with the interior being placed at D. The accuracy of the method was based on experience and practice and regarded as acceptable. This eventually changed with the advancement of statics when the method was disproved.

2.3.1.4 The Catenary - Hooke

Original arch design determined by Leonardo Da Vinci, Vincenzo Viviani, and Jesuit François Derand relied heavily on geometry and tracing (Fig. 2.3). This continued into the early 17th centuries through the work of Robert Hooke.

Hooke worked as the Curator of Experiments to the Royal Society. During this time he experimented on model arches without the use of mathematical analysis. In 1675, Robert Hooke published a book aiding the theory of geometry by determining the perfect shape of an arch to be the shape of a catenary or hanging chain. "As hangs the flexible line, so but inverted will stand the rigid arch" (Kurrer, 2012, pg. 214).

2.3.1.5 The Catenary - Gregory and Bernoulli

Nearly twenty years later, in 1697, David Gregory expanded upon Hooke's theory. He did not limit his thinking to only arches of catenary shape but to other figures as well by adding the concept of catenary shape containment within the arch. "When an arch of any other figure is supported, it is because in its thickness some catenaria is included...if any thrust line can be found lying within the masonry, the arch will stand" (Heyman, 1998, pg. 80). Jakob Bernoulli furthered the hypothesis by calculating the curvature of the catenary.

Gregory also defined abutment thrust stating that "the same force that a chain exerts inward, an arch of equal form exerts outward" (Benvenuto, 1991, pg. 327). However, by the end of the late 1600's, geometry lost ground to the scientific and mathematical theory of statics.

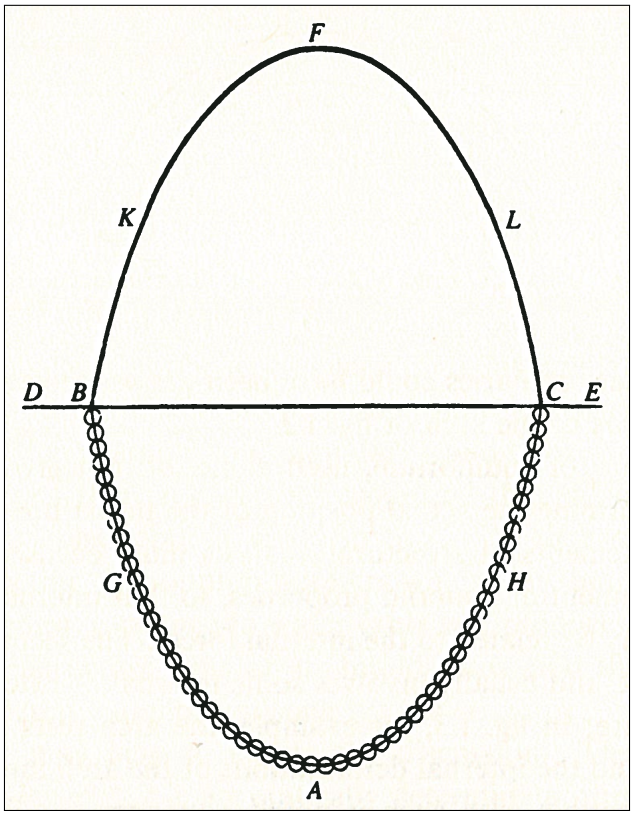

Figure 2.4: Hooke's hanging chain, (Heyman, 1997)

2.3.1.6 Introduction of Thrust - Fabri

Honoré Fabri began the transition from geometric analysis to thrust line. Fabri analyzed a semicircular arch as a 3-pin system loaded at C by assuming the thrust lines to be straight lines from the springing to the crown (Fig. 2.5). If the thrust line lied completely within the arch, the arch remained stable. Fabri used the model to geometrically determine the arch and abutment thickness by circumscribing a semicircular arch at the tangent of the thrust line (assumed thrust line at 45 deg).

$$\begin{aligned} \text{Dead} &= 2R = 2(CB) \\ \text{Horizontal Thrust} &= R = BD \qquad (1/2 \text{ Dead Load}) \end{aligned} \tag{2.1}$$

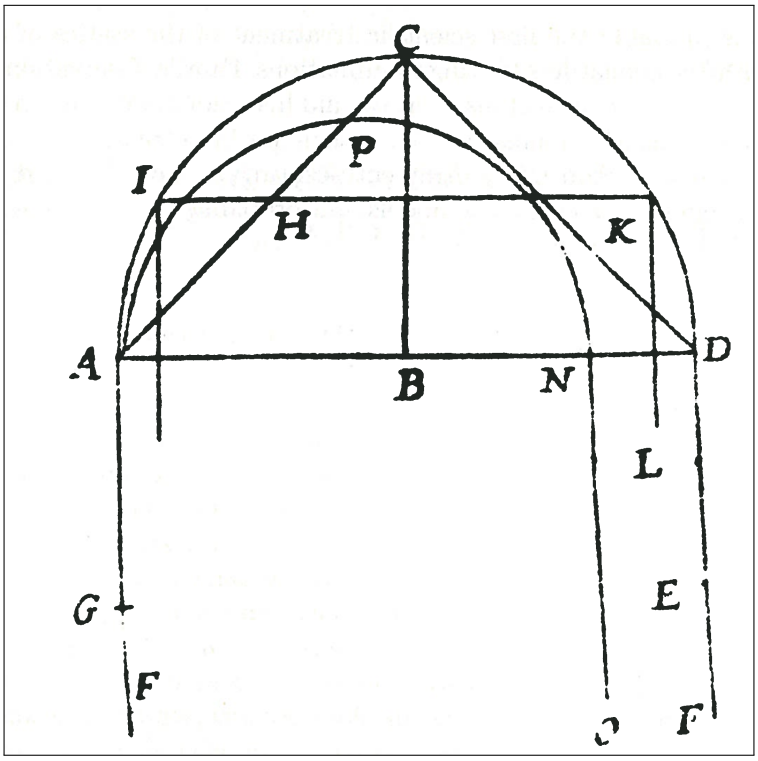

Figure 2.5: Fabri's Arch Thrust Model, (Benvenuto, 1991)

The forces calculated are found to be about 5 percent higher than computed via the elastic theory. Fabri's geometric analysis was a conservative approach to calculating the arch and abutment thickness.

$$d_1 = ND = 2R(3 - 2\sqrt{2}) = 0.343R \qquad \text{(Thickness)} \tag{2.2}$$

$$r = R - d_1 = BN = R(4\sqrt{2} - 5) = 0.657R \text{ (Radius)} \tag{2.3}$$

Though Fabri still utilized geometric analysis, he was one of the first theorists to introduce the concept of thrust line into arch and abutment design.

2.3.2 Wedge Theory/ Collapse Analysis

2.3.2.1 Static Analysis - de La Hire

Philippe de la Hire's work is recognized as the first globally accepted scientific and static analysis of an arch. In 1695, as one of the leading members of the Académie Royale des Sciences de Paris (Benvenuto, 1991, pg. 321), he presented his *Traité de méchanique*. His arch theory developed from the need of a scientific verification for masonry arch design. In his text, de la Hire examined a semicircular arch assembled from voussoirs with predetermined weights. The voussoirs were assumed perfectly smooth with no friction implying the line of thrust must act perpendicular to the joints. The keystone was assumed a wedge resting on neighboring wedges implying that the weight of the keystone was supported by forces perpendicular to the joints. De la Hire determined that the forces within each individual voussoir were proportional to the sides of a triangle perpendicular to the force. For example, we can look at the voussoir next to the keystone in Fig. 2.6.

$$Q2 : F1 : Fr = LO : LC : CO \tag{2.4}$$

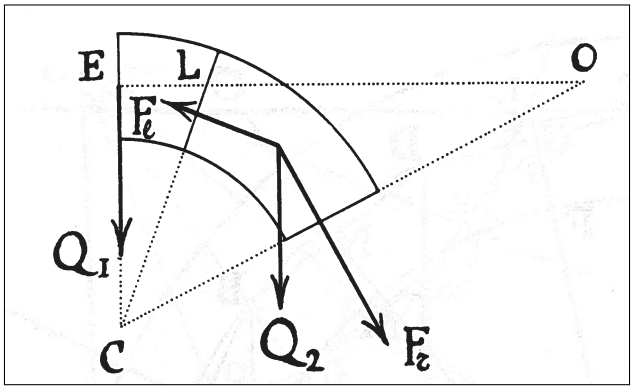

Figure 2.6: De la Hire's construction for determining the size of the voussoirs of an arch, (de la Hire, 1679) (Adapted by (Benvenuto, 1991))

This method can be performed for all voussoirs except the last one located at the springing. According to the theory, the weight at the springing would be infinite since the resulting weight

and thrust forces are parallel along with the corresponding sides of the force triangle. The issue only arises due to the assumption of infinitely smooth voussoirs.

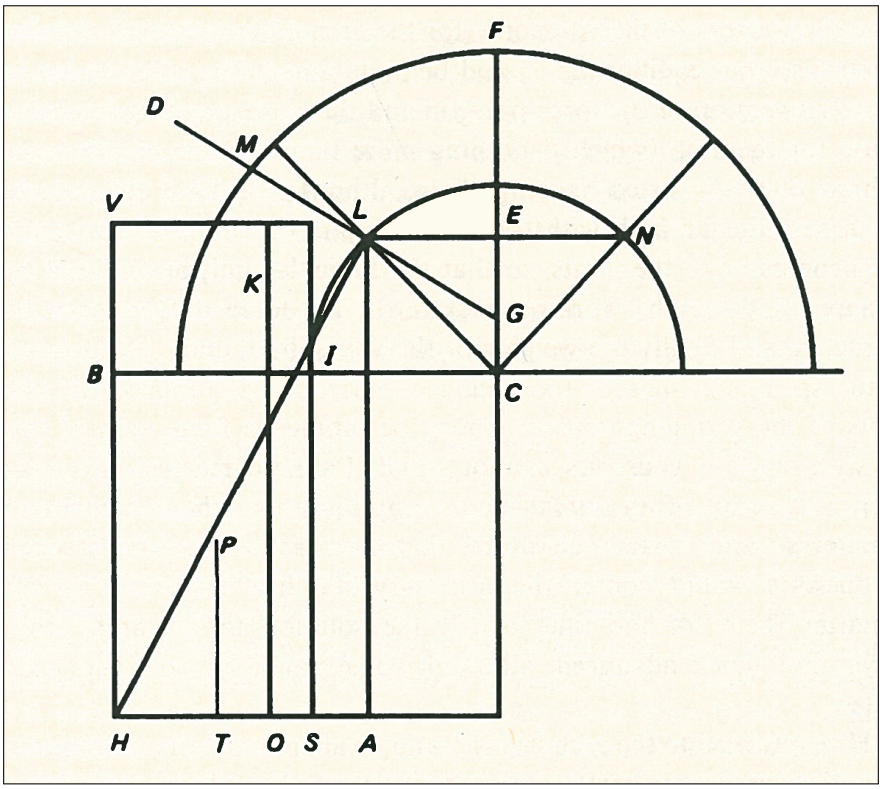

Figure 2.7: Mechanism of the semi-circular arch, (de la Hire, 1712) (Adapted by (Heyman, 1998))

On February 27, 1712, Philippe de la Hire submitted a memoir, entitled *Sur la construction des voûtes dans les edifices*, to the Académie Royale (de la Hire, 1712). In his memoir, he revisited the arch and determined the voussoirs were no longer frictionless but rather friction was assumed so large, sliding failure could not occur. This meant the thrust lines were no longer fixed as perpendicular at the joints.

He also introduced the wedge and lever to the static behavior of the arch. The new parameters were used to determine arch thrust for abutment design, utilizing mechanics and graphical analysis.

De la Hire developed an ultimate load theory proposing three ideas regarding the analysis of a round arch. First, "an arch breaks in an intermediate section between the impost and the keystone, at about 45 degrees". The newly formed wedge drops, due to its weight, pushing the abutments

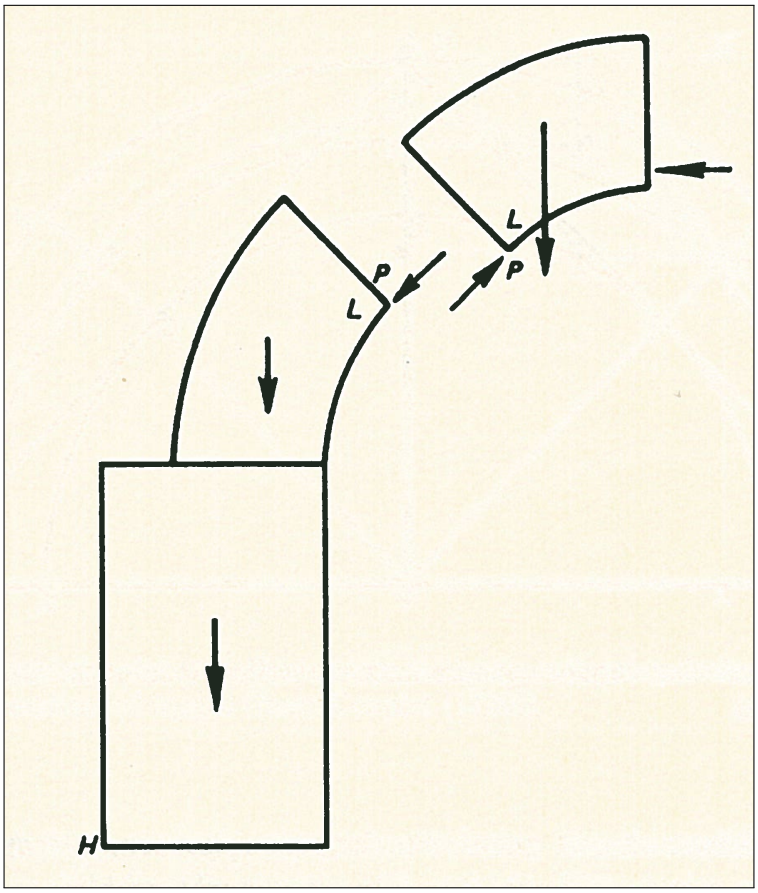

Figure 2.8: The statics of the arch, (de la Hire, 1712) (Adapted by (Heyman, 1998))

and causing rotation. Second, "the three zones bounded by the disconnections of the voussoirs are so stable that they form a single body". Third, the thrust at the hinge was determined to act tangentially to the intrados. Knowing the weight of the upper portion of the arch, the resulting thrust could be determined.

The component of the thrust, D, acted perpendicular to the lever arm, LH 2.7, which was then traced to the base of the abutment determining the abutment width. The weight of the abutment and base were represented on the other end of the lever arm by Q acting at T. Rather than focusing on geometry, the focus is placed on the weight of these stabilizing parts. Through the initial graphical analysis, de la Hire developed a mathematical proof and equation to determine the necessary abutment width. From Fig. 2.7 the following relationship were made.

$$LG : CG = P_c : D \tag{2.5}$$

If we set LE = f (half chord), CE = e, SA = a, CF = r, EF = s, LA = g, TO = h, OS = t, the abutment height HB = b, and the width HS = y, the following equations can be derived

$$CG = e - \frac{f}{g}(y - a) \tag{2.6}$$

$$LG = \sqrt{f^2 + \frac{f^2}{g^2}(y + a)^2} \tag{2.7}$$

$$D = P_c \frac{eg - fy - fa}{f\sqrt{g^2 + (y + a)^2}} \tag{2.8}$$

Since the design assumed constant thickness of the abutment, the weight can be considered proportional to the area. Therefore, the weight of the abutment equaled $b*y$. De la Hire accounted for the weight, $P^{'}$, of segment ILM with an imaginary increase of the abutment height BV. The total weight, P, to be applied at a distance of HT = $y/2$ from H is given by

$$P = by + \frac{(\frac{1}{2}y + h)P'}{\frac{1}{2}y} \tag{2.9}$$

The law of levers can then be applied

$$D * HL = P * HT \tag{2.10}$$

$$HL = \sqrt{(y + a) + g^2} \tag{2.11}$$

Finally the abutment width is computed by the following relationship

$$\frac{1}{2}bfy^2 + \frac{1}{2}P'fy + P'fh = P_c eg - P_c fy - P_c fa \tag{2.12}$$

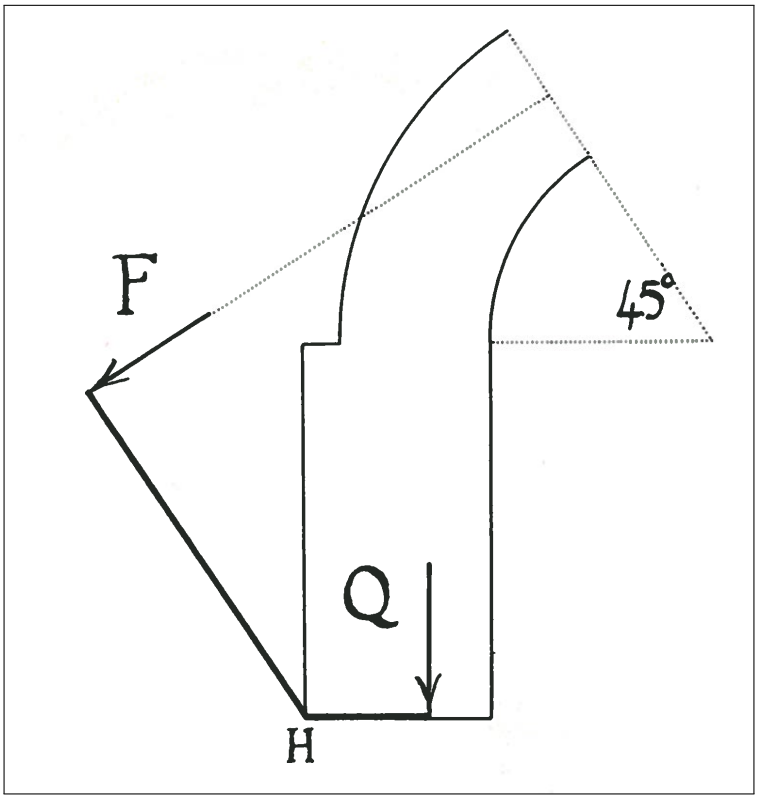

Figure 2.9: Belidor's Variant of de la Hire's method, (Benvenuto, 1991)

2.3.2.2 Wedge Theory - Belidor

In 1729, Bernard Forest de Belidor took a similar approach to de la Hire except changed the critical hinging point to 45 degrees, computing a thrust of $\sqrt{2W}$ (W is the weight of the voussoir above the hinge). He also changed the location of the thrust to act perpendicular at the center of the joint rather than the intrados (Fig. 2.9). The new, easier determined thrust value compounded upon the theory to develop an equation for abutment width.

From Fig. 2.10, we can derive an equation for determining the abutment width, y, where l is the height, b is the distance between the intrados of the abutment and the vertical line passing through center of gravity of *MmKk*, and c is the distance between the intrados and the vertical line from L. We can simplify Fig. 2.10 by setting $LY = y + c$, $HY = l +$ *OC*, and $HN = HY$ - $NY = HY$ - $LY = l +$ *OC* - $(y+c)$. The figure can be further simplified by setting $f =$ *OC* $+ l$ - c and *HN*

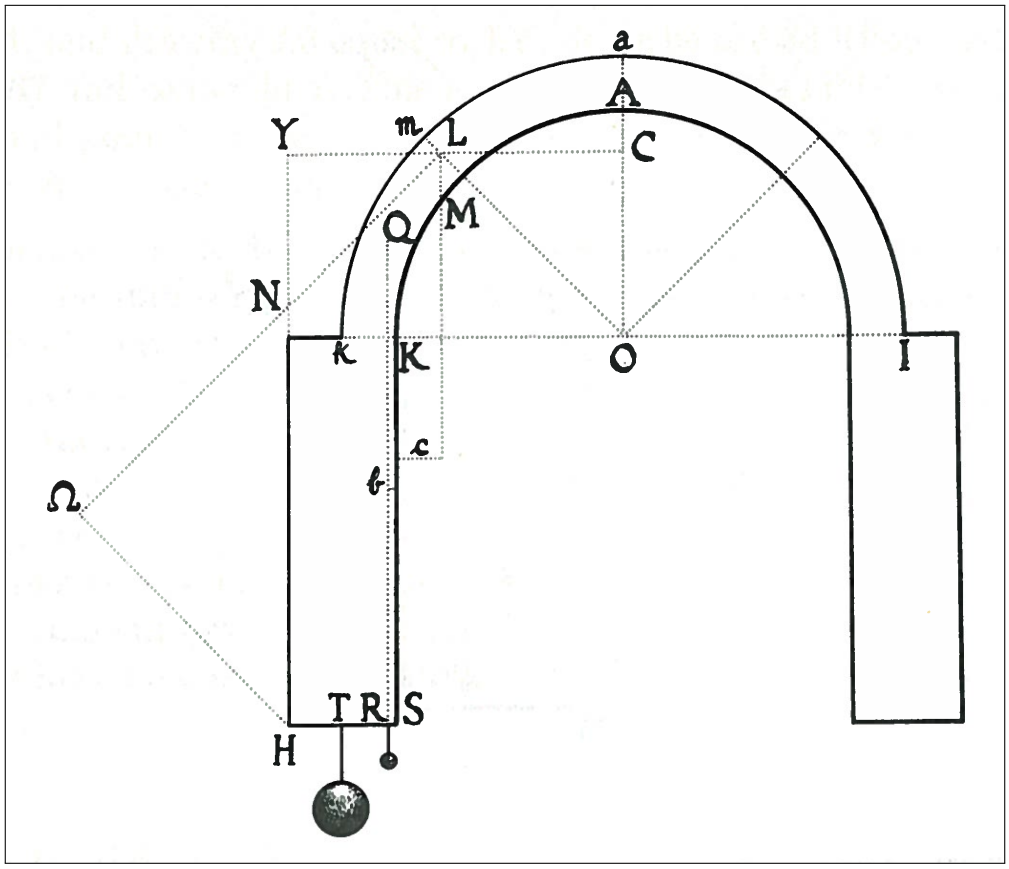

Figure 2.10: Belidor's Model, (Benvenuto, 1991)

$= f$ - y, designating the lever arm

$$H\Omega = \frac{\sqrt{2}(f-y)}{2} \tag{2.13}$$

Using these assumption, Belidor derived the equilibrium equation

$$P_c(f-y) = l\frac{y^2}{2} + P_c(y-b) \tag{2.14}$$

and the final equation for the required abutment width

$$y = -\frac{2P_c}{l} + \sqrt{\frac{4{P_c}^2 + 2P_c l(f+b)}{l^2}} \tag{2.15}$$

Similar to de La Hire, Belidors wedge theory neglected friction. However, Belidor came to the conclusion that mortar or a bond would be required. "The theory of La Hire and Belidor

was accepted throughout continental Europe almost without question during the rest of the 18th century" (Kurrer, 2012, pg. 208).

2.3.2.3 Collapse Analysis - Couplet

The work of Claude Antoine Couplet (Couplet, 1731) and (Couplet, 1732) laid the basis of future arch analysis. His two memoirs to the Académie Royal des Science, *De la poussée des voûtes* and *Seconde partie de l'examen de la poussé des voûtes* expanded and improved upon the theories of de la Hire and Belidor. Couplet determined the three key postulates about masonry behavior. First, masonry has no tensile strength. Second, masonry has infinite compressive strength. Third, sliding failure cannot occur (Heyman, 1998, pg. 83).

Utilizing equilibrium (statics) and deformation (mechanics), Couplet became the first to develop techniques for determining the size and thrust of voussoirs. With a known keystone weight, the said keystone can be decomposed into equivalent forces perpendicular to the joints of the adjoining voussoirs. The equivalent forces were extended to the center of gravity of the neighboring voussoir. A vertical line could then be drawn from the equivalent force to the perpendicular force of the voussoir. The vertical component determined the weight of the wedge and the perpendicular component determined the thrust (Fig. 2.11).

Couplet's final major achievement was the development of a ratio, dependent on the arch radius, to determine the least thickness of a semicircular arch carrying only self weight. Utilizing collapse mechanism, in particular the four-bar chain, he broke the arch into four segments at 45 degrees. The points of rotation were regarded as hinges through which the thrust must pass. The failure mode was analyzed to determine a t/R=0.101 (Fig. 2.12).

$$t_{min,c} = 0.101 \times R \tag{2.16}$$

All masonry arches less than the minimum thinkness were considered unstable. The theory was later refined by Jacques Heyman realizing the critical hinging did not occur at the intrados at

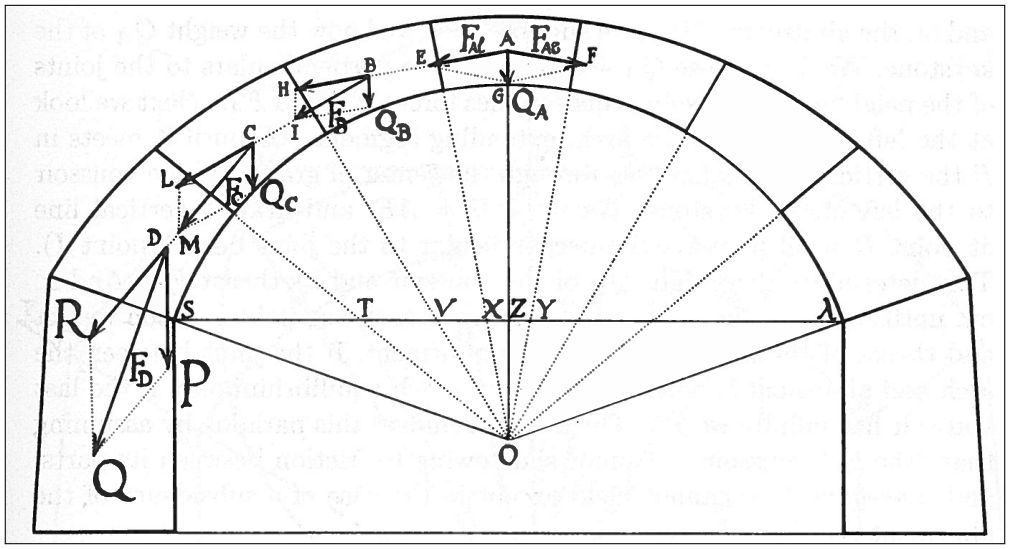

Figure 2.11: Couplet's voussoir size and thrust determination, (Couplet, 1731) (Adapted by (Benvenuto, 1991))

45 degrees but rather 58.9 degrees. The value was refined to

$$t_{min,h} = 0.106 \times R \tag{2.17}$$

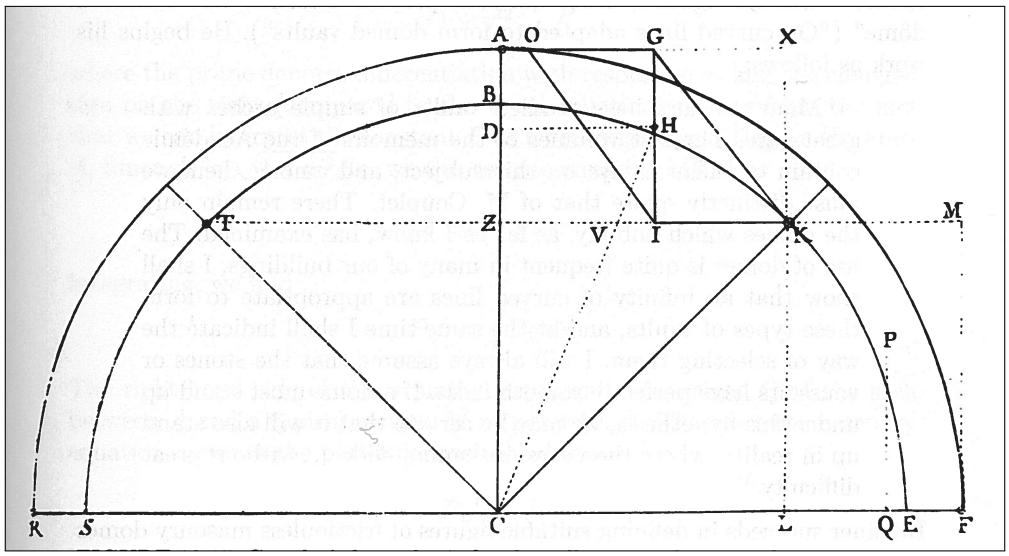

Figure 2.12: Couplet's Hypothesis for the collapse mechanism of an arch, (Couplet, 1732) (Adapted by (Benvenuto, 1991))

2.3.2.4 Voussoir Rotation Theorem - Coulomb

In 1773, Charles Auguste Coulomb published his work (Coulomb, 1773) determining the dimensions of vaults and arches, the rupture locations, and the limit state of rest with cohesion and friction. The first three corollaries contributed to vault dimensioning. His first corollary focused on an infinitely thin vault as seen in Fig. 2.13(c). He defined P and Q as the loads located at M. Given the relationship of similar triangles, it can be determined that

$$\frac{dx}{dy} = \frac{P}{Q} \tag{2.18}$$

Assuming the horizontal thrust is constant and equal to P at the crown location, a, and that the resultant vertical forces equal the weight of the vault, the relationship derived above can be modified to

$$\frac{dx}{dy} = \frac{P}{\int q ds} \tag{2.19}$$

with the curve of the vault calculated by the left hand side of the equation and the weight being attained by the other. From one known element, the other can be easily attained.

In the second corollary, Coulomb determined the vault width at any point with only the self-weight load condition. Through rigorous derivations, Coulomb developed the following equation

$$r + h = \sqrt{r^2 + 2P(\frac{ds}{dx})^2} \tag{2.20}$$

where r equals the radius of curvature of the intrados of the vault and h is the width at the location of interest. However, Coulomb found two problems with his theory. First, the resultants of the forces must always be perpendicular to the joints for the method to be valid. Second, the formulation is not completely reliable due to the infinite growth of h as θ approaches 0.

Coulomb's third corollary looked to determine the direction of the joints between the voussoirs, given the known intrados and extrados. The corollary determines the joints for the vaults and arch case (Fig. 2.13(a)), along with the platband condition seen in Fig. 2.13(b). Through derivations that we will overlook, the location and direction of the joint is determined for each case.

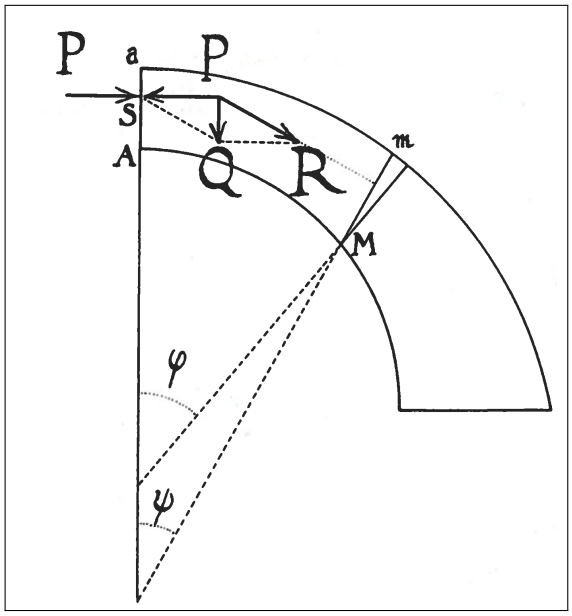

(a) Circular arch joint direction determination, (Coulomb, 1773) (Adapted by (Benvenuto, 1991))

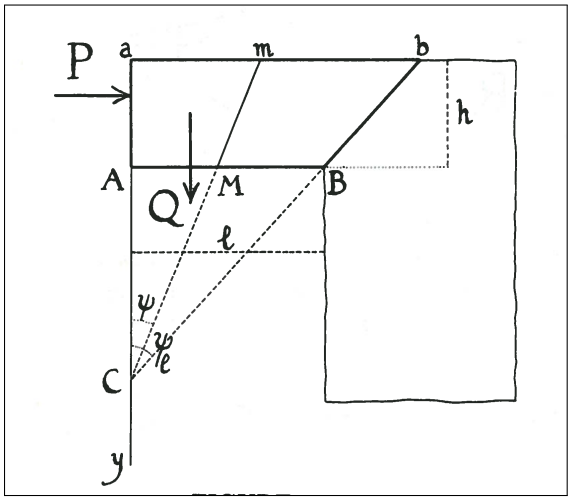

(b) Platband joint direction determination, (Coulomb, 1773) (Adapted by (Benvenuto, 1991))

Coulomb's most memorable contribution to masonry arch design comes in his final corollary involving cohesion and friction. By calculating the rupture location and limit states of the arch, Coulomb determined the maximum value of arch thrust through extreme value calculation of differential calculus. He determined the arch thrust for four cases (Fig. 2.13(c)): keystone sliding downward (*1*), keystone sliding upward (*2*), rotation about M (*3*), and rotation about m (*4*). Coulomb used statically determinate collapse mechanisms rather than the four-pin collapse mechanisms of Couplet. In cases *1* and *2*, Coulomb first developed his laws of friction. He stated that the friction force must be applied in the direction opposite of the tendency to slide. Applying the friction coefficient to the equation of equilibrium, the horizontal thrust at the crown, P, was determined. The maximum and minimum value of P was calculated to prevent collapse of the arch by sliding.

Coulomb's voussoir rotation theory looked mainly upon the cases of *3* and *4*, rotation about M and m (Fig. 2.13(d)). He determined a half arch was maintained in equilibrium by a horizontal thrust acting at the capstone. Coulomb's analysis introduced the idea of maximum and minimum allowable thrust to keep the arch in equilibrium, dependent upon the location of the hinge. By

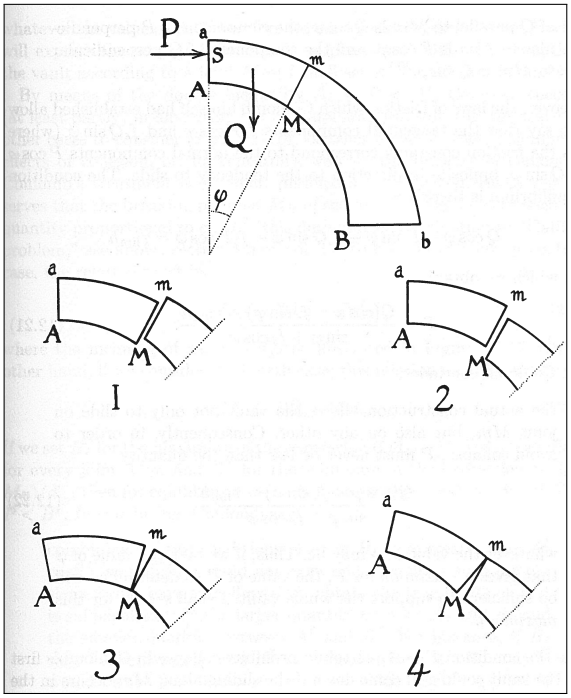

(c) Four limit cases for considering friction and cohesion, (Coulomb, 1773) (Adapted by (Benvenuto, 1991))

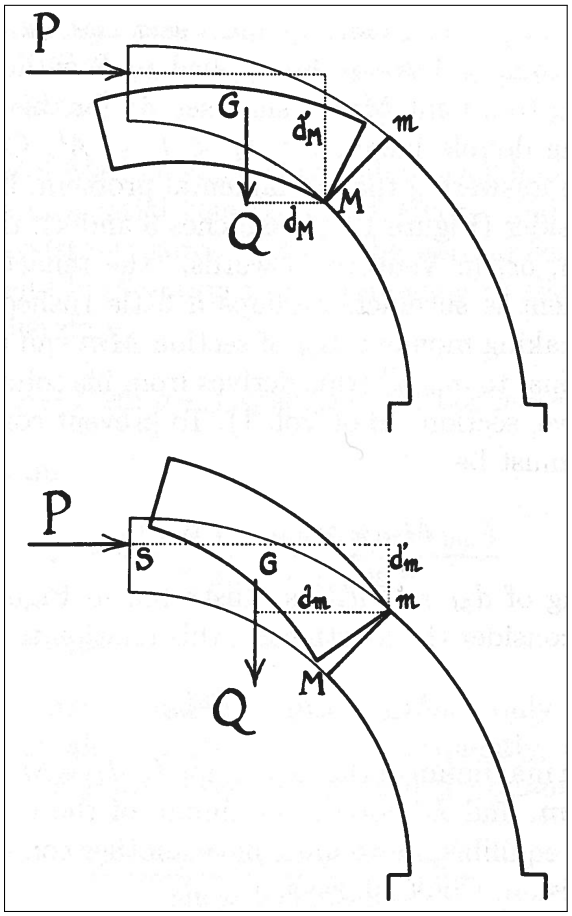

(d) Coulomb's voussoir rotation principle, (Coulomb, 1773) (Adapted by (Benvenuto, 1991))

assuming the hinge location about the intrados, M, the equivalent thrust was determined. The location of the hinge was moved until the maximum thrust was found. This was the minimum value required to maintain stability of the arch. The process was then repeated by assuming hinging about the extrados, m. Once again the hinge was relocated until a minimum value was found, or the maximum value for arch stability. The maximum and minimum values of all four cases control the design.

2.3.2.5 Voussoir Rotation Theorem Advancement

Though Coulomb was not correct in determining the critical hinging location in the arch, his theory was a stepping stone for future research. In 1820, Audoy improved upon Coulomb's

method and determined the location of the "fracture joints at the intrados which correspond to the maximum horizontal thrust at the key in the case of sliding or rotating" (Benvenuto, 1991, pg. 429). Barlow later solidified the theory of maximum and minimum thrust in 1846 by creating a 6 voussoir arch model with wood acting as mortar. Removing select pieces of wood, he developed hinging and thrust lines, determining the line of resistance and line of impression (limits of least and greatest horizontal abutment thrust) (Heyman, 1998, pg. 92).

2.3.3 Line of Thrust Theory

The line of thrust theory was introduced through recognizing the need to achieve "load bearing system synthesis" (Kurrer, 2012, pg. 216) in order to analyze the arch as a whole. The chain models introduced by Hooke and Gregory analyzed a whole system, however, lacked the ability to analyze individual elements. The load bearing system analysis of de la Hire and Couplet was limited to individual load bearing elements and their addition to form the model arch. Neither the chain models nor the addition of individual wedges could properly analyze the arch and saw no progress until Gerstner in the early 1800s.

2.3.3.1 Introduction of Line of Thrust Theory - Gerstner

Franz Joseph Ritter von Gerstner brought about the "merger of the loadbearing system synthesis with loadbearing system analysis" (Kurrer, 2012, pg. 216). In 1831, Gerstner accomplished this through the introduction of the line of thrust theory and formulation of the three prime tasks. First task: "Determine the loading case for given loading case". Second task: "Determine loading case for a given arch center of gravity axis such that said axis coincides with the line of thrust". Third task: "Take into account the line of thrust for given loading case and masonry arch center of gravity axis" (Kurrer, 2012, pg. 217). The line of thrust theory favored the third task through the recognition that a masonry arch's stability is dependent on the number of statically possible lines of thrust. Eventually the focus changed from the infinite number of statically possible thrust lines to the true line of thrust.

2.3.3.2 True Line of Thrust - Moseley

The true line of thrust was considered as the true acting thrust found within the arch for a given loading. The topic of true thrust presented great debate in the 1800's. The first exploration of the topic came from Henry Moseley in 1833. Moseley proposed the principle of the line of resistance and line of pressure, stating that the line of minimum resistance would identify the true line of thrust. The line of resistance was created by connecting the intersections of the thrust resultants with the joints. The line of pressure was created from the direction of the resultant pressures in the joints (Fig. 2.13).

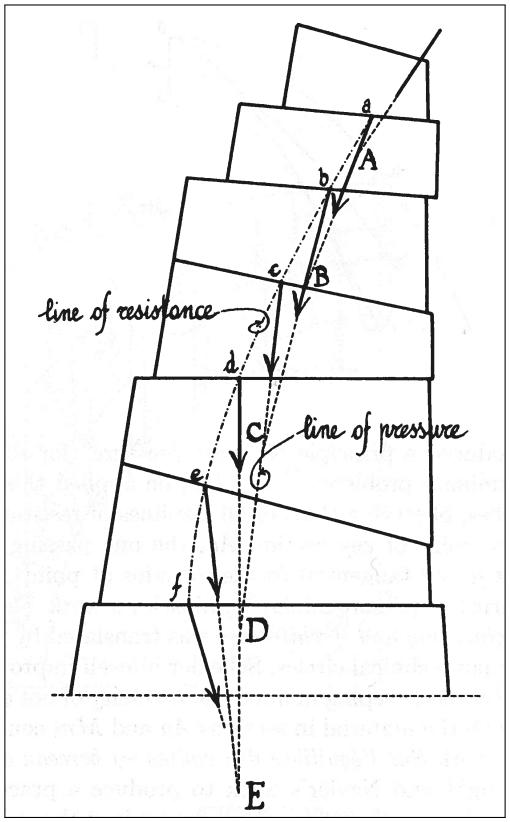

Figure 2.13: Line of resistance and line of pressure, (Moseley, 1839) (Adapted by (Benvenuto, 1991))

"For equilibrium to exist, the line of resistance must be entirely inside the interior of the arch; if it crosses the extrados or intrados below a certain angle, the arch will break near its point

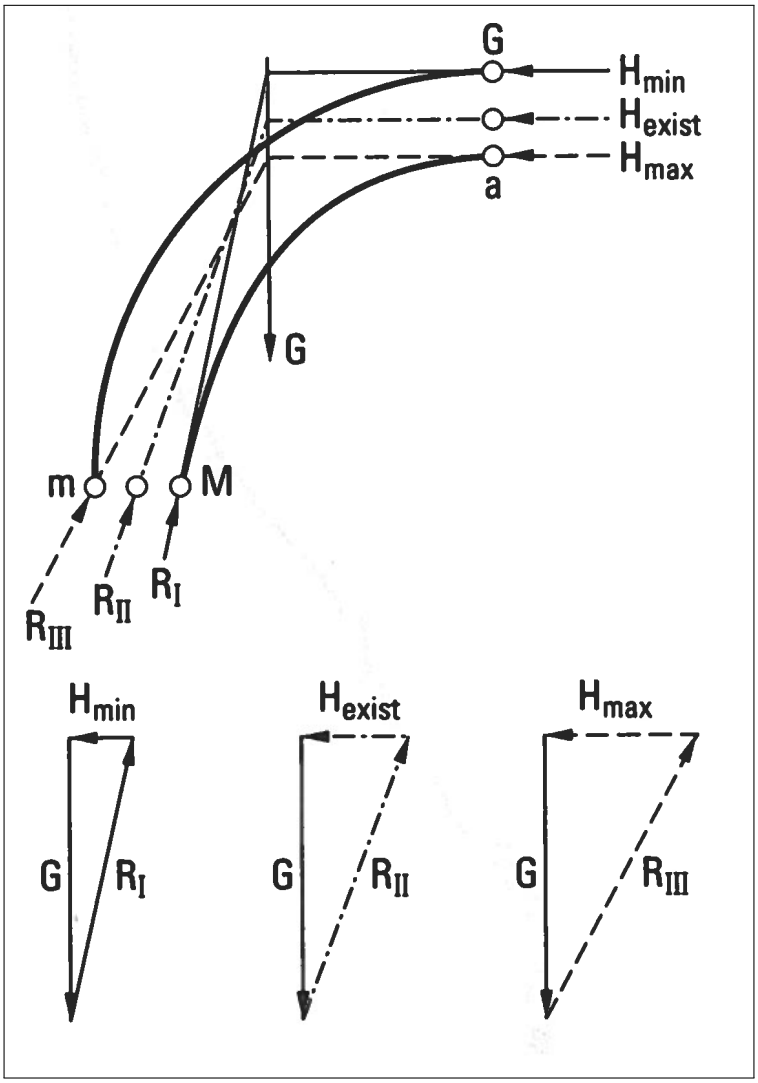

Figure 2.14: Significant equilibrium conditions after Moseley and Scheffler, (Kurrer, 2012)

of intersection with the line" (Benvenuto, 1991, pg. 432). Moseley determined the true line of thrust must pass through the extrados at the key and the intrados at the springing, since this was the minimum arch thrust. However, he did not examine of the case of maximum thrust. Rotation occurs at the locations where the line of resistance is tangent to the intrados or extrados.

Moseley also included the concept of friction in his analysis. He stated that the angle, ρ, at

which the line of pressure crosses the joint must be connected with the friction in the joint.

$$\begin{array}{lcll} \phi & = & \tan^{-1} f & \text{friction angle} \\ \rho & > & \phi & \text{sliding will occur} \\ \rho & < & \phi & \text{no sliding} \end{array} \tag{2.21}$$

2.3.3.3 True Line of Thrust - Scheffler

An infinite number of lines of pressure can be drawn within the arch, but which is the correct, true line of thrust? This was main topic of opposition to the viewpoint of Moseley. Scheffler quickly counters by stating that it's unclear to determine which of the infinite force systems occur in nature. "According to Scheffler, the minimal line of thrust is the true line of thrust only for masonry arches with a rigid mass of voussoirs. However, as the material of the voussoirs is not rigid, but rather elastic, the true line of thrust lies between the minimum and maximum lines" confirming the idea of limit analysis presented by Coulomb (Kurrer, 2012, pg. 219). Scheffler led the initial push toward the idea of elastic material properties and elastic analysis.

2.3.4 Stress Analysis

2.3.4.1 Uniform Stress Distribution - Young and Huerta

Thomas Young worked on his masonry arch theory from 1801 to 1816. His theory consisted of six parts, however, we will only focus on the first part: the resistance of materials. In this portion of Young's masonry arch theory, he developed a law of distribution of stress over the arch cross section when an axial force is applied eccentrically to the neutral axis position. The neutral axis position is described by Young as "the distance of the neutral point from the axis is to the depth, as the depth to twelve times the distance of the force, measured in the transverse section" (Huerta, 2005, pg. 202) and can be seen below.

$$z = \frac{d^2}{12y} \tag{2.22}$$

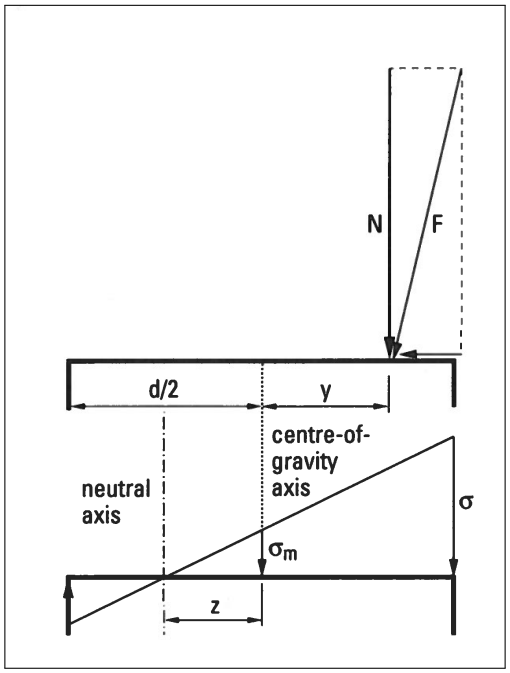

Figure 2.15: Stress distribution over the cross section after Young, (Huerta, 2005) (Adapted by (Kurrer, 2012))

Huerta advances Young's theory with the following mathematical explanation. The axial stress, σ, at the extreme right (Fig. 2.15) can be written as

$$\sigma = \sigma_m \left(\frac{d + 6y}{d} \right) \tag{2.23}$$

where the average stress,

$$\sigma_m = \frac{N}{db} \tag{2.24}$$

When the applied force neared the edge of the cross-section, the force distribution exhibited compressive forces near the applied force and tension away from the force. Indirectly, Young made the determination of the middle third rule. "If the axial force N is applied in the middle-third of the depth d of the arch, then all the stresses are compressive" (Kurrer, 2012, pg. 88). Ensuring compression throughout the arch instills confidence in the overall stability and safety of the arch. As stated previously, a "load bearing structure will not collapse when an equilibrium condition can be found that does not infringe the hinge condition" (Kurrer, 2012, pg. 236). If no tension is found

within the structure, no hinges will form and the structure will remain stable.

2.3.4.2 Middle Third - Navier

Claude - Louis Navier introduced stress analysis to masonry arch theory, which laid the foundation to what became the basis of strength analysis. Navier's masonry arch theory observed the voussoir rotation theory of Coulomb. In addition he "permits horizontal loads, assuming a triangular distribution for the compressive stress in the joints under consideration" (Kurrer, 2012, pg. 220). He considered the stress distributed over every point in the transverse joints which allows for a more realistic distribution of the compressive forces which the material resists (Fig. 2.16).

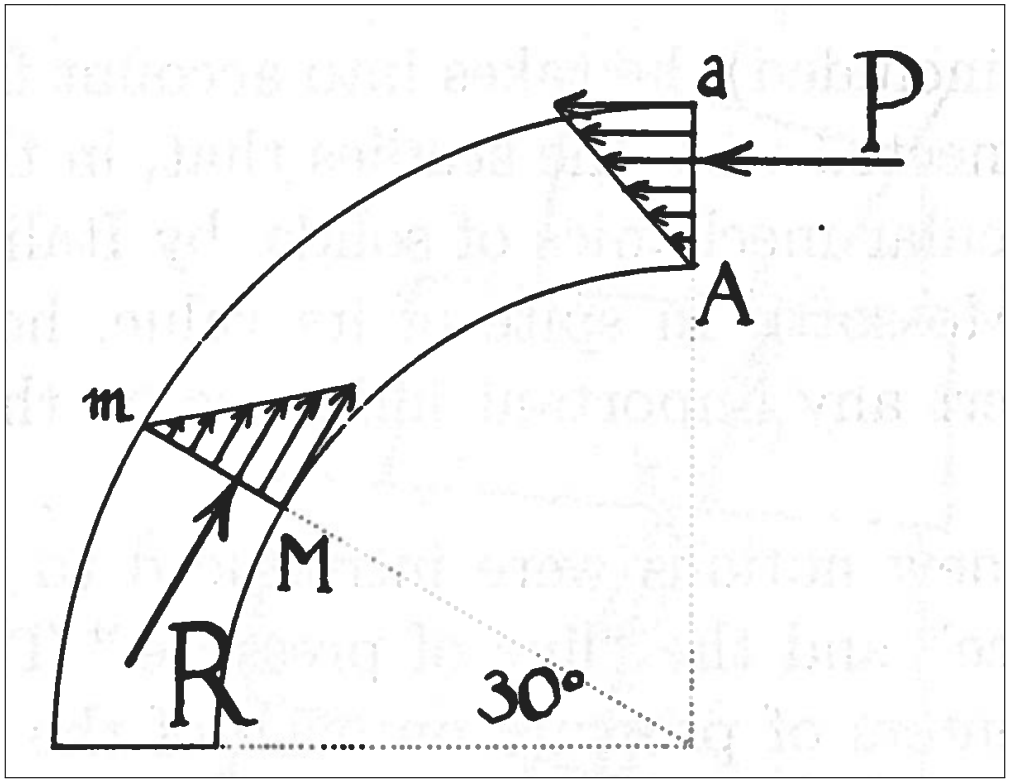

Figure 2.16: Navier's stress distribution, (Navier, 1826) (Adapted by (Benvenuto, 1991))

Even though Navier introduced stress analysis into masonry arch theory and elastic theory, he could not relate the elastic theory developed for timber and iron construction to masonry arches. This was due more to the time frame and lack of experimentation and material knowledge than

a lapse on Navier's part. The "force-deformation behavior of masonry arch materials in the service condition was not yet researched experimentally until the final third of the 19th century, in particular by Johann Bauschinger". Also "the small compressions under service conditions could not be quantified reliably with the testing apparatus available at that time". Finally, "deformation measurements on the generally oversized masonry arch structures could not be meaningful because the effects of arch settlement, dimensional stability, etc. were in the same order of magnitude as the deformations under service conditions" (Kurrer, 2012, pg. 220).

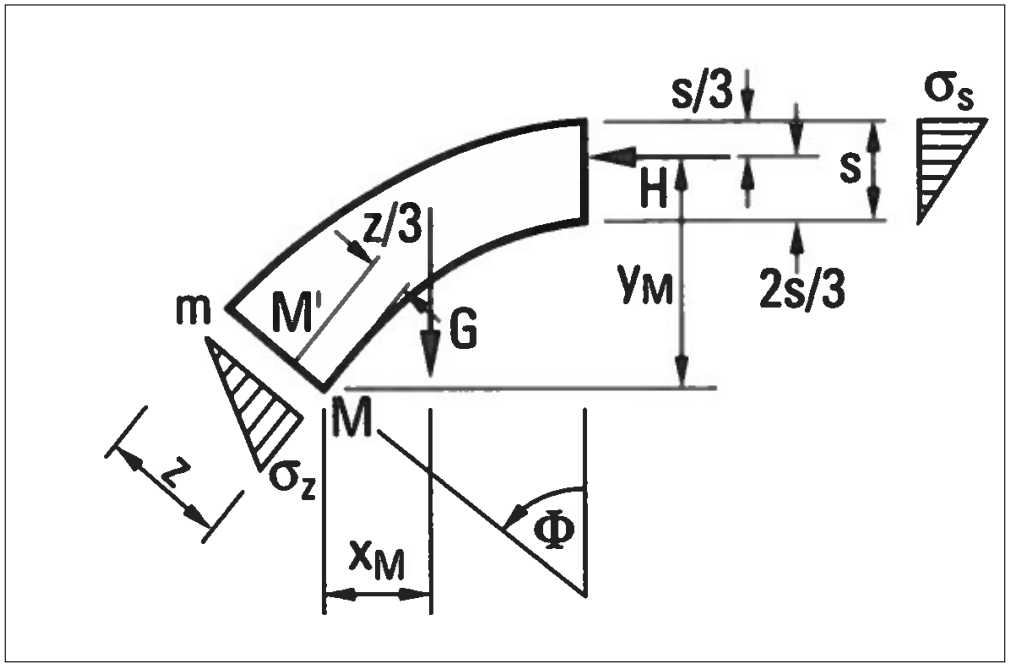

Figure 2.17: Distributed stress analysis in masonry arches, (Navier, 1826)

However, Navier did come to the conclusion that "the resultant of normal pressure at the joint must pass at a distance from the most compressed edge equal to a third of the actual width of that joint" and that "the pressure on this edge is twice as much as the one that would occur in the hypothesis of a uniform repartition on the whole surface of the joint" (Benvenuto, 1991, pg. 431). Navier, along with Young discussed previously, noticed the importance of thrust occurring within the middle third of the member to maintain uniform compressive stress across the member face (Fig. 2.17).

2.3.4.3 Advancement of Stress Analysis - Bandhauer

Without the creation of elastic theory, alternatives for analyzing the stress distributions in the joints of masonry arches continued development. In 1831, Bandhauer introduced a new approach of stress distribution at voussoir joints and the idea of a factor of safety. Bandhauer determined that the thrust line of a catenary arch with a factor of safety of one must follow the given calculation or failure may occur. However, as the factor of safety grows average compression line can deviate from the given calculation without the fear of failure. "It is this and only this condition that we have to thank for the stability of all our free-standing masonry arches designed according to the catenary" (Kurrer, 2012, pg. 221).

Bandhauer's stress concept developed from this new approach resulted in the compressive stress equation seen below

$$\sigma_B(v) = \frac{N}{bd} \times \frac{1}{1-v} \tag{2.25}$$

where d is the thickness, b is the width, N is the normal force applied at the eccentricity, e and

$$v = \frac{2e}{d} \tag{2.26}$$

Converting Eq. 2.25 to the dimensionless form allowed the creation of Bandhauer's hyperbolic function of compressive stress distribution.

$$\frac{\sigma_B(v)}{\sigma_m} = \frac{1}{1-v} \tag{2.27}$$

For comparison, Young's equation (Eq. 2.23) is also converted to the dimensionless form

$$\frac{\sigma(v)}{\sigma_m} = 3v + 1 \tag{2.28}$$

In Fig. 2.18 seen below, Bandhauer's equation differs from the compressive stress distribution developed by Young and Navier for N applied in the middle third of the cross section.

The equations of Young, Navier and Bandhauer all equate equal values at *v=0* and *v=2/3*. The difference is found as the equations approach *v=1*. As Bandhauer's hyperbolic function ap-

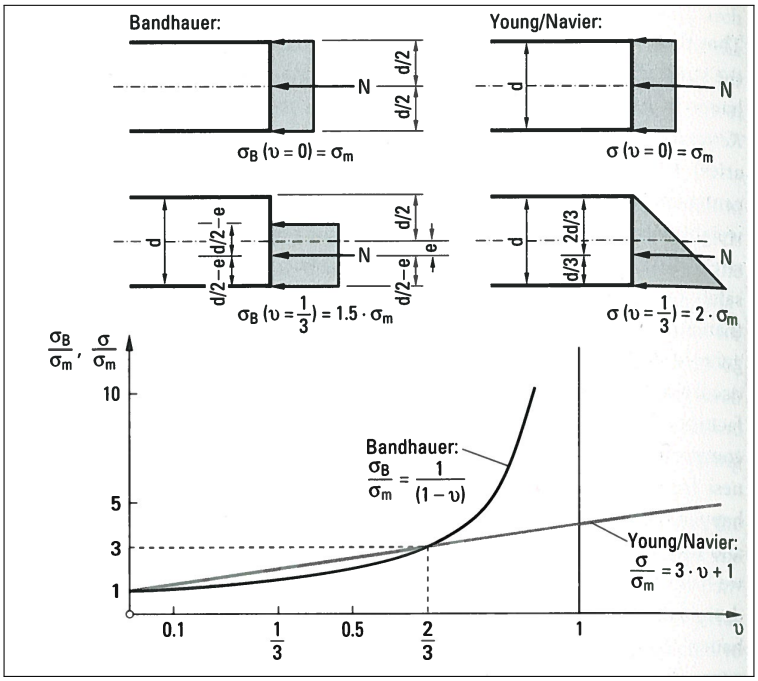

Figure 2.18: Stresses at the extreme fibers in the masonry arch cross-section according to Bandhauer and Young/Navier, (Kurrer, 2012)

proaches 1, it goes to infinity in accordance with the conditions set by Couplet and Heyman of infinite compressive strength. In comparison, the equation of Young/ Navier continues linearly as it approaches 1. Bandhauer's hyperbolic functions mimics today's equation of load carrying capacity.

$$\sigma_B(v = 2/3) = B_R = \frac{N_T}{bd} \times \frac{1}{1 - \frac{2}{3}} = 3\frac{N_T}{bd} \tag{2.29}$$

or

$$N_T = \frac{1}{3} bdB_R \tag{2.30}$$

where B_R equals the standardized compressive strength of masonry.

2.3.5 Elastic Theory - Winkler

In 1860, Saavedra was the first individual to try elastic theory with masonry arches. However, his approach was far too complex and not practical for the design of masonry arch structures. With

minimal results, his theory was placed on the back burner to make room for the theorems of Rankine and Winkler. Rankine "postulated the theorem that the stability of a masonry arch is guaranteed when a line of thrust due to a given loading case can be drawn through the middle-third of all arch cross sections" (Kurrer, 2012, pg. 223). Rankine combined the middle third rule with thrust line theory which was used in analysis until the 1960's.

From 1867 to 1868, Wrinkler developed the influence line concept for 3-pin, 2-pin, and fixed arches. However, his more notable achievement comes about in 1879 with his presentation on the concept of elastic arch theory. Winkler adapted his elastic arch theory to the analysis of masonry arches. He first defined the line of thrust as "the geometrical position of the point at which the resultants intersect the masonry joints" (Kurrer, 2012, pg. 225). He next determined the position of the line of thrust. In the final step, he differentiated the normal state from the disrupted state.

Winkler also identified disruptions such as "incompletely cured mortar, temperature changes, yielding centering during construction and, first and foremost, sinking abutments after striking the centering, which lead to visible cracks and considerable changes to the course of the line of thrust" (Kurrer, 2012, pg. 225). He proposed that the correct line of thrust can be determined through elastic analysis when the arch is subjected to normal state conditions.

In Winkler's elastic theorem he derived three elasticity conditions to determine the position of the line of thrust in a masonry arch with three degrees of static indeterminacy. No rotation ($\Delta\phi = 0$) and no horizontal ($\Delta u = 0$) or vertical ($\Delta v = 0$) movement.

$$\begin{aligned} \Delta\phi &= 0 = \int d\gamma = \int \tfrac{1}{EI_z} \times M(s)ds \\ \Delta u &= 0 = \int \Delta ds_x = \int \tfrac{1}{EI_z} \times M(s)yds \\ \Delta v &= 0 = \int \Delta ds_y = \int \tfrac{1}{EI_z} \times M(s)xds \end{aligned} \tag{2.31}$$

where M is the bending moment with the arc coordinate s, E is the elastic modulus, and I_z is the second moment of area about the z-axis.

The Winkler Theorem states that "for a constant thickness, the line of thrust close to the [correct] one [is] the one for which the sum of the squares of the deviations from the center-of-gravity axis is a minimum" (Winkler, 1880, pg. 128).

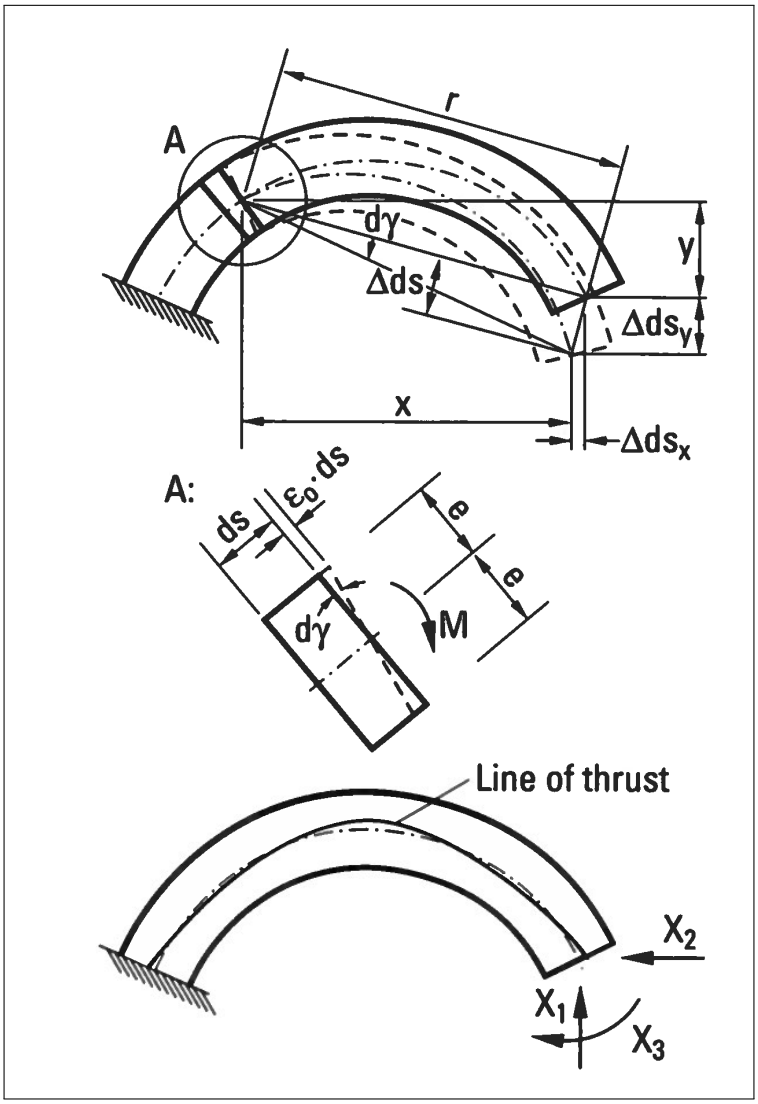

Figure 2.19: Winkler's determination of the position of the line thrust in masonry arch using elastic theory, (Kurrer, 2012)

$$I = \int [z(s)]^2 \times ds = \text{Minimum} \tag{2.32}$$

Eq. 2.32 must satisfy the following conditions

$$\frac{\mathrm{d}I}{\mathrm{d}a} = 0 \tag{2.33}$$

$$\frac{\mathrm{d}I}{\mathrm{d}b} = 0 \tag{2.34}$$

$$\frac{\mathrm{d}I}{\mathrm{d}c} = 0 \tag{2.35}$$

where a, b, and c are unknown position parameters. The vertical support reaction, X_1, the horizontal thrust, X_2 and the moment, X_3 from Fig. 2.19 can be used for the position parameters.

2.3.6 Ultimate Load Theory - Heyman

Even though Drucker is credited as first suggesting the use of ultimate load analysis for investigating the equilibrium and failure of voussoir arches, the memorable contribution to this topic comes from Jacques Heyman. In 1966, Heyman published a discussion of the ultimate load theory for all masonry load bearing structures, including plane arches, domes, fan vaults, groined vaults, towers, and spires (Kurrer, 2012, pg. 233). Heyman required three principles be met in order to conduct the ultimate load analysis of masonry construction. All three principles aligned with those of Couplet, infinite compressive strength, zero tensile strength, and no sliding occurs. "When the masonry material satisfies these conditions, the component of the resultant of the effective stresses acting perpendicular to the cross-sectional area must be a compressive force N for each cross-section whose intersection point lies within the cross-section" (Kurrer, 2012, pg. 233). If N acts at the edge of the cross-section, a hinge forms leading to a yield surface bounded by two straight lines.

$$M = Ne \tag{2.36}$$

$$-h \leq e \leq h \tag{2.37}$$

The normal force must act within the yield surface of AOB. If N passes outside the yield surface, the thrust passes outside the masonry arch section and the structure is deemed unstable.

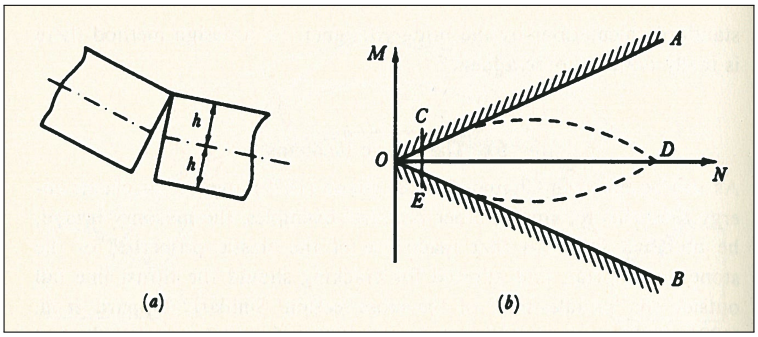

Figure 2.20: The yield surface for masonry, (Heyman, 1998)

In today's design principles for masonry arches, the ultimate load theorem of Heyman, first hinted by Coulomb through voussoir rotation, is most often utilized to analyze stability.

If we replace the stone of infinite strength (Fig. 2.20) with a stone of finite crushing strength, the yield zone is reduced to the curved boundary *OCDEO*. Even though the zone narrows to point *D*, this has little effect on the majority of all masonry design. "A typical value of permitted stress used in the nineteenth-century design...is 10 [percent] of the crushing strength; nominal stresses are likely to be less than this, but even at 10 [percent] the portion of the yield surface is the slightly curvilinear triangle *OCE*" (Heyman, 1998, pg. 94).

To aid his ultimate load analysis, Heyman proposed a geometric factor of safety. "If the real arch has twice the thickness of the limiting arch, then the geometrical factor of safety is 2" (Kurrer, 2012, pg. 237). The limiting arch must be determined from the most unfavorable loading case. Elaborate calculations, often including virtual displacements, were required for the exact value. However, from the concept of simply passing a thrust line through the arch, it was easy to show.

Heyman also proved that the ultimate load analysis enabled the equilibrium approach for the analysis of loadbearing structures. This tool was made useful for determining the structural stability of the masonry. "It is not the task of the structural engineer to determine the true equilibrium condition for a particular loadbearing structure, but rather sensible equilibrium conditions" (Kurrer, 2012, pg. 237).

2.4 Shells

2.4.1 Introduction

"A dome is a rounded vault forming a roof over a large interior space" (Heyman, 1997, pg. 27). This characteristic alone brought interest to dome and vault research as theorists searched for new and aesthetically pleasing forms of shelter. The majority of the properties of the masonry arch hold true for the dome, resulting in far more research in the field of arches. However, some unique properties are seen only in the dome and require special attention.

2.4.2 The Hen's Egg - Viviani

The basic shape of a dome is a shell of revolution where every horizontal section is circular, similar to that of the hen's egg. Vincenzo Viviani spent immense time studying the egg's shape and its extraordinary strength. Even with its thin and fragile shell, the shell cannot be broken with pressure applied between the thumb and finger when held in the longitudinal axis. Instead a high local pressure is required to crack the shell. Given the high strength with respect to the thin shell, the egg formed the basis of experimentation and development of the dome.

2.4.3 Structural Theory

The shell is considered as a curved surface or plate with a small thickness compared to the size of the shelled structure. The interior forces of the shell resist self weight and external loads and are able to carry a wide range of loadings. The major concern of the shell's carrying capacity lies not with the thickness, as in an arch, but solely with local compressive buckling. However, as discussed previously with arches, masonry has an extremely high compressive strength, ensuring no local buckling danger. Similar the masonry arch, the masonry dome exhibits low compressive stresses. Fig. 2.21 displays a uniform, thin walled hemisphere solely supporting self weight. The shell is supported at its base by a uniform compressive stress, σ. The radius, a, thickness, t, and unit weight, ρ, will help aid the illustration.

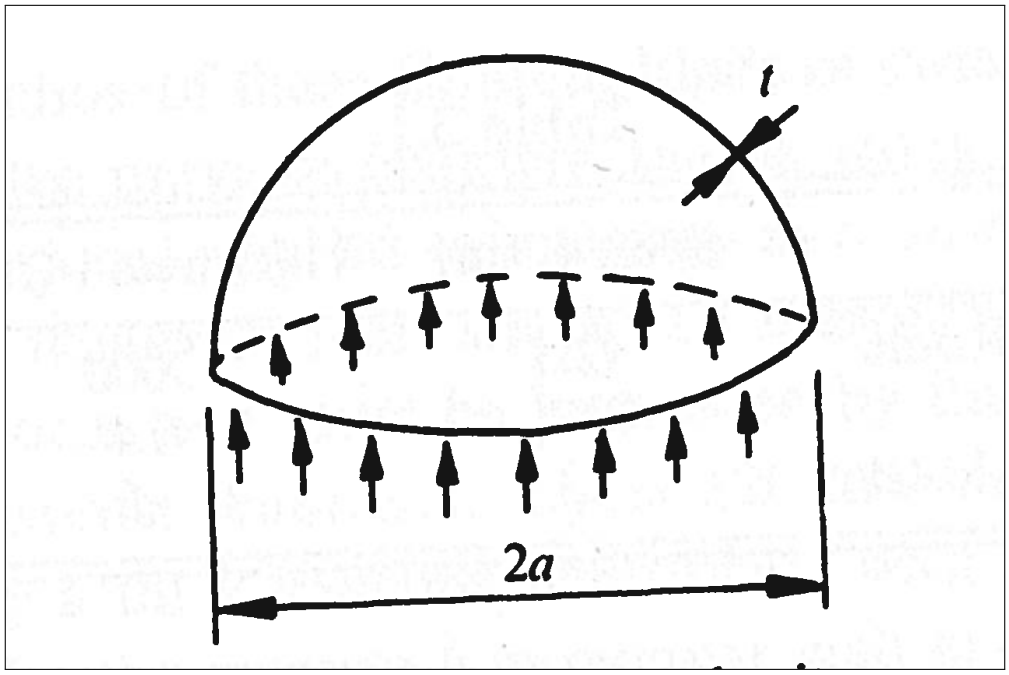

Figure 2.21: Hemispherical shell under its own weight, (Heyman, 1997)

$$\text{Volume} = 2\pi a^2 t \tag{2.38}$$

$$\text{Diametral ring area} = 2\pi a t \tag{2.39}$$

$$\sigma(2\pi a t) = \rho(2\pi a^2 t) \tag{2.40}$$

$$\sigma = \rho a \tag{2.41}$$

The proof shows that the compressive stress is unreliant on the dome thickness but rather the radius.

Another unique characteristic comparing the structural theory of the arch to the dome deals with the keystone. The masonry arch requires the keystone to stand where as the crown of the dome is not required. This is due to the multi-directional distribution of stress. Since the hoop stresses are always in compression, a full circle around the dome is enough to support itself. The segmental dome allowed for a oculus (skylight) along with large bell towers and spires to extend from the dome at the opening. Famous examples of segmental, incomplete hemisphere, domes are

the Santa Maria del Fiore and the Pantheon in Rome.

2.4.4 Analysis

Initial methods of dome analysis followed that of the masonry arch, utilizing statics or Hooke's hanging chain. Hooke's hanging chain represented the thrust line within the dome. This static approach allowed the dome to carry a wide range of loadings. This methodology was performed by Poleni in the study of the cracking of the St. Peter's dome in Rome and will be discussed in a later section. Similarly to the arch, no matter the shape, an outward thrust was observed at the supports. However, domes often require buttresses due to the lack of lateral strength from the supporting walls.

The second and more recognized method of dome analysis is the membrane theory. The membrane theory assumes "that the surface has no stiffness against bending, so that the forces in the shell are purely tensile or compressive" (Heyman, 1997, pg. 28). However, since masonry has no tensile properties, only compression is considered. The theory analyzes the transmission of stresses through the shell to the base. Using differential equations and an infinitesimally small element cut from the shell, the stress resultants within the dome can be found (see Fig. 2.22 and 2.23).

The stress resultants N_ϕ and N_θ act on the cut edges of the element. N_ϕ represents the stresses along the meridian which increase from the crown to the base. N_θ accounts for the parallel circles, or hoop stresses. The meridian stresses are compressive throughout the shell which are the same stresses accounted for by the hanging chain theory. However, Mascheroni, discussed in a later section, discovered that the hoop stresses switch from compression to tension between the crown and the base. From the crown (90 degrees) to 51.82 degrees the stresses are in compression and then switch to tension increasing toward the base (Fig. 2.24). Steel rings or buttresses are required to prevent the tensile forces from controlling at the base of the dome and limits the outward thrust at the supports.

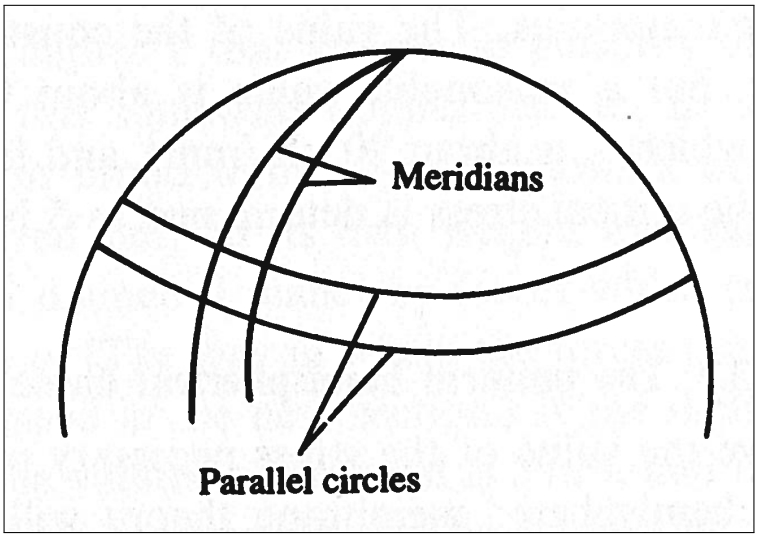

Figure 2.22: Meridians and parallels defining an element of the shell, (Heyman, 1997)

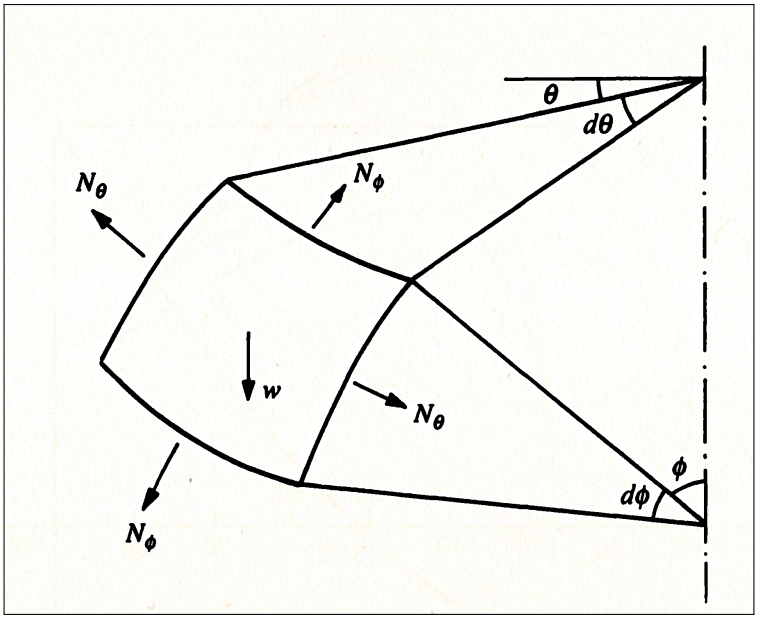

Figure 2.23: Equilibrium of a small element of shell, (Heyman, 1997)

2.4.5 Vault Research

2.4.5.1 Ideal Vault - Bossut

The French mathematician, Abbe Charles Bossut, set his sight on the formulation of the ideal vault, neglecting friction and cohesion between the vousoirs. Bossut assumed smooth, frictionless

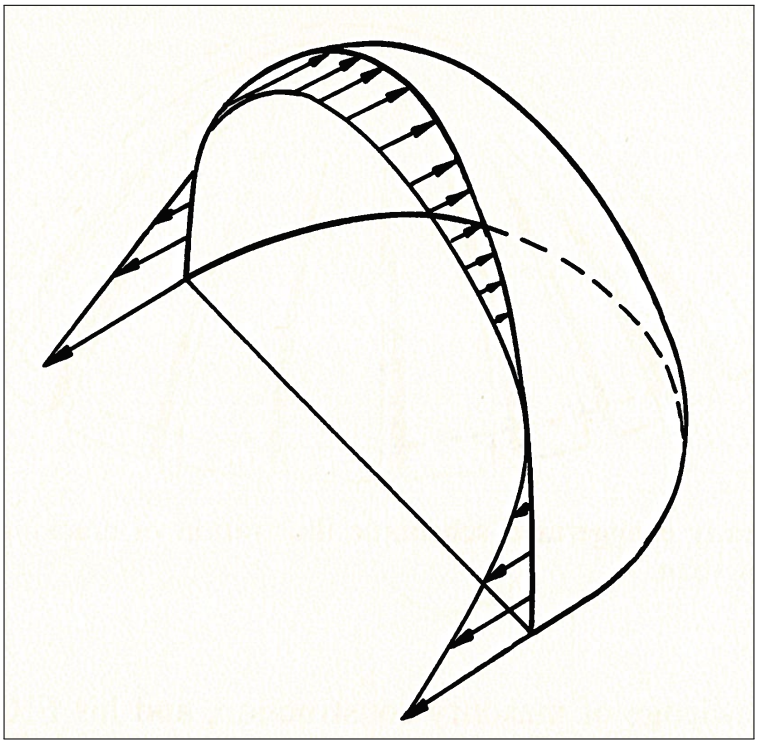

Figure 2.24: Hoop stress resultants necessary for the equilibrium of a hemispherical shell, (Heyman, 1997)

blocks with joints perpendicular to the intrados. The weights of the blocks along with all non-vertical forces were assigned to F_1 and F_2 (Fig. 2.25). The forces were then decomposed into the internal forces F_{1l}, F_{1r}, F_{2l} and F_{2r}. From equilibrium

$$F_{1r} = F_{2l} \tag{2.42}$$

Utilizing the theorem of sines

$$F_l = F\frac{\sin\alpha}{\sin\beta} \tag{2.43}$$

$$F_r = F\frac{\sin\gamma}{\sin\beta} \tag{2.44}$$

$$\tag{2.45}$$

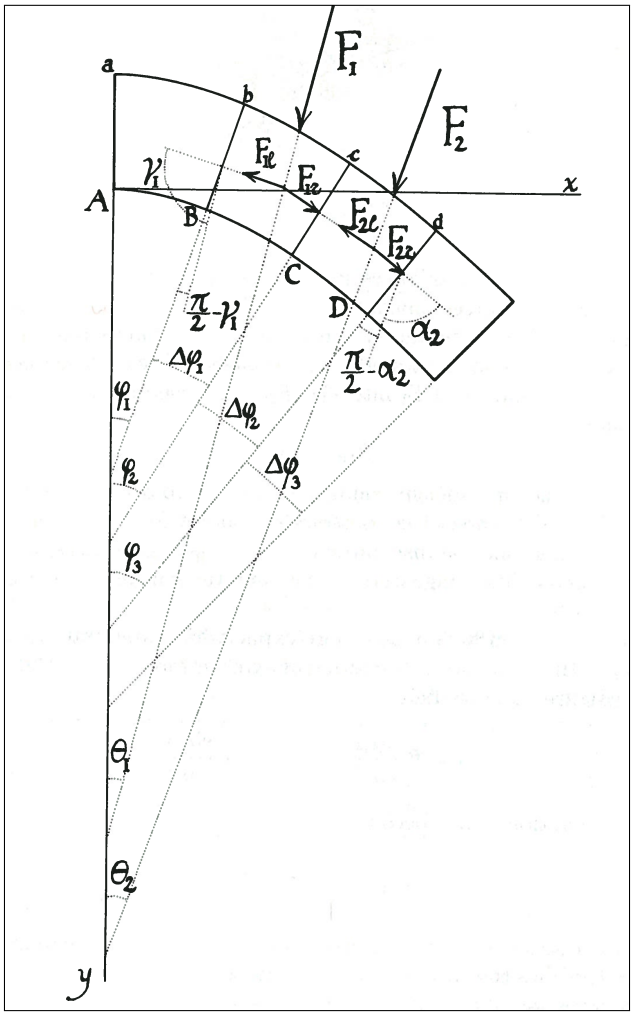

Figure 2.25: Bossut's ideal vault formulation, (Benvenuto, 1991)

Eq. 2.42 becomes

$$\frac{F_1}{F_2} = \frac{\sin\alpha_2 \sin\beta_1}{\sin\gamma_1 \sin\beta_2} \tag{2.46}$$

The angles α, β and γ were written as functions of ϕ which described the rotation of the intrados curve, and θ which gave the direction of the exterior force (Benvenuto, 1991, pg. 378). If we set $\Delta\phi_1 = \phi_2 - \phi_1$ and $\Delta\phi_2 = \phi_3 - \phi_2$

$$\beta_1 = \Delta\phi_1 \tag{2.47}$$

$$\beta_2 = \Delta\phi_2 \tag{2.48}$$

$$\frac{\pi}{2} - \gamma_1 = \phi_1 - \theta_1 \tag{2.49}$$

$$\frac{\pi}{2} - \alpha_2 = \phi_3 - \theta_2 \tag{2.50}$$

Substituting into Eq. 2.46

$$\frac{F_1}{F_2} = \frac{\sin\Delta\phi_1}{\sin\Delta\phi_2}\frac{\cos(\phi_3 - \theta_2)}{\cos(\phi_1 - \theta_1)} \tag{2.51}$$

$$\frac{F_1}{F_2} = \frac{\sin\Delta\phi_1}{\sin\Delta\phi_2}\frac{\cos\phi_3\cos\theta_2 + \sin\phi_3 sin\theta_2}{\cos\phi_1\cos\theta_1 + \sin\phi_1\sin\theta_1} \tag{2.52}$$

Bossut's formulation dictated that if the path of the intrados and the direction of the forces were known, the ratio of forces could be found throughout the geometry.

Expanding upon his original formulation, Bossut converted his analysis into differential terms. Bossut assumed the vault, of basic arch shape, was composed of an infinite number of infinitesimal blocks. The variables of Eq. 2.52 are modified to their differential form. Let F_1 and F_2 become continuous

$$F_1 = f ds \tag{2.53}$$

$$F_2 = (f + df)ds \tag{2.54}$$

$$\cos\theta_1 = \cos\theta(s) \tag{2.55}$$

$$\sin\theta_1 = \sin\theta(s) \tag{2.56}$$

$$\cos\theta_2 = \cos\theta(s) + d[\cos\theta(s)] \tag{2.57}$$

$$\sin\theta_2 = \sin\theta(s) + d[\sin\theta(s)] \tag{2.58}$$

$$\tag{2.59}$$

From the curve of Fig. 2.26, the following relations can be made

$$\cos\phi_1 = \frac{dx(s)}{ds} \tag{2.60}$$

$$\sin\phi_1 = \frac{dy(s)}{ds} \tag{2.61}$$

$$\cos\phi_3 = \frac{dx(s)}{ds} + 2\frac{d^2x(s)}{ds^2}ds \tag{2.62}$$

$$\sin\phi_3 = \frac{dy(s)}{ds} + 2\frac{d^2y(s)}{ds^2}ds \tag{2.63}$$

$$\tag{2.64}$$

Substituting the relations above into Eq. 2.52 we obtain

$$f\cos\theta\left(2r\frac{d^2x}{ds^2} + \frac{dr}{ds}\frac{dx}{ds}\right) + f\sin\theta\left(2r\frac{d^2y}{ds^2} + \frac{dr}{ds}\frac{dy}{ds}\right) + r\frac{dx}{ds}\frac{d}{ds}\left(f\cos\theta\right) + r\frac{dy}{ds}\frac{d}{ds}\left(f\sin\theta\right) = 0 \tag{2.65}$$

Bossut's new form of analysis allowed him to determine the solution to two problems. First, the figure of the vault can be determined from the known forces. Second, the forces can be determined from the known vault figure.

Bossut put his formulation of the best vault figure to practice through the analysis of four different cases. He first looked at the homogeneous, uniform arch, subject only to self-weight loading. Through formulating equations and slight derivation, the homogeneous catenary was determined, confirming the results of Gregory. The second case included a variable vertical loading condition. The results once again presented the catenary but this time was proportional to the increasing vertical force. The third case examined the arch loaded normal to the axis, similar to hydrostatic pressure. The results matched that of a suspended rope. Finally, Bossut looked at the case of the dome vault. Each groin is considered separately as an arch of variable thickness (Fig. 2.27)

2.4.5.2 Domes of Finite Thickness - Mascheroni

In 1785, Lorenzo Mascheroni published his methodology for the principle problems in constructing arches and domes and the calculation of domes of finite thickness. In this review, we will

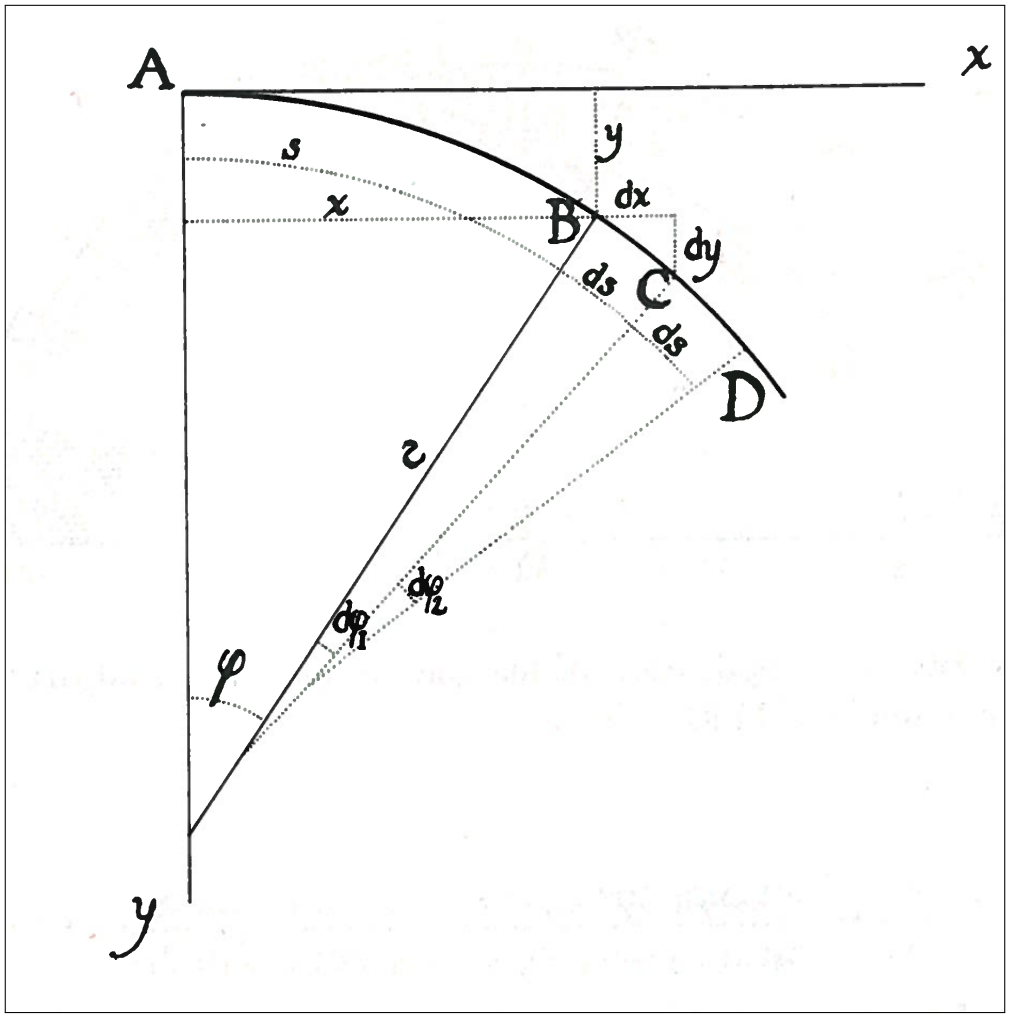

Figure 2.26: Infinitesimal vault, (Benvenuto, 1991)

focus on the later. In calculating the shape of a dome of finite thickness, Mascheroni first reviewed the work of Bouguer. Bouguer stated that the resultant of the horizontal thrust and vertical force from weight must be perpendicular to the joint between the voussoirs of an arch. However, the resultant force must be at an oblique angle to the joint in the case of a dome. Bouguer derived the relationship of

$$\frac{Q}{P} > \tan\phi \tag{2.66}$$

$$Q = P\frac{dy}{dx} \tag{2.67}$$

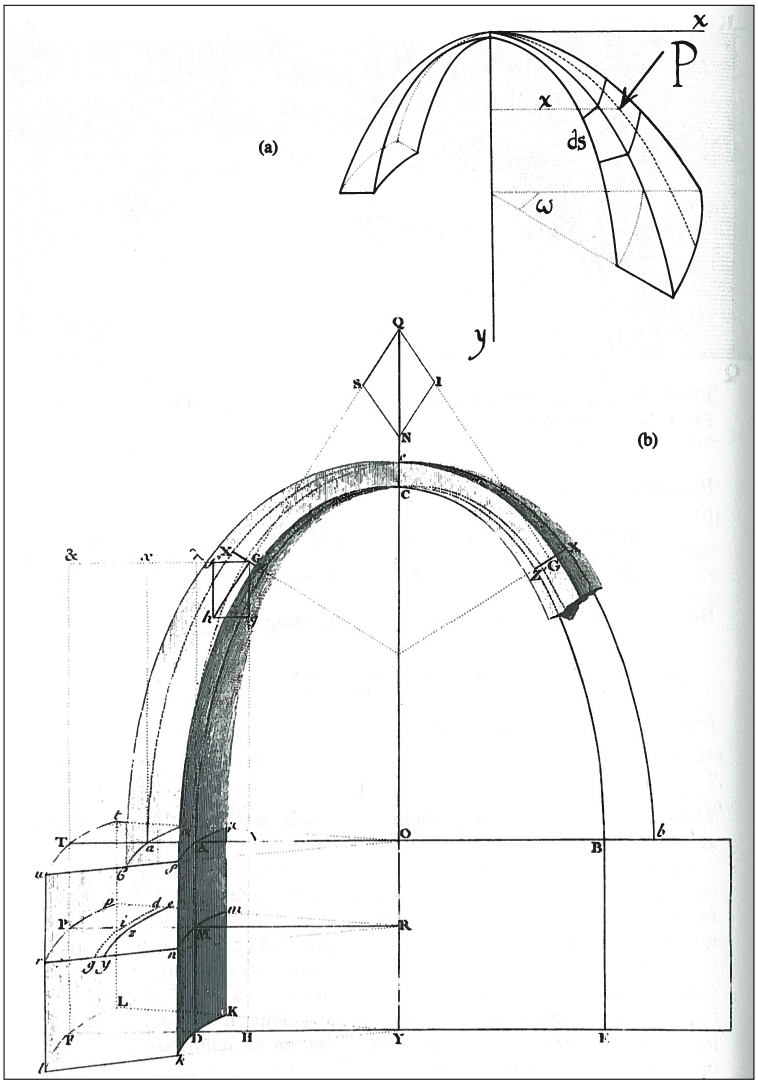

Figure 2.27: Bossut's figure for his studies of domes, (Benvenuto, 1991)

to ensure an oblique resultant force angle. He determined that if this condition held true in all joints around the dome, the forces would "hinder and annul each other" (Benvenuto, 1991, pg. 420). Even though his realization was wrong, the idea of a possible oblique resultant is correct. The resultant "can be oblique to *Mn* [the joint], because the stresses created by each element of the dome include not only compressive forces along the meridians, but also lateral internal forces along the other principal direction" (Benvenuto, 1991, pg. 421). Given the use of masonry, only compression can be considered because voussoirs cannot exert tensile stress on each other.

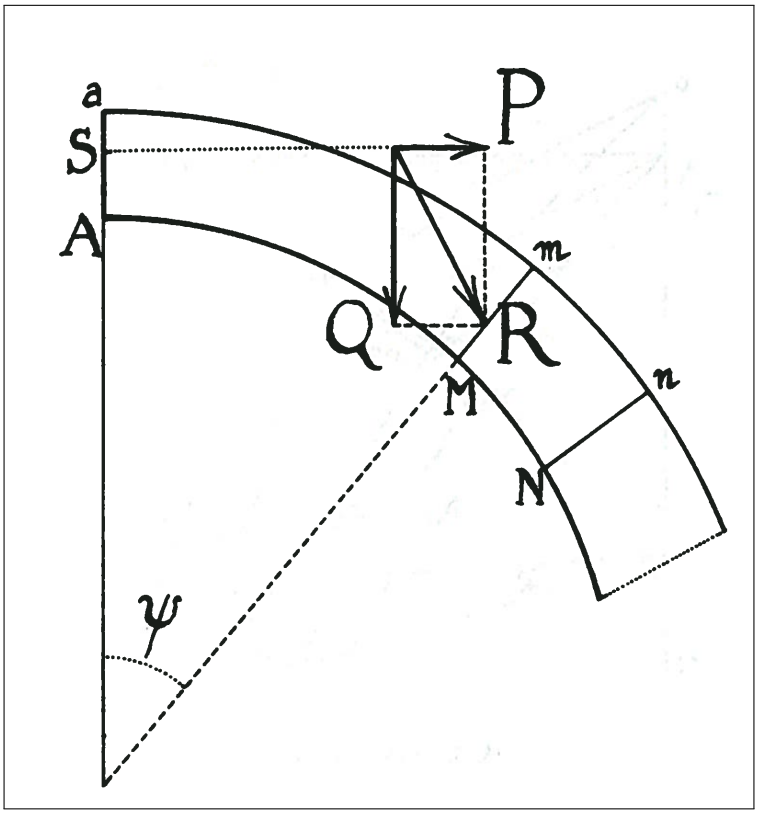

Figure 2.28: Bouguer's analysis of domes and oblique forces, (Benvenuto, 1991)

Mascheroni analyzed the ideal conditions to simplify the analysis. He assumed the joints were perpendicular to the intrados and that the thickness of the dome was very small compared to its radius. The simplifications allowed the reduction of the element volume Mn' (Fig. 2.29) to

$$\text{Vol}(Mn') = \left(hds + \frac{1}{2}h^2 d\phi \right) x \tag{2.68}$$

Since $\frac{1}{2}h^2 d\phi$ is negligible compared to $hxds$, Eq. 2.68 is reduced to

$$\text{Vol}(Mn') = hxds \tag{2.69}$$

Since the groin volume, Mn', is proportional to the wieght, Q, Eq. 2.67 can be rewritten as

$$\int hxds > P\frac{dy}{dx} \tag{2.70}$$

Through logarithms and differentiating, Eq. 2.71 is derived and can be used to determine

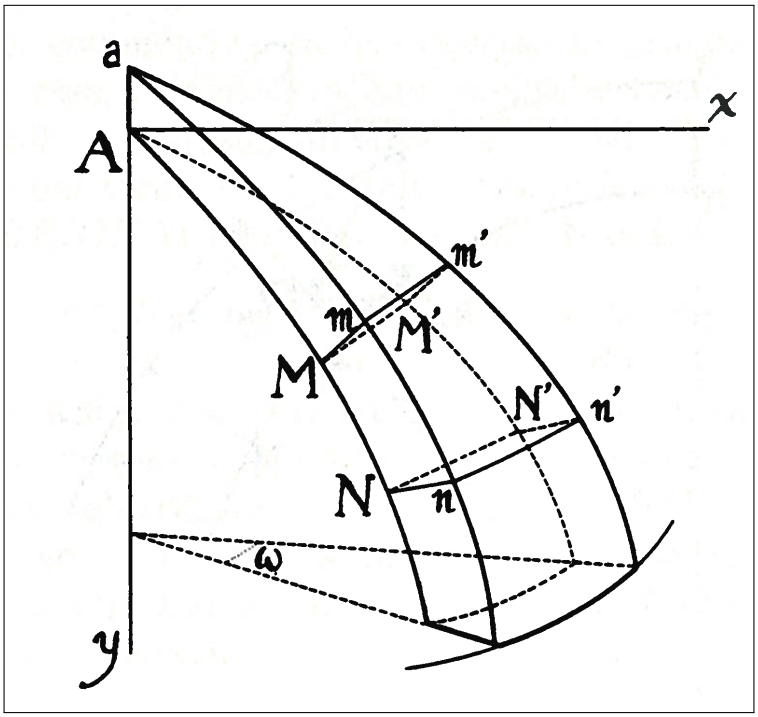

Figure 2.29: Mascheroni's simplified analysis of finite domes, (Benvenuto, 1991)

the size of the wedge from a known intrados curve.

$$\frac{hxds}{\int hxds} > \frac{dy'}{y'} \tag{2.71}$$

where $y' = \frac{dy}{dx}$

The final contribution of Mascheroni came about through expanding upon the suggestion of Bouguer to determine the scale of teh voussoir size from a known arch curve. But instead of the voussoir proportions, Mascheroni shifts the view to a round dome of constant thickness and the conditions that must satisfy equilibrium. Assuming a arch intrados curve of $x = \sqrt{2Ry - y^2}$ and basic calculation, Eq. 2.71 becomes

$$(R - y)(2R - y) > R^2 \tag{2.72}$$

Solving for y the following relationship is derived

$$y < \frac{3 - \sqrt{5}}{2} R = 0.382R \tag{2.73}$$

Mascheroni realized that a "dome of uniform thickness cannot be hemispheric, because its keystone cannot exceed 0.382R - that is, the generating arch of the dome cannot be more than $51°49'50''$. In the lower zones of such a structure, the lateral stress between groins changes from compression to tension, and the structure would need to be hooped" (Benvenuto, 1991, pg. 425).

2.4.5.3 Salimbeni

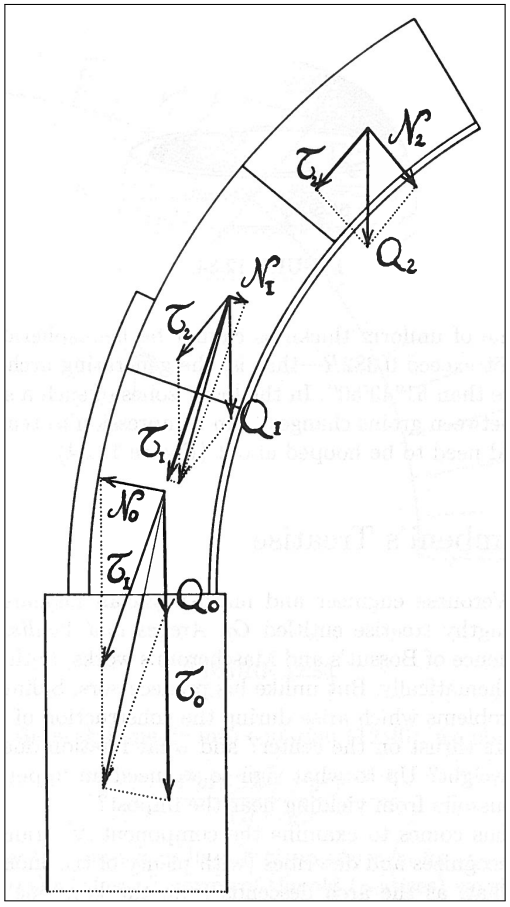

Figure 2.30: Salimbeni's graphical analysis of force transfer in a dome, (Salimbeni, 1787) (Adapted by (Benvenuto, 1991))

Mascheroni's final realization of tensile forces found in the dome was confirmed by the Veronese engineer and mathematician, Leonardo Salimbeni. In Salimbeni's published work, he studied the component, N, transverse to the intrados. As N progresses through the groin of the

dome and away from the keystone, the value decreases until the sign changes. It is observed that the springing yields outward rather than inward as observed in the arch. Salimbeni sought the solution to the location of the transfer of forces but could only develop a graphical solution rather than an exact formulation.

2.5 St. Peter's Basilica, Rome - Case Study

2.5.1 Introduction

In 1742, the dome of Saint Peter's Basilica, at Rome, showed severe cracking. Pope Benedict XIV deemed it necessary to conduct a study of the dome with a detailed analysis and report of the conclusion. The Pope assigned three mathematicians to review the state of the dome. Frs. Ruggiero Guiseppe Boscovich, Thomas le Seur, and Francois Jacquir analyzed the dome utilizing virtual work (Benvenuto, 1991, pg. 352). They broke the dome into a simple static scheme for the laws of mechanics to be applied. The conclusions presented a case of total separation between the drum and buttresses and between the interior and exterior portion of the base. Given the results, the three mathematicians deemed the dome unsafe and susceptible to collapse. They advised the dome be reinforced with iron rings to prevent a possible collapse.

Unsatisfied with the results, the pope wanted confirmation of the hypothesis of collapse. In 1743, Giovanni Poleni was appointed by Pope Benedict XIV to review the work of the mathematicians and provide his own conclusion. In Poleni's report of the dome, he focused on the cracks, the restoration and tension rings (Poleni, 1748).

2.5.2 Three Mathematicians Model

Frs. Ruggiero Guiseppe Boscovich, Thomas le Seur, and Francois Jacquir developed a geometric model to explain the domes damage, Fig. 2.31. The model presented the movement of the dome and allowed for the evaluation of its stability. Due to sagging of the drum and buttresses, each groin exhibited subsidence at its upper end and opening or separation at the lower end (López,

2006, pg. 1958). The three mathematicians also modeled the pilasters of the dome, concluding that they bent outward aiding in the sagging of the dome.

Poleni was asked to review the model of the mathematicians, concluding that a dome subjected to the magnitude of movement presented in the model could not possibly stand. Disproving their model, Poleni stated that the movement could not have occurred without separating the sections, as seen from his own developed model, Fig 2.32. The damage to the actual dome should coincide with that of his own geometric model, which it did not.

Poleni also went into detail on the supporting structural components. Poleni analyzed the drum as a whole, rather than just the pilasters like the mathematicians, along with the piers and buttresses. In fact, majority of the damage viewed in the dome, occurred over the piers and were entirely neglected by the mathematicians. Poleni first looked at the theory of the drum pilasters developed by the mathematician's model. He concludes that since the pilasters stood perpendicular, in order for outward movement to occur, the pilaster's initial design would have required an inward bend which is highly doubtful. However, the drum did subside, which Poleni attributed to a couple factors. He focused on the material bond of the drum, stating that the main reason for damage is due to the constant pressure of the full weight of the dome resting on the faulty masonry wall sections. He also attributed damage to the buttresses inability to support the forces distributed from the main arches (López, 2006, pg. 1964). These two factors contributed to a slight spreading and sagging of the dome, but nothing to the extent of the movement modeled by the three mathematicians which would result in total separation of the sections.

2.5.3 Poleni's Analysis

After disproving the model of the 3 mathematicians, Poleni dove into the theories of arches, vaults, and domes. He viewed principles related to the stability of vaulted structures and found that the same type of damage was observed in the drum and buttresses. Since the dome consisted of wedges and vousoirs, "whatever is said of the parts of a [vousoir] arch, must equally apply to the vault and dome" (López, 2006, pg. 1967). In other words, the wedges support one another

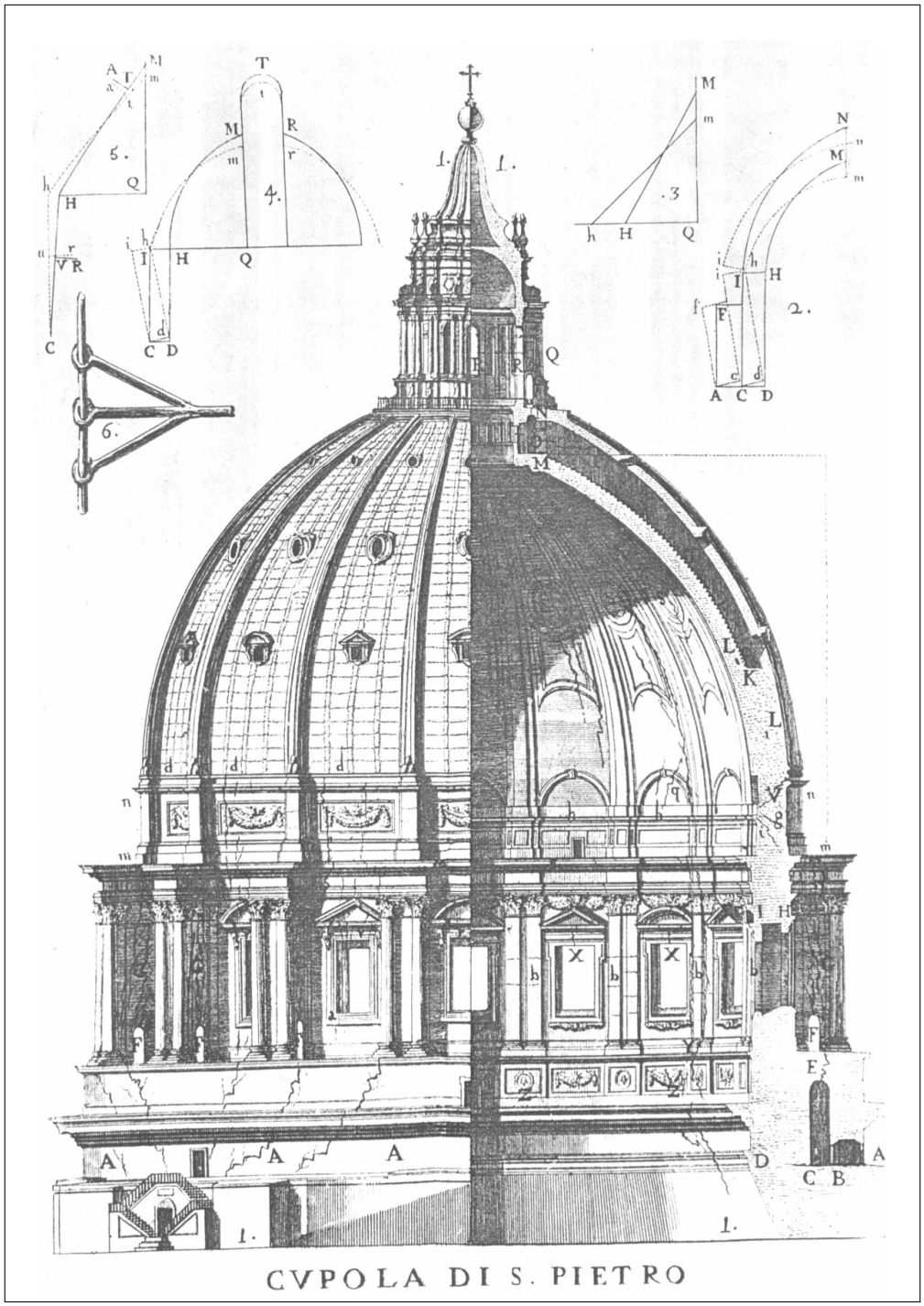

Figure 2.31: Cracked section and structural analysis of the dome of Saint Peter's, (Poleni, 1748) (Adapted by (López, 2006))

preventing a collapse due to gravity.

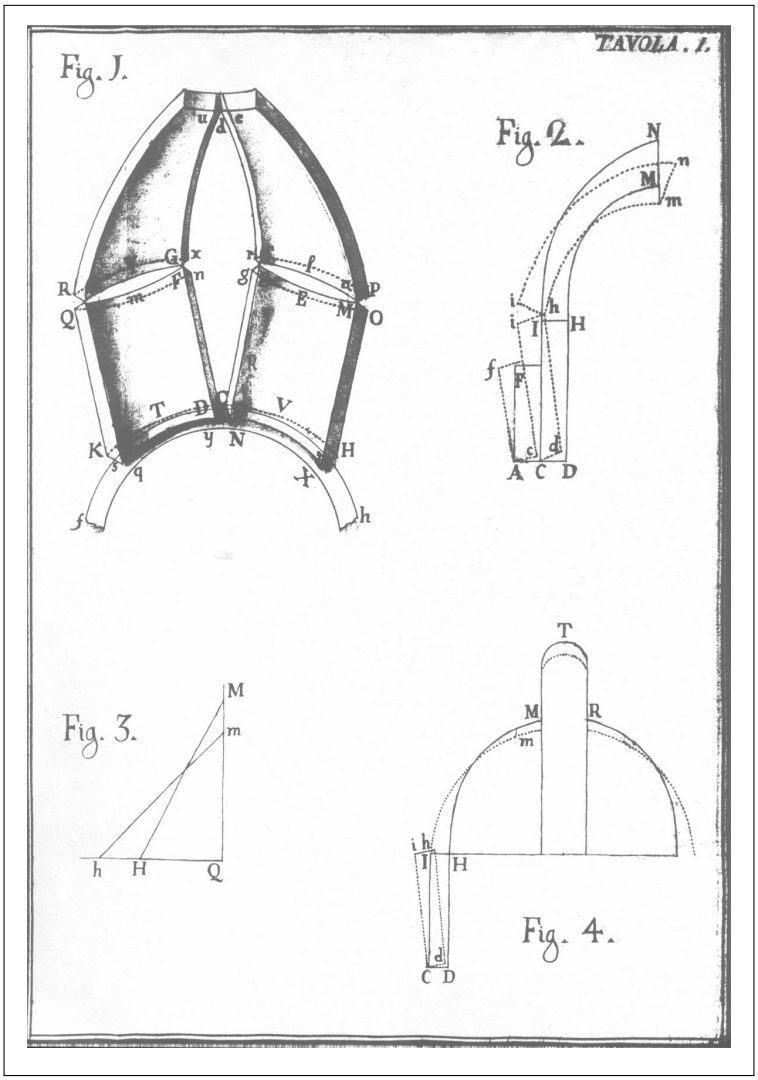

Figure 2.32: Poleni's analysis model, (Poleni, 1748) (Adapted by (López, 2006))

Poleni first referenced Coulomb and his work with the distribution of thrust forces. He differentiated the dome's pressure into its horizontal and perpendicular components. As the thrust neared the base, it more closely aligned with the vertical with less outward thrust (Fig 2.33). This realization allowed Poleni to conclude that the gothic dome configuration is better than the semicircle. He attributed this gothic shape of the dome as the main factor for stability. Referencing Stirling and Gregory on the relationship between the catenary and the geometric shape of an arch, Poleni applied Stirling's theory of spheres to the form of the dome (Fig. 2.34).

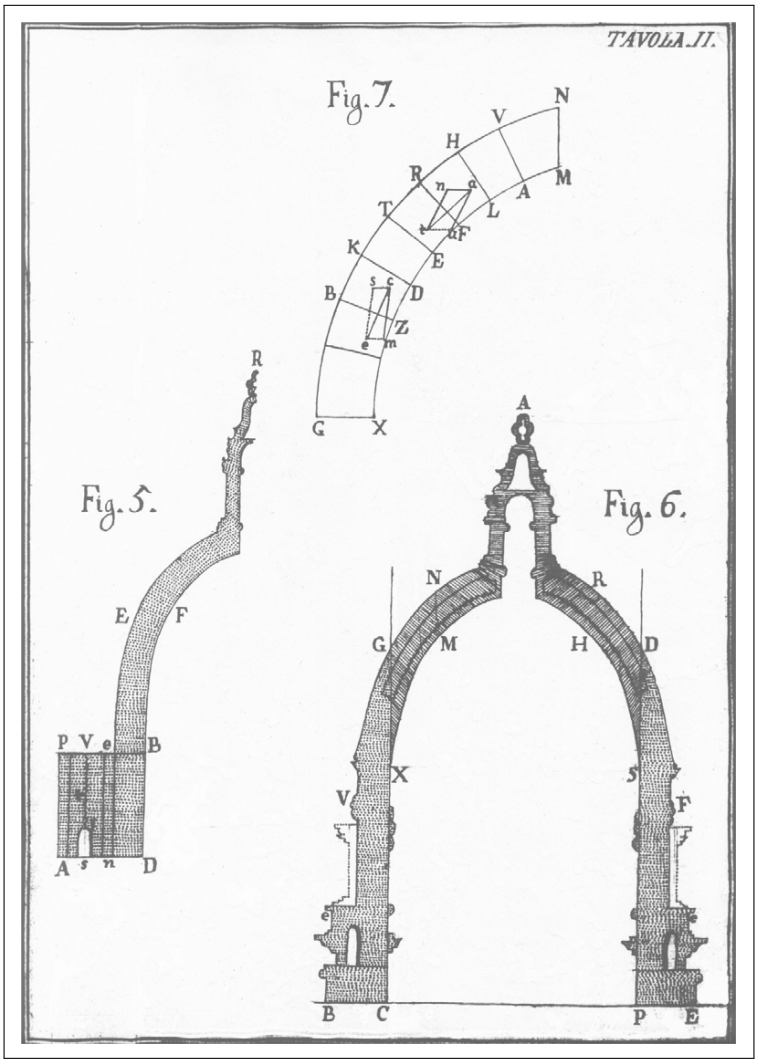

Figure 2.33: Cross sections of the dome of Saint Peter's, (Poleni, 1748) (Adapted by (López, 2006))

For stability, the line of thrust should be contained everywhere within the masonry. He divided the dome into 50 half spherical lunes which were subdivided into 16 wedges. He then selected one 2D arch formed by the lunes for analysis. The position and weight of each wedge was determined in order to accurately interpret the weight and accompanying thrust of the dome. Using weighted balls proportional to the recorded segments, a flexible string was hung confirming the shape of the dome as acceptable (Fig. 2.35) for supporting the weight and thrust of the structure.

Poleni also analyzed the affects of cold, heat, humidity, and drying on the various construction materials, along with the influence of friction and imperfections due to craftmen's work and external forces such as earthquakes.

2.5.4 Recommendations

Poleni attributed the damage seen in the dome to defective building materials and methods, rather than an unstable structure. The vertical cracking of the dome came about from the yielding of the drum resting on main arches due to the immense weight that the latter have to bear when compared to the piers. This was confirmed by the fact that the ribbing, "essential elements of vault" (López, 2006) were in nearly perfect condition. The damage was not viewed as serious due to the lack of horizontal cracks. Poleni recommended restoring the structure to its original state as much as possible. He suggested repairing the cracks, especially in the main arches, by filling the cracks with bronze wedges, specially cut stone, and fine plaster.

The final recommendation was to reinforce the dome with six new iron rings. Though the dome was in no danger of collapsing, Poleni felt it fitting to support against any further damage. Iron rings were to be placed in the drum to reinforce the cylindrical surface. Also two new rings were to be added to the dome in addition to monitoring of the old rings.

2.5.5 Conclusion

Poleni ultimately determined the dome of St. Peter's in Rome to be safe and unsusceptible to collapse. The conclusion came about through detailed static analysis, physical structural inspection and the theory of Hooke's hanging chain. Poleni utilized the dome's thrust components to determine that the stability of the structure was highly dependent on its geometry. He successfully confirmed this hypothesis through use of the weighted hanging chain, finding that the chain remained within the thickness of the entire structural shell. This became the first case that statics and structural mechanics were applied successfully to a real architectural problem.

2.6 Conclusion

In this chapter, we focused on the historical development of the arch and dome theories of analysis along with the structural theory of masonry design. The emphasis was placed on the origination of the theory and how it progressed throughout history to our current methodologies. Though the review was not extensive, it allows for proper insight into multiple examples of pre-emodern era analysis arch and shell analysis.

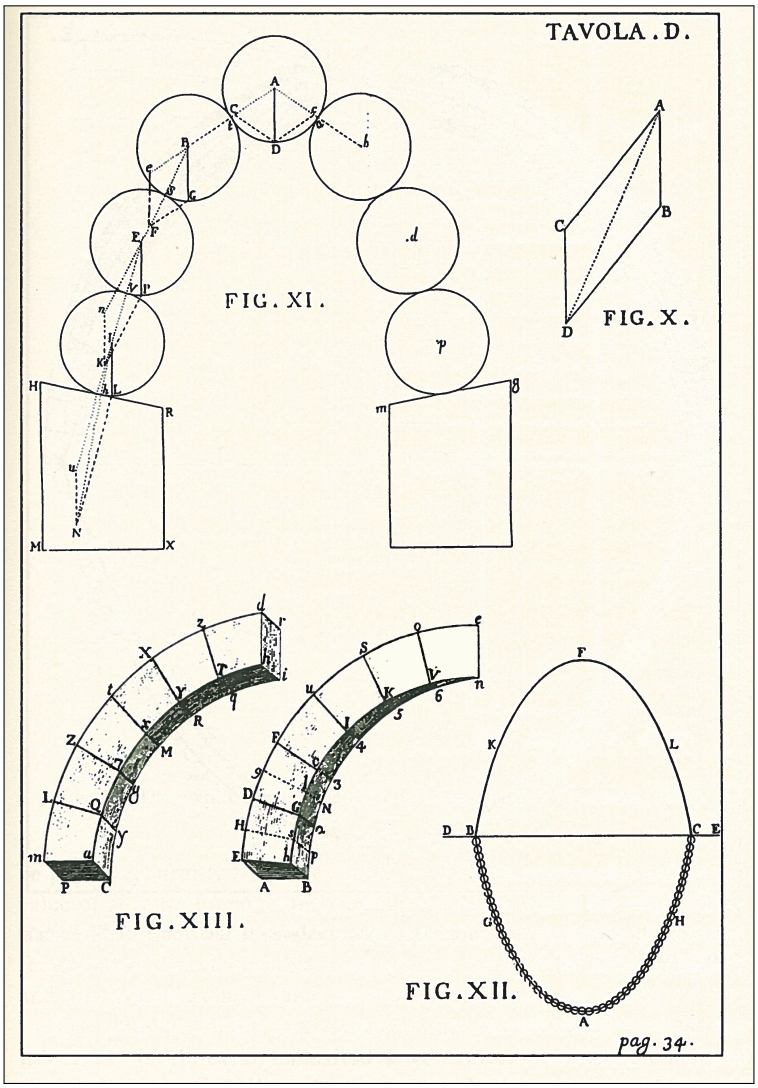

Figure 2.34: Illustrations of the mechanics of masonry arches, (Poleni, 1748) (Adapted by (Heyman, 1998))

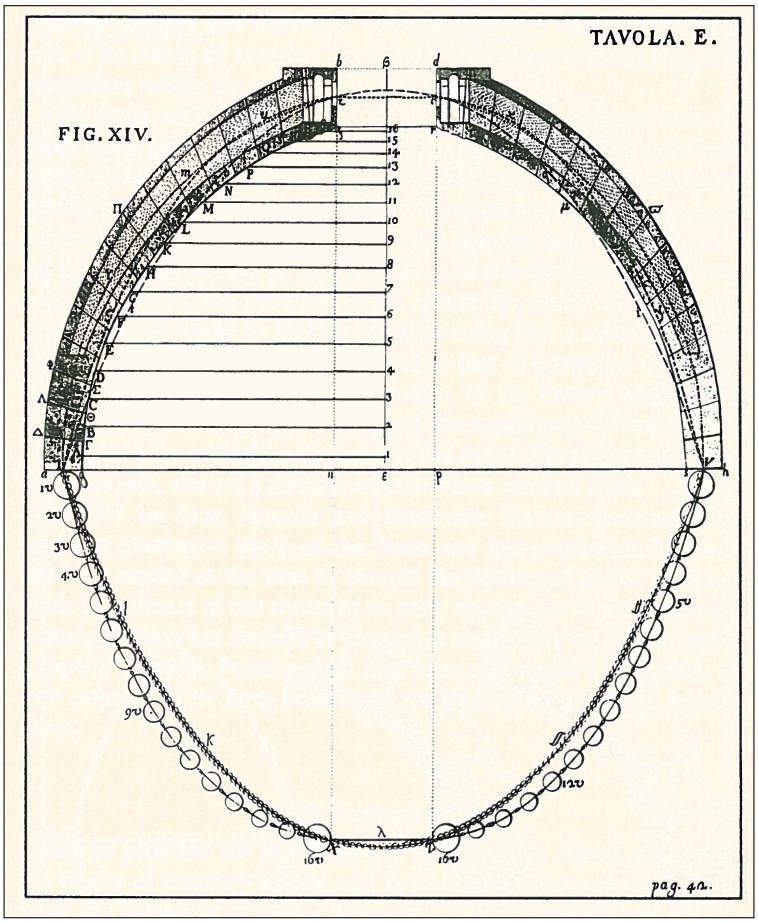

Figure 2.35: The hanging chain applied to the analysis of the dome of St Peter's, (Poleni, 1748)

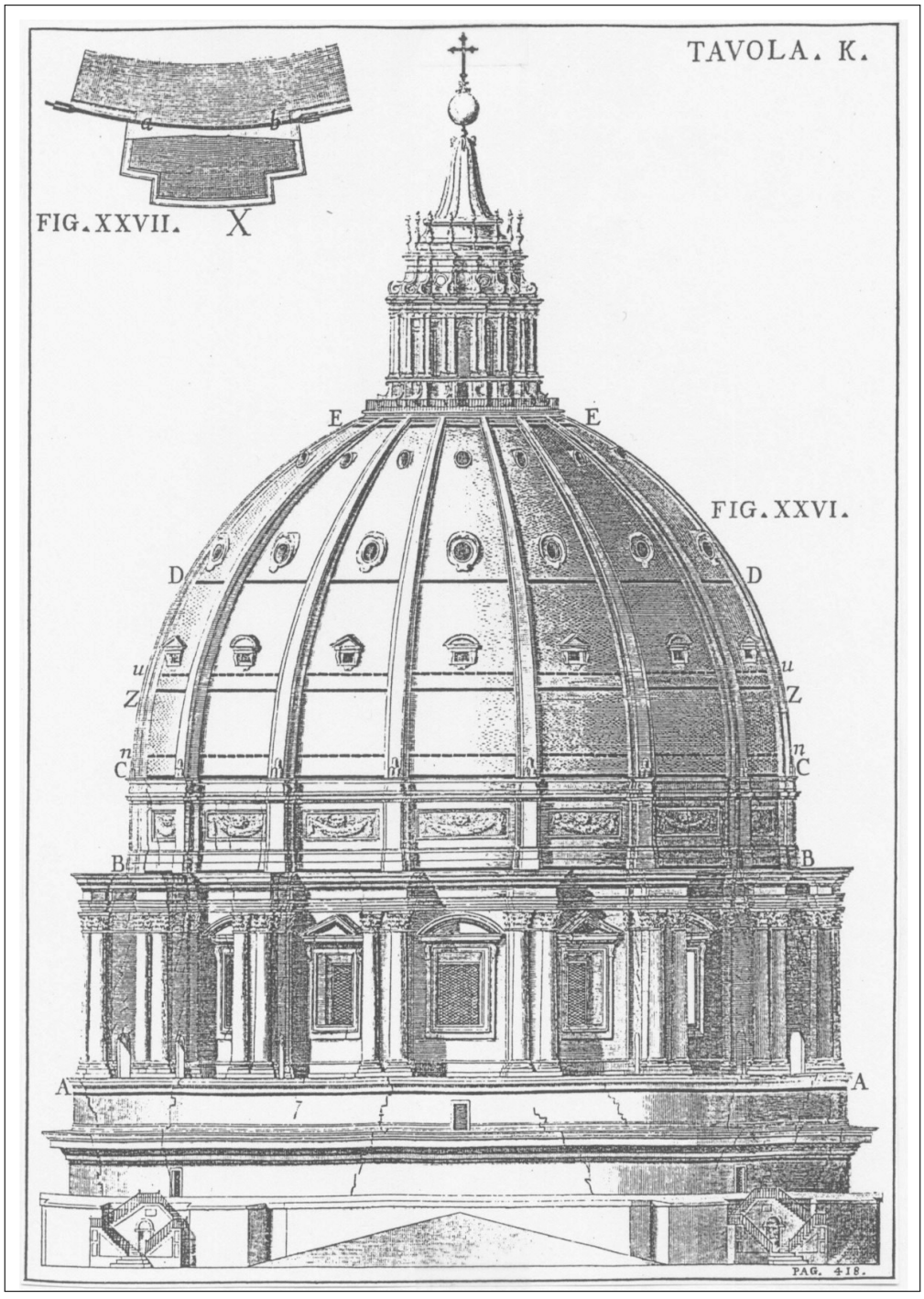

Figure 2.36: The location of the six new rings placed around the dome of Saint Peter's, (Poleni, 1748) (Adapted by (López, 2006))

Chapter 3

Beams, Plates and Shells

3.1 Introduction

The previous chapter focused exclusively on the historical theory of masonry arch and shell design. In hopes of grasping an appreciation for hand calculations, we reviewed the historical analysis of arch and shell design in an age where computers were obsolete. We will now continue with the idea of hand calculations by introducing the derivations of the differential equations of a beam and plate subject to flexure. Before we can continue with the discussion of shells, we must first understand the basics. We will build up from the basic beam, progress to the plate, and finally begin the discussion of thin shells.

Chapter three begins by viewing a beam in flexure and determining the equation of curvature through equilibrium, compatibility and stress-strain relations. After deriving the differential equation governing a beam, we advance to the plate. Once again, we utilize our three fundamental relations of equilibrium, compatibility, and stress-strain to derive the differential equation of a beam in flexure. The section is summed up by the development of table comparing the elasticity and plate theory equations.

The chapter continues with the derivation of the equation for thin shells. Following the previous two methodologies, utilizing our fundamental relations, we develop a set of simultaneous equations with 11 equations and 11 unknowns containing five stress resultants, three stress couples, and three displacements. The section is, once again, summed up in a table displaying the equations for each fundamental relation. The chapter concludes with a discussion of the methodology of the

theory of shallow shells and the membrane theory. The governing assumptions and equations for each theory are derived.

It must be noted that in order for the reader to fully understand the derivations of this chapter, they must understand the figures representative of the equations. All equations and derivations are produced directly from the provided figures found within.

3.2 Beam

3.2.1 Curvature Equation

In order to properly understand the shell theory discussed in the next chapter, we must first understand the derivation of a simple beam subjected to flexural loading. This required deriving the basic curvature equation for a beam in flexure utilizing properties and relations defined through mechanics of materials. Let us consider a segment of a beam (between point 1 and point 2), Fig.

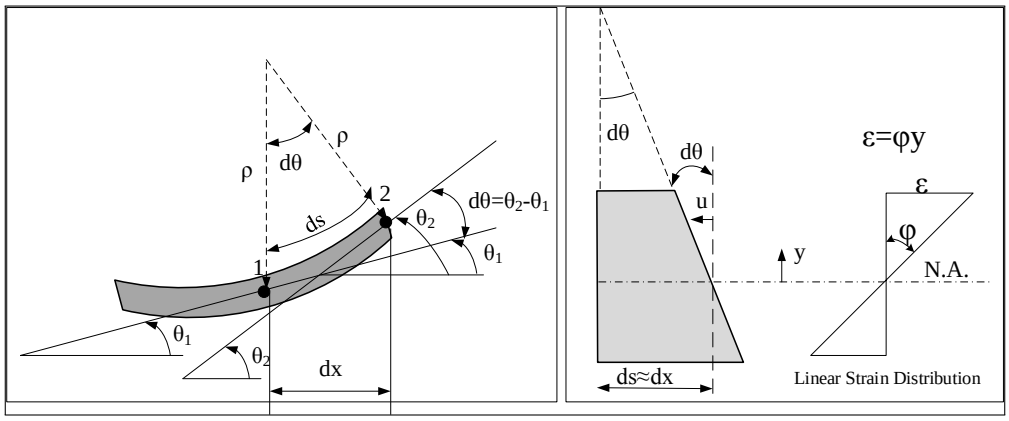

Figure 3.1: Curvature of a Flexural Element

3.1. The slope is denoted by θ, the change in slope per unit length is the curvature ϕ, the radius of curvature is ρ. From mechanics of material we have the following relationship

$$\phi = \frac{1}{\rho} = \frac{d\theta}{dx} \tag{3.1}$$

assuming the flexure only induces a small displacement, $ds \approx dx$ and $\theta = \frac{dy}{dx}$. The approximate equation of curvature, Eq. 3.1, can be rewritten as

$$\phi = \frac{1}{\rho} = \frac{d\theta}{dx} = \frac{d^2y}{dx^2} \tag{3.2}$$

Next, we shall derive the exact expression for the curvature. From Fig. 3.1, we have

$$\tan\theta = \frac{dy}{dx} \tag{3.3}$$

Defining t as

$$t = \frac{dy}{dx} \tag{3.4}$$

and combining with Eq. 3.3 we obtain

$$\theta = \tan^{-1} t \tag{3.5}$$

Applying the chain rule to $\phi = \frac{d\theta}{ds}$ we have

$$\phi = \frac{d\theta}{dt}\frac{dt}{ds} \tag{3.6}$$

ds can be rewritten as

$$\left.\begin{array}{rcl} ds &=& \sqrt{dx^2 + dy^2} \\ &=& \sqrt{1 + \left(\frac{dy}{dx}\right)^2}dx \\ t &=& \frac{dy}{dx} \end{array}\right\} ds = \sqrt{1+t^2}dx \tag{3.7}$$

Next combining Eq. 3.6 and 3.7 we obtain

$$\left.\begin{array}{rcl} \phi &=& \frac{d\theta}{dt}\frac{dt}{\sqrt{1+t^2}dx} \\ \theta &=& \tan^{-1} t \\ \frac{d\theta}{dt} &=& \frac{1}{1+t^2} \end{array}\right\} \quad \left.\begin{array}{rcl} \phi &=& \frac{1}{1+t^2}\frac{1}{\sqrt{1+t^2}}\frac{dt}{dx} \\ \frac{dt}{dx} &=& \frac{d^2y}{dx^2} \end{array}\right\} \phi = \frac{\frac{d^2y}{dx^2}}{\left[1 + \left(\frac{dy}{dx}\right)^2\right]^{\frac{3}{2}}} \tag{3.8}$$

Thus the slope θ, curvature ϕ, radius of curvature ρ are related to the y displacement at a point x along a flexural member by

$$\phi = \frac{1}{\rho} = \frac{\frac{d^2y}{dx^2}}{\left[1 + \left(\frac{dy}{dx}\right)^2\right]^{\frac{3}{2}}} \tag{3.9}$$

If the displacements are very small, we will have $\frac{dy}{dx} << 1$, thus Eq. 3.9 reduces to

$$\phi = \frac{d^2y}{dx^2} = \frac{1}{\rho} \tag{3.10}$$

3.2.2 Differential Equation of the Elastic Curve

We will next derive the basic curvature equation for a beam in flexure utilizing the differential equation of the elastic curve. Referencing Figure 3.1, a positive $d\theta$ at the upper fibers will cause a differential shortening represented by du.

$$du = -yd\theta \tag{3.11}$$

Dividing both sides by dx,

$$\underbrace{\frac{du}{dx}}_{\varepsilon} = -y\frac{d\theta}{dx} \tag{3.12}$$

Combining this with Eq. 3.2, we derive the fundamental relationship between curvature (ϕ), elastic curve (i.e. displacement) (y), and linear strain (ε).

$$\frac{1}{\rho} = \phi = -\frac{\varepsilon}{y} \tag{3.13}$$

Note that so far we have made no assumptions about the material properties (i.e. it can be elastic or inelastic). However, we will focus solely on the elastic case:

$$\left.\begin{array}{rcl} \varepsilon & = & \frac{\sigma}{E} \\ \sigma & = & -\frac{My}{I} \end{array}\right\} \varepsilon = -\frac{My}{EI} \tag{3.14}$$

Combining Eq. 3.14 with Eq. 3.13 yields

$$\phi = \frac{1}{\rho} = \frac{d\theta}{dx} = \frac{d^2y}{dx^2} = \frac{M}{EI} \tag{3.15}$$

This is the fundamental differential equation governing for beams.

3.3 Plates (Adapted from Pilkey & Wunderlich)

Building off the basis of beam flexure, Sec. 3.2, we will next discuss the transverse deformation of plates. The approach followed will be consistent with the finite element formulation, Fig. 3.2.

3.3.1 Fundamental Relations

3.3.1.1 Equilibrium

Consider an arbitrary plate element with the given stresses, Fig.3.3.

The resultants, per unit width, are given by

$$
\begin{aligned}
\text{Membrane Force} \quad \mathbf{N} &= \int_{-\frac{t}{2}}^{\frac{t}{2}} \boldsymbol{\sigma} \mathrm{d}z \quad \begin{cases} N_{xx} &= \int_{-\frac{t}{2}}^{\frac{t}{2}} \sigma_{xx} \mathrm{d}z \\ N_{yy} &= \int_{-\frac{t}{2}}^{\frac{t}{2}} \sigma_{yy} \mathrm{d}z \\ N_{xy} &= \int_{-\frac{t}{2}}^{\frac{t}{2}} \sigma_{xy} \mathrm{d}z \end{cases} \\
\text{Bending Moments} \quad \mathbf{M} &= \int_{-\frac{t}{2}}^{\frac{t}{2}} \boldsymbol{\sigma} z \mathrm{d}z \quad \begin{cases} M_{xx} &= \int_{-\frac{t}{2}}^{\frac{t}{2}} \sigma_{xx} z \mathrm{d}z \\ M_{yy} &= \int_{-\frac{t}{2}}^{\frac{t}{2}} \sigma_{yy} z \mathrm{d}z \\ M_{xy} &= \int_{-\frac{t}{2}}^{\frac{t}{2}} \sigma_{xy} z \mathrm{d}z \end{cases} \\
\text{Transverse Shear Forces} \quad \mathbf{V} &= \int_{-\frac{t}{2}}^{\frac{t}{2}} \boldsymbol{\tau} \mathrm{d}z \quad \begin{cases} V_x &= \int_{-\frac{t}{2}}^{\frac{t}{2}} \tau_{xz} \mathrm{d}z \\ V_y &= \int_{-\frac{t}{2}}^{\frac{t}{2}} \tau_{yz} \mathrm{d}z \end{cases}
\end{aligned}
\tag{3.16-a}
$$

Note that in plate theory, we ignore the effect of the membrane forces. Those in turn will be accounted for in shells.

The equation of equilibrium is derived by considering an infinitesimal element $tdxdy$ subjected to an applied transverse load p_z. We would have to consider three equations of equilibrium, Fig. 3.4:

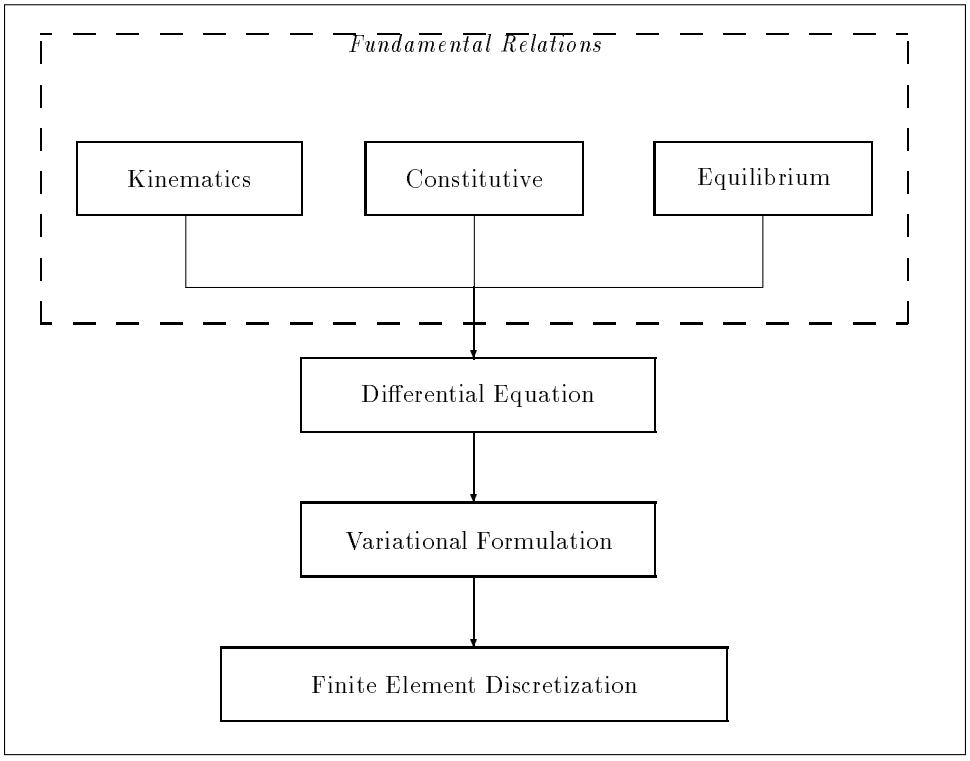

Figure 3.2: Finite Element Formulation

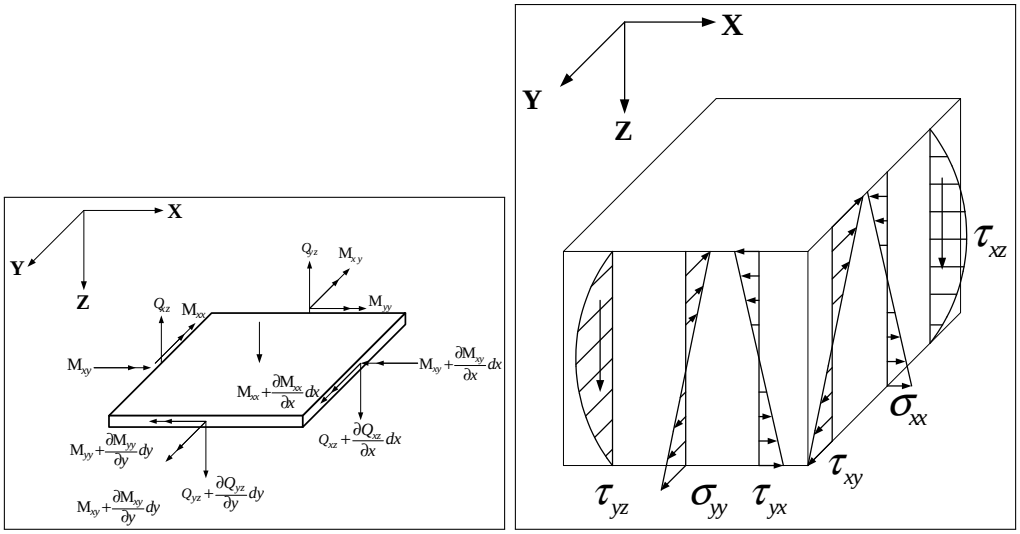

Figure 3.3: Stresses in a Plate

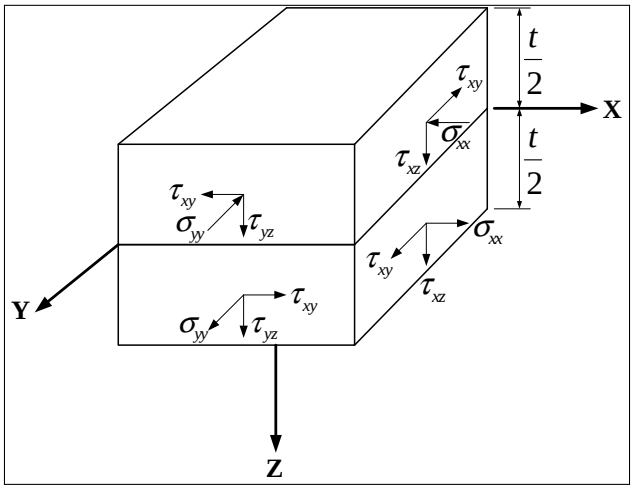

Figure 3.4: Free Body Diagram of an Infinitesimal Plate Element

Summation of Forces in the z direction

$$\frac{\partial V_x}{\partial x}\mathrm{d}x\mathrm{d}y + \frac{\partial V_y}{\partial y}\mathrm{d}x\mathrm{d}y + p_z\mathrm{d}x\mathrm{d}y = 0 \tag{3.17}$$

or

$$\frac{\partial V_x}{\partial x} + \frac{\partial V_y}{\partial y} + p_z = 0 \tag{3.18}$$

Summation of Moments about the x axis

$$\frac{\partial M_{xy}}{\partial x}\mathrm{d}x\mathrm{d}y + \frac{\partial M_{yy}}{\partial y}\mathrm{d}x\mathrm{d}y - V_y\mathrm{d}x\mathrm{d}y = 0 \tag{3.19}$$

or

$$\frac{\partial M_{xy}}{\partial x} + \frac{\partial M_{yy}}{\partial y} - V_y = 0 \tag{3.20}$$

Summation of Moments about the y axis

$$\frac{\partial M_{yx}}{\partial y} + \frac{\partial M_{xx}}{\partial x} - V_x = 0 \tag{3.21}$$

Since $M_{xy} = M_{yx}$, those equations can be expressed in matrix form as

$$\underbrace{\left[\begin{array}{ccc|cc} \frac{\partial}{\partial x} & 0 & \frac{\partial}{\partial y} & -1 & 0 \\ 0 & \frac{\partial}{\partial y} & \frac{\partial}{\partial x} & 0 & -1 \\ 0 & 0 & 0 & \frac{\partial}{\partial x} & \frac{\partial}{\partial y} \end{array}\right]}_{\mathbf{L}^T} \underbrace{\left\{\begin{array}{c} M_{xx} \\ M_{yy} \\ M_{xy} \\ \hline V_x \\ V_y \end{array}\right\}}_{\mathbf{M}} + \left\{\begin{array}{c} 0 \\ 0 \\ p_z \end{array}\right\} = \left\{\begin{array}{c} 0 \\ 0 \\ 0 \end{array}\right\} \tag{3.22}$$

Note that the left matrix corresponds to L^T where the 1 term has been substituted by -1

3.3.1.2 Kinematic Relations

From Fig. 3.5 we have five displacements u, v, w, θ_{xx} and θ_{yy}. However, two of the three displacements, u, v can be expressed in terms of the θ_{xx} and θ_{yy} which are the rotations of the plate

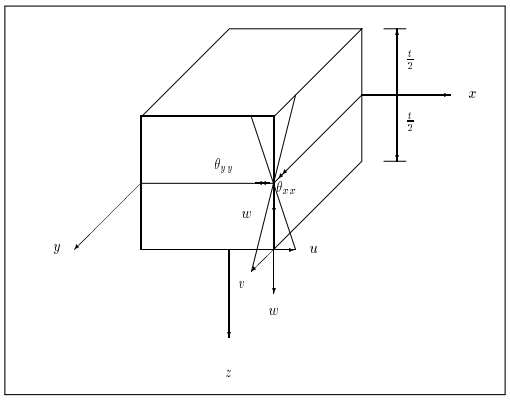

Figure 3.5: Displacements in a Plate

middle surface, with the third displacement being the transverse one w. We will use a notation consistent with the traditional one adopted for plate bending, rather than one consistent with the coordinate directions as used in finite element. Since we are focusing on thin plates, the middle surface will be assumed to remain without strain, and the plane sections remain plane. Based on

the plane section remaining plane assumption, we have,

$$\begin{Bmatrix} u \\ v \\ w \end{Bmatrix} = \begin{bmatrix} z & 0 & 0 \\ 0 & z & 0 \\ 0 & 0 & 1 \end{bmatrix} \begin{Bmatrix} \theta_{xx} \\ \theta_{yy} \\ w \end{Bmatrix} \tag{3.23}$$

However, from mechanics of material, we know the relation $\epsilon = Lu$ or

$$\underbrace{\begin{Bmatrix} \varepsilon_{xx} \\ \varepsilon_{yy} \\ \varepsilon_{zz} \\ \gamma_{xy} \\ \gamma_{xz} \\ \gamma_{yz} \end{Bmatrix}}_{\boldsymbol{\varepsilon}} = \underbrace{\begin{bmatrix} \frac{\partial}{\partial x} & 0 & 0 \\ 0 & \frac{\partial}{\partial y} & 0 \\ 0 & 0 & \frac{\partial}{\partial z} \\ \frac{\partial}{\partial y} & \frac{\partial}{\partial x} & 0 \\ \frac{\partial}{\partial z} & 0 & \frac{\partial}{\partial x} \\ 0 & \frac{\partial}{\partial z} & \frac{\partial}{\partial y} \end{bmatrix}}_{\mathbf{L}} \underbrace{\begin{Bmatrix} u \\ v \\ w \end{Bmatrix}}_{\mathbf{u}} \tag{3.24}$$

Since w corresponds to the transverse deflection of the middle surface, and does not vary with z, then $\varepsilon_{zz} = 0$. Substituting Eq. 3.23, we obtain

$$\left\{\begin{array}{c} \varepsilon_{xx} \\ \varepsilon_{yy} \\ \varepsilon_{zz} \\ \hline \gamma_{xy} \\ \hline \gamma_{xz} \\ \gamma_{yz} \end{array}\right\} = \left\{\begin{array}{c} z\theta_{xx,x} \\ z\theta_{yy,y} \\ 0 \\ \hline z(\theta_{xx,y} + \theta_{yy,x}) \\ \hline (\theta_{xx} + w_{,x}) \\ (\theta_{yy} + w_{,y}) \end{array}\right\} = \left\{\begin{array}{c} z\kappa_{xx} \\ z\kappa_{yy} \\ 0 \\ \hline 2z\kappa_{xy} \\ \hline \gamma_{xz} \\ \gamma_{yz} \end{array}\right\} \tag{3.25}$$

Note that this equation assumes that the displacement w is small compared to the thickness of the plate, and the rotation is small. Because the rotation is small, its square is negligible with respect to unity, and hence the curvature

$$\kappa = \frac{\frac{\partial \theta}{\partial x}}{(1+\theta^2)^{3/2}} \approx \frac{\partial \theta}{\partial x} \tag{3.26}$$

is equal to the rate of change of rotation. Hence, the kinematic relation for the transverse displacement of a plate is

$$\underbrace{\left\{\begin{array}{c}\kappa_{xx}\\ \kappa_{yy}\\ \hline 2\kappa_{xy}\\ \hline \gamma_{xz}\\ \gamma_{yz}\end{array}\right\}}_{\boldsymbol{\kappa}} = \underbrace{\left[\begin{array}{ccc}\frac{\partial}{\partial x} & 0 & 0\\ 0 & \frac{\partial}{\partial y} & 0\\ \hline \frac{\partial}{\partial y} & \frac{\partial}{\partial x} & 0\\ \hline 1 & 0 & \frac{\partial}{\partial x}\\ 0 & 1 & \frac{\partial}{\partial y}\end{array}\right]}_{\mathbf{L}} \underbrace{\left\{\begin{array}{c}\theta_{xx}\\ \theta_{yy}\\ \hline w\end{array}\right\}}_{\mathbf{u}} \tag{3.27}$$

3.3.1.3 Constitutive Relations

For three dimensional continuum, the strain-stress relation is

$$\left\{\begin{array}{c}\varepsilon_{xx}\\ \varepsilon_{yy}\\ \varepsilon_{zz}\\ \hline \gamma_{xy}\\ \gamma_{xz}\\ \gamma_{yz}\end{array}\right\} = \frac{1}{E}\left[\begin{array}{ccc|ccc}1 & -\nu & -\nu & & & \\ -\nu & 1 & -\nu & & \mathbf{0} & \\ -\nu & -\nu & 1 & & & \\ \hline & & & 2(1+\nu) & 0 & 0\\ & \mathbf{0} & & 0 & 2(1+\nu) & 0\\ & & & 0 & 0 & 2(1+\nu)\end{array}\right]\left\{\begin{array}{c}\sigma_{xx}\\ \sigma_{yy}\\ \sigma_{zz}\\ \hline \tau_{xy}\\ \tau_{xz}\\ \tau_{yz}\end{array}\right\} \tag{3.28}$$

However from Eq. 3.25, $\varepsilon_{zz} = 0$. Therefore we can neglect σ_{zz} which is much smaller than the other stresses. Inverting the previous equation yields

$$\underbrace{\left\{\begin{array}{c}\sigma_{xx}\\ \sigma_{yy}\\ \tau_{xy}\\ \hline \tau_{xz}\\ \tau_{yz}\end{array}\right\}}_{\boldsymbol{\sigma}} = \underbrace{\frac{E}{1-\nu^2}\left[\begin{array}{ccc|cc}1 & \nu & 0 & & \\ \nu & 1 & 0 & \multicolumn{2}{c}{\mathbf{0}}\\ 0 & 0 & \frac{1-\nu}{2} & & \\ \hline & & & \frac{1-\nu}{2} & 0\\ \multicolumn{3}{c|}{\mathbf{0}} & 0 & \frac{1-\nu}{2}\end{array}\right]}_{\mathbf{D}}\underbrace{\left\{\begin{array}{c}\varepsilon_{xx}\\ \varepsilon_{yy}\\ \gamma_{xy}\\ \hline \gamma_{xz}\\ \gamma_{yz}\end{array}\right\}}_{\boldsymbol{\varepsilon}} \tag{3.29}$$

Note that the shear modulus is $\mu = \frac{E}{2(1+\nu)}$.

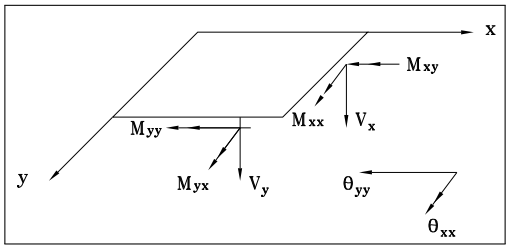

Figure 3.6: Positive Moments and Rotations

We now seek to write the moments in terms of the curvatures, Fig. 3.6. Introducing the stresses from Eq. 3.29 into Eq. 3.16-a, and using Eq. 3.25 we derive the first term

$$\begin{aligned} M_{xx} &= \int_{-\frac{t}{2}}^{\frac{t}{2}} \sigma_{xx} z \mathrm{d}z = \int_{-\frac{t}{2}}^{\frac{t}{2}} \frac{E}{1-\nu^2}(\varepsilon_{xx} + \nu\varepsilon_{yy}) z \mathrm{d}z = \int_{-\frac{t}{2}}^{\frac{t}{2}} \frac{E}{1-\nu^2}(z\kappa_{xx} + \nu z\kappa_{yy}) z \mathrm{d}z \\ &= \frac{E}{1-\nu^2}(\kappa_{xx} + \nu\kappa_{yy}) \int_{-\frac{t}{2}}^{\frac{t}{2}} z^2 \mathrm{d}z = \frac{Et^3}{12(1-\nu^2)}(\kappa_{xx} + \nu\kappa_{yy}) \end{aligned} \tag{3.30-a}$$

Following a similar procedure for the other two terms, we obtain the following moment-curvature relation

$$\underbrace{\begin{Bmatrix} M_{xx} \\ M_{yy} \\ M_{xy} \end{Bmatrix}}_{\mathbf{M}} = \underbrace{\frac{Et^3}{12(1-\nu^2)} \begin{bmatrix} 1 & \nu & 0 \\ \nu & 1 & 0 \\ 0 & 0 & \frac{1-\nu}{2} \end{bmatrix}}_{\mathbf{D}} \underbrace{\begin{Bmatrix} \kappa_{xx} \\ \kappa_{yy} \\ 2\kappa_{xy} \end{Bmatrix}}_{\boldsymbol{\kappa}} \tag{3.31}$$

The $\frac{Et^3}{12(1-\nu^2)}$ term is referred to as the flexural rigidity and is analogous to the flexural stiffness EI of a beam (if the plate has unit width, and $\nu = 0$, then $EI = Et^3/12$).

3.3.2 Plate Theories: Kirchhoff

In the following section the derived equations from our fundamental relations will be applied to the plate theory of Kirchhoff. This theory, is primarily applicable to thin plates in which shear deformations can be neglected as assumed previously. This formulation is analogous to the conventional Euler-Bernoulli beam theory.

3.3.2.1 Fundamental Relations

Kinematic Relations : Since shear deformations are neglected, $\gamma_{xz} = \gamma_{yz} = 0$ and thus the last two relation of Eq. 3.25 reduce to

$$\theta_{xx} = -w_{,x} \quad \text{and} \quad \theta_{yy} = -w_{,y} \tag{3.32}$$

and the first three strains become

$$\epsilon_{xx} = -z\frac{\partial^2 w}{\partial x^2}; \qquad \epsilon_{yy} = -z\frac{\partial^2 w}{\partial y^2}; \qquad \gamma_{xy} = -2z\frac{\partial^2 w}{\partial x \partial y}; \tag{3.33}$$

or

$$\underbrace{\begin{Bmatrix} \kappa_{xx} \\ \kappa_{yy} \\ 2\kappa_{xy} \end{Bmatrix}}_{\boldsymbol{\kappa}} = \underbrace{\begin{Bmatrix} -\frac{\partial^2}{\partial x^2} \\ -\frac{\partial^2}{\partial y^2} \\ -2\frac{\partial}{\partial x}\frac{\partial}{\partial y} \end{Bmatrix}}_{\mathbf{L}} \underbrace{\begin{Bmatrix} w \end{Bmatrix}}_{\mathbf{u}} \tag{3.34}$$

Constitutive Relation : The constitutive relation of Eq. 3.31 still applies

$$\underbrace{\begin{Bmatrix} M_{xx} \\ M_{yy} \\ M_{xy} \end{Bmatrix}}_{\mathbf{M}} = \underbrace{\frac{Et^3}{12(1-\nu^2)} \begin{bmatrix} 1 & \nu & 0 \\ \nu & 1 & 0 \\ 0 & 0 & \frac{1-\nu}{2} \end{bmatrix}}_{\mathbf{D}} \underbrace{\begin{Bmatrix} \kappa_{xx} \\ \kappa_{yy} \\ 2\kappa_{xy} \end{Bmatrix}}_{\boldsymbol{\kappa}} \tag{3.35}$$

Equilibrium : The equilibrium equation, as expressed by Eq. 3.22 is also still valid. If we were to substitute the second and third relations into the first one, we would obtain the following equilibrium relation in terms of the moments

$$\frac{\partial^2 M_{xx}}{\partial x^2} + 2\frac{\partial^2 M_{xy}}{\partial x \partial y} + \frac{\partial^2 M_{yy}}{\partial y^2} + p_z = 0 \tag{3.36}$$

(Note the similarity with the corresponding equations for beam flexure $\frac{d^2M}{\mathrm{d}x^2} - V_x = 0$)

3.3.2.2 Differential Equation

If we combine the kinematic and constitutive relation equations, 3.34 and 3.35, we obtain

$$\left\{ \begin{array}{c} M_{xx} \\ M_{yy} \\ M_{xy} \end{array} \right\} = -\frac{Et^3}{12(1-\nu^2)} \left[\begin{array}{c} \frac{\partial^2}{\partial x^2} + \nu \frac{\partial^2}{\partial y^2} \\ \frac{\partial^2}{\partial y^2} + \nu \frac{\partial^2}{\partial x^2} \\ (1-\nu) \frac{\partial}{\partial x} \frac{\partial}{\partial y} \end{array} \right] \left\{ \begin{array}{c} w \end{array} \right\} \tag{3.37}$$

Finally, we substitute the equilibrium equation, 3.36, into the previous one,

$$\frac{\partial^4 w}{\partial x^4} + 2\frac{\partial^4 w}{\partial x^2 \partial y^2} + \frac{\partial^4 w}{\partial y^4} = \frac{p_z}{\frac{Et^3}{12(1-\nu^2)}} \tag{3.38}$$

or

$$\nabla^4 w = \frac{p_z}{\frac{Et^3}{12(1-\nu^2)}} \tag{3.39}$$

Note the similarity with the corresponding equation for beams

$$\frac{\partial^2}{\partial x^2} EI \frac{\partial^2 w}{\partial x^2} = p_z \quad \text{or} \quad \frac{\partial^4}{\partial x^4} = \frac{p_z}{EI} \tag{3.40}$$

3.3.2.3 Stresses

Combining the stress-strain relation of Eq. 3.29, with Eq. 3.33, and 3.37, the stresses can be expressed in terms of the moments

$$\sigma_{xx} = \frac{M_{xx}}{\frac{t^3}{12}} z; \qquad \sigma_{yy} = \frac{M_{yy}}{\frac{t^3}{12}} z; \qquad \tau_{xy} = \frac{M_{xy}}{\frac{t^3}{12}} z \tag{3.41}$$

Again we note the analogy with the flexural stress expression in beams $\sigma = \frac{My}{I}$. Using the three dimensional equilibrium equation:

$$\begin{aligned} \frac{\partial \sigma_{xx}}{\partial x} + \frac{\partial \tau_{xy}}{\partial y} + \frac{\partial \tau_{xz}}{\partial z} &= 0 \\ \frac{\partial \tau_{yx}}{\partial x} + \frac{\partial \sigma_{yy}}{\partial y} + \frac{\partial \tau_{yz}}{\partial z} &= 0 \\ \frac{\partial \tau_{zx}}{\partial x} + \frac{\partial \tau_{zy}}{\partial y} + \frac{\partial \sigma_{zz}}{\partial z} &= 0 \end{aligned} \tag{3.42-a}$$

integrating the first equation yields

$$\begin{aligned}\tau_{xz} &= -\int_{t/2}^{z}\left(\frac{\partial\sigma_{xx}}{\partial x}+\frac{\partial\tau_{xy}}{\partial y}\right)\mathrm{d}z = \int_{z}^{t/2}\frac{12z}{t^3}\left(\frac{\partial M_{xx}}{\partial x}+\frac{\partial M_{xy}}{\partial y}\right)\mathrm{d}z \\ &= \frac{12}{t^3}\int_{z}^{t/2} zV_x\mathrm{d}z \end{aligned} \tag{3.43-a}$$

Finally

$$\tau_{xz}=\frac{3V_x}{2t}\left[1-\left(\frac{2z}{t}\right)^2\right] \quad \text{and} \quad \tau_{yz}=\frac{3V_y}{2t}\left[1-\left(\frac{2z}{t}\right)^2\right] \tag{3.44}$$

Thus, the shear stress distribution across the plate thickness is parabolic (though they tend to be very small compared to τ_{xy}) and the peak shear stresses occur at the middle surface ($z=0$) where

$$\tau_{xz}|_{max}=\frac{3}{2}\frac{V_x}{t} \quad \text{and} \quad \tau_{yz}|_{max}=\frac{3}{2}\frac{V_y}{t} \tag{3.45}$$

Finally, it can be shown that σ_{zz} varies cubically.

3.3.2.4 Variational Formulation

Prior to the finite element discretization, we seek to obtain from the previously derived relations a variational formulation of the problem. The internal virtual work is given by

$$\delta W_i=-\int_A \delta\epsilon^T\sigma\mathrm{d}A=-\int_A \delta\kappa^T M\mathrm{d}A \tag{3.46}$$

where $M=D\kappa$ is obtained from Eq. 3.35, and $\kappa=Lu$ is obtained from Eq. 3.34. Accounting for the external virtual work, we obtain

$$\delta W=\delta W_i+\delta W_e=\underbrace{-\int_A \delta u^T(L^TDL)u\mathrm{d}A}+\underbrace{\int_A \delta u^T p_v\mathrm{d}A+\int_{\Gamma_p} u^T p\mathrm{d}\Gamma}=0 \tag{3.47}$$

where p_v contains the applied transverse loading p_z, and p the edge loading p_s. Substituting for the L^TDL terms (Eq. 3.34) we obtain

$$\begin{aligned} K^e &= L^TDL=\lfloor\ -\tfrac{\partial^2}{\partial x^2}\quad -\tfrac{\partial^2}{\partial y^2}\quad -2\tfrac{\partial}{\partial x}\tfrac{\partial}{\partial y}\ \rfloor\frac{Et^3}{12(1-\nu^2)}\begin{bmatrix}1&\nu&0\\ \nu&1&0\\ 0&0&\frac{1-\nu}{2}\end{bmatrix}\begin{Bmatrix}-\frac{\partial^2}{\partial x^2}\\ -\frac{\partial^2}{\partial y^2}\\ -2\frac{\partial}{\partial x}\frac{\partial}{\partial y}\end{Bmatrix} \\ &= K \\ &\quad \left[\frac{\partial^2}{\partial x^2}\left(\frac{\partial^2}{\partial x^2}+\nu\frac{\partial^2}{\partial y^2}\right)+2(1-\nu)\frac{\partial}{\partial x}\frac{\partial}{\partial y}\left(\frac{\partial}{\partial x}\frac{\partial}{\partial y}\right)+\frac{\partial^2}{\partial y^2}\left(\frac{\partial^2}{\partial y^2}+\nu\frac{\partial^2}{\partial x^2}\right)\right] \end{aligned} \tag{3.48-a}$$

Finally, noting that $u = w$, the virtual work becomes

$$\delta W_e = -K \int_A \delta w \left(L w p_z\right) \mathrm{d}A + \int_{\Gamma_p} \delta w p_s \mathrm{d}\Gamma = 0 \tag{3.49}$$

where $K = Et^3/12(1-\nu^2)$.

3.3.3 Summary

Table 3.1 summarizes some of the major equations governing plate bending, and contrasts them with the equivalent elasticity ones. Now that we have fully reviewed the derivation of the beam and plate subjected to flexure, we can increase the difficulty one step farther and begin the discussion of thin shells.

3.4 Thin Shell Theory

As discussed previously in Sec. 2.4.3, a thin shell is a curved surface or plate whose thickness is small compared to the dimensions and radii of curvature, r_x and r_y, of the shelled structure. This section will focus on the derivation of the differential equation of thin shells. This will be achieved by first establishing equilibrium of a differential element cut from the shell, and next by ensuring that each element remains continuous with the element adjacent after deformation, through achieving strain compatibility.

3.4.1 Definitions and Assumptions

3.4.1.1 Definitions

Before we begin, a few terms must be defined to allow for clarity of the subject. The stress resultants and stress couples are integrated over the shell thickness and are defined as the total forces and moments acting per unit length at the middle surface (the face created by bisecting the thin shell thickness).

In order to properly determine the stress resultants and couples, we will first consider the infinitesimal segment shown in Fig. 3.7 and more particularly the edge along the y axis. From

Elasticity	**Plate Theory** (Kirchhoff)
Kinematic	
$\underbrace{\begin{Bmatrix}\varepsilon_{xx}\\ \varepsilon_{yy}\\ \varepsilon_{zz}\\ \varepsilon_{xy}\\ \varepsilon_{xz}\\ \varepsilon_{yz}\end{Bmatrix}}_{\boldsymbol{\varepsilon}} = \underbrace{\begin{bmatrix}\frac{\partial}{\partial x} & 0 & 0\\ 0 & \frac{\partial}{\partial y} & 0\\ 0 & 0 & \frac{\partial}{\partial z}\\ \frac{\partial}{\partial y} & \frac{\partial}{\partial x} & 0\\ \frac{\partial}{\partial z} & 0 & \frac{\partial}{\partial x}\\ 0 & \frac{\partial}{\partial z} & \frac{\partial}{\partial y}\end{bmatrix}}_{\mathbf{L}} \underbrace{\begin{Bmatrix}u_x\\ u_y\\ u_z\end{Bmatrix}}_{\mathbf{u}}$	$\underbrace{\begin{Bmatrix}\kappa_{xx}\\ \kappa_{yy}\\ 2\kappa_{xy}\end{Bmatrix}}_{\boldsymbol{\kappa}} = \underbrace{\begin{Bmatrix}-\frac{\partial^2}{\partial x^2}\\ -\frac{\partial^2}{\partial y^2}\\ -2\frac{\partial}{\partial x}\frac{\partial}{\partial y}\end{Bmatrix}}_{\mathbf{L}} \underbrace{\{\ w\ \}}_{\mathbf{u}}$
	$\underbrace{\begin{Bmatrix}\kappa_{xx}\\ \kappa_{yy}\\ 2\kappa_{xy}\end{Bmatrix}}_{\boldsymbol{\kappa}} = \underbrace{\begin{bmatrix}\frac{\partial}{\partial x} & 0\\ 0 & \frac{\partial}{\partial y}\\ \frac{\partial}{\partial y} & \frac{\partial}{\partial x}\end{bmatrix}}_{\mathbf{L}_f} \underbrace{\begin{Bmatrix}\theta_{xx}\\ \theta_{yy}\end{Bmatrix}}_{\boldsymbol{\theta}}; \underbrace{\begin{Bmatrix}\gamma_{xz}\\ \gamma_{yz}\end{Bmatrix}}_{\boldsymbol{\gamma}} = \underbrace{\begin{bmatrix}\frac{\partial}{\partial x} & 1 & 0\\ \frac{\partial}{\partial y} & 0 & 1\end{bmatrix}}_{\mathbf{L}_s} \underbrace{\begin{Bmatrix}w\\ \theta_{xx}\\ \theta_{yy}\end{Bmatrix}}_{\mathbf{u}}$
Equilibrium	
$\underbrace{\begin{bmatrix}\frac{\partial}{\partial x} & 0 & 0 & \frac{\partial}{\partial y} & \frac{\partial}{\partial z} & 0\\ 0 & \frac{\partial}{\partial y} & 0 & \frac{\partial}{\partial x} & 0 & \frac{\partial}{\partial z}\\ 0 & 0 & \frac{\partial}{\partial z} & 0 & \frac{\partial}{\partial x} & \frac{\partial}{\partial y}\end{bmatrix}}_{\mathbf{L}^T} \underbrace{\begin{Bmatrix}\sigma_{xx}\\ \sigma_{yy}\\ \sigma_{zz}\\ \sigma_{xy}\\ \sigma_{xz}\\ \sigma_{yz}\end{Bmatrix}}_{\boldsymbol{\sigma}} + \rho \underbrace{\begin{Bmatrix}b_x\\ b_y\\ b_z\end{Bmatrix}}_{\rho\mathbf{b}} = 0$	$\underbrace{\begin{bmatrix}\frac{\partial}{\partial x} & 0 & \frac{\partial}{\partial y} & -1 & 0\\ 0 & \frac{\partial}{\partial y} & \frac{\partial}{\partial x} & 0 & -1\\ 0 & 0 & 0 & \frac{\partial}{\partial x} & \frac{\partial}{\partial y}\end{bmatrix}}_{\mathbf{L}^T} \underbrace{\begin{Bmatrix}M_{xx}\\ M_{yy}\\ M_{xy}\\ V_x\\ V_y\end{Bmatrix}}_{\mathbf{M}} + \begin{Bmatrix}0\\ 0\\ p_z\end{Bmatrix} = \begin{Bmatrix}0\\ 0\\ 0\end{Bmatrix}$
	$\underbrace{\left[\begin{array}{ccc\|cc}\frac{\partial}{\partial x} & 0 & \frac{\partial}{\partial y} & -1 & 0\\ 0 & \frac{\partial}{\partial y} & \frac{\partial}{\partial x} & 0 & -1\\ 0 & 0 & 0 & \frac{\partial}{\partial x} & \frac{\partial}{\partial y}\end{array}\right]}_{\mathbf{L}^T=\lfloor\ \mathbf{L}_f^T\quad \mathbf{L}_s^T\ \rfloor} \underbrace{\left\{\begin{array}{c}M_{xx}\\ M_{yy}\\ \hline M_{xy}\\ \hline V_x\\ V_y\end{array}\right\}}_{\mathbf{M}} + \begin{Bmatrix}0\\ 0\\ p_z\end{Bmatrix} = \begin{Bmatrix}0\\ 0\\ 0\end{Bmatrix}$
Constitutive	
$\underbrace{\begin{Bmatrix}\sigma_{xx}\\ \sigma_{yy}\\ \sigma_{zz}\\ \sigma_{xy}\\ \sigma_{yz}\\ \sigma_{zx}\end{Bmatrix}}_{\boldsymbol{\sigma}} = \alpha \underbrace{\begin{bmatrix}1 & \beta & \beta & 0 & 0 & 0\\ \beta & 1 & \beta & 0 & 0 & 0\\ \beta & \beta & 1 & 0 & 0 & 0\\ 0 & 0 & 0 & \gamma & 0 & 0\\ 0 & 0 & 0 & 0 & \gamma & 0\\ 0 & 0 & 0 & 0 & 0 & \gamma\end{bmatrix}}_{\mathbf{D}} \underbrace{\begin{Bmatrix}\varepsilon_{xx}\\ \varepsilon_{yy}\\ \varepsilon_{zz}\\ \varepsilon_{xy}\\ \varepsilon_{yz}\\ \varepsilon_{zx}\end{Bmatrix}}_{\boldsymbol{\varepsilon}}$	$\underbrace{\begin{Bmatrix}M_{xx}\\ M_{yy}\\ M_{xy}\end{Bmatrix}}_{\mathbf{M}} = K \underbrace{\begin{bmatrix}1 & \nu & 0\\ \nu & 1 & 0\\ 0 & 0 & \frac{1-\nu}{2}\end{bmatrix}}_{\mathbf{D}} \underbrace{\begin{Bmatrix}\kappa_{xx}\\ \kappa_{yy}\\ 2\kappa_{xy}\end{Bmatrix}}_{\boldsymbol{\kappa}}$
	$\underbrace{\left\{\begin{array}{c}M_{xx}\\ M_{yy}\\ M_{xy}\\ \hline V_x\\ V_y\end{array}\right\}}_{\mathbf{M}} = \underbrace{\left[\begin{array}{ccc\|c}K\begin{bmatrix}1 & \nu & 0\\ \nu & 1 & 0\\ 0 & 0 & \frac{1-\nu}{2}\end{bmatrix} & & & \mathbf{0}\\ \hline & & & \\ \mathbf{0} & & & \zeta\begin{bmatrix}1 & 0\\ 0 & 1\end{bmatrix}\end{array}\right]}_{\mathbf{D}} \underbrace{\begin{Bmatrix}\kappa_{xx}\\ \kappa_{yy}\\ 2\kappa_{xy}\\ \gamma_{xz}\\ \gamma_{yz}\end{Bmatrix}}_{\boldsymbol{\kappa}}$
$\alpha = \frac{E(1-\nu)}{(1+\nu)(1-2\nu)}; \beta = \frac{\nu}{1-\nu}; \gamma = \frac{1-2\nu}{2(1-\nu)}$	$K = \frac{Et^3}{12(1-\nu^2)}; \qquad \zeta = \frac{5}{6}\mu t$
Virtual Work	
$\delta\Pi = \int_\Omega \delta(\mathbf{Lu})^T \mathbf{D}\boldsymbol{\epsilon}\mathrm{d}\Omega - \int_\Omega \delta\mathbf{u}^T\mathbf{b}\mathrm{d}\Omega - \int_{\Gamma_t} \delta\mathbf{u}^T\hat{\mathbf{t}}\mathrm{d}\Gamma = 0$	$\delta W = -\int_A \delta w\,(KLwp_z)\,\mathrm{d}A + \int_{\Gamma_p} \delta w p_s \mathrm{d}\Gamma = 0$
	$\delta W = -K\left[\int_A \delta\boldsymbol{\theta}^T\mathbf{K}_f^e\boldsymbol{\theta}\mathrm{d}A + \frac{6k_s(1-\nu)}{t^2}\int_A \delta\mathbf{u}^T\mathbf{K}_s^e\mathbf{u}\mathrm{d}A\right] + \int_A \delta\mathbf{u}^T\mathbf{p}_V\,\mathrm{d}A + \int_\Gamma \delta\mathbf{u}^T\mathbf{p}\mathrm{d}\Gamma = 0$

Table 3.1: Comparison of Governing Equations in Elasticity and Plate Bending

equilibrium we have

$$\underbrace{N_{xx} r_y d\alpha_y}_{\text{Resultant force on neutral axis}} = \underbrace{\int_{-\frac{h}{2}}^{+\frac{h}{2}} \boldsymbol{\sigma}_{xx}(r_y - z) d\alpha_y dz}_{\text{internal force}} \tag{3.50}$$

Dividing both sides by $r_y d\alpha_y$, we obtain the membrane force acting along the x axis

$$N_{xx} = \int_{-\frac{h}{2}}^{+\frac{h}{2}} \boldsymbol{\sigma}_{xx} \left(1 - \frac{z}{r_y}\right) dz \tag{3.51}$$

The $\left(1 - \frac{z}{r_y}\right)$ term, which was not present in Eq. 3.50, accounts for the fact that our section is really a wedge rather than rectangular.

The differential element of consideration can be seen in Fig. 3.7. along with the stress

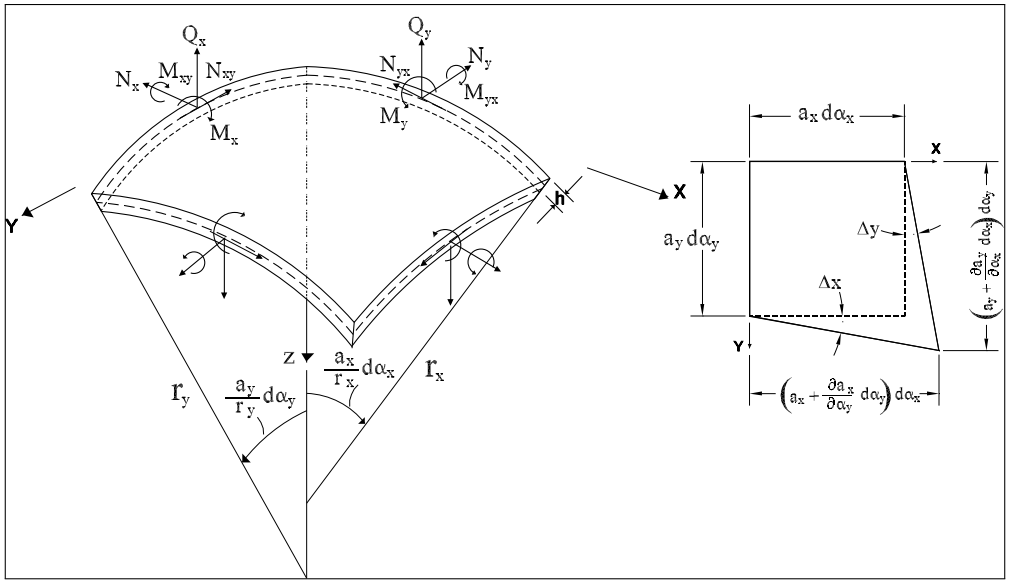

Figure 3.7: Differential Shell Element, Forces, (Billington, 1965)

resultants and stress couples in Fig. 3.8 The vectors of stress resultants are seen in Fig. 3.9 and the vectors of stress couples in Fig. 3.10. The derivation of the following stress resultants and stress couples follow the same formulation as the membrane force N_{xx} from Eq. 3.51.

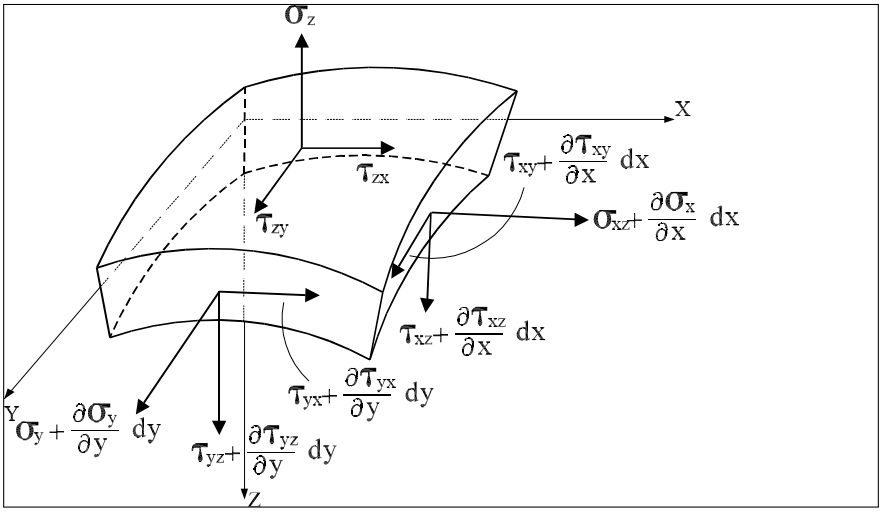

Figure 3.8: Differential Shell Element, Stresses, (Billington, 1965)

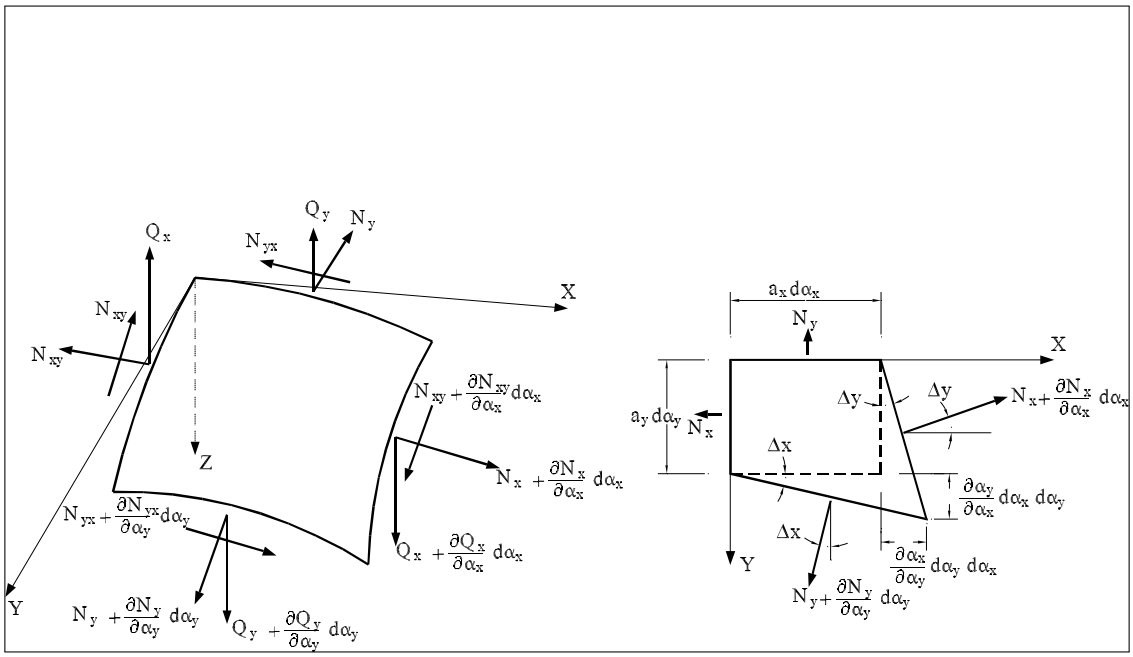

Figure 3.9: Differential Shell Element, Vectors of Stress Resultants, (Billington, 1965)

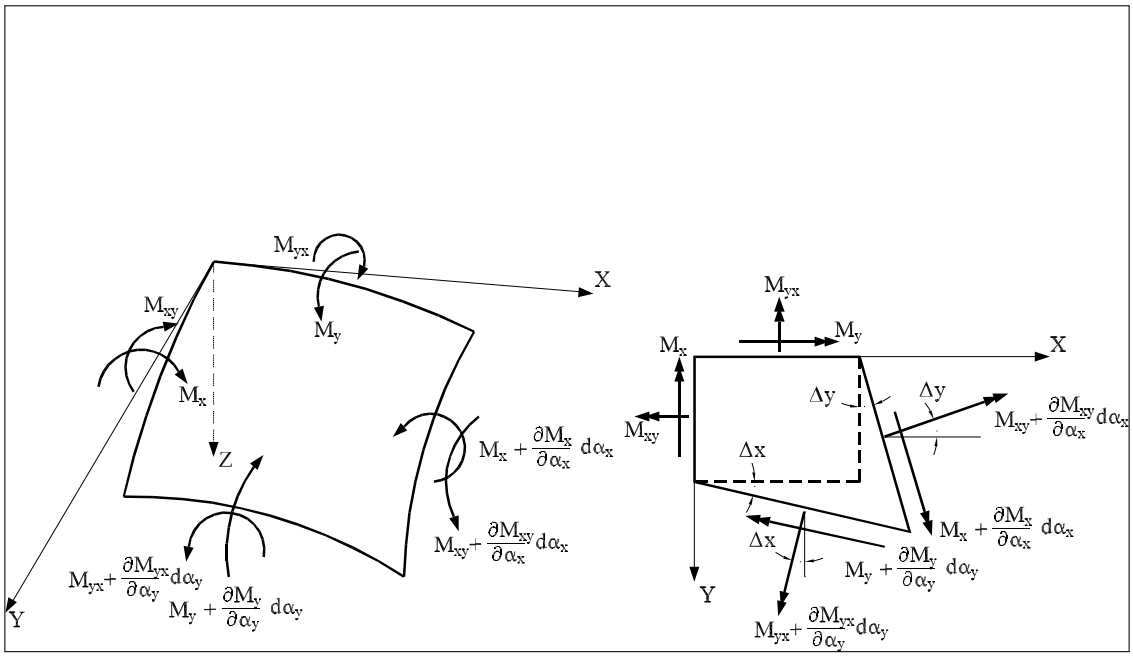

Figure 3.10: Differential Shell Element, Vectors of Stress Couples, (Billington, 1965)

Membrane Force

$$N = \int_{-\frac{h}{2}}^{+\frac{h}{2}} \boldsymbol{\sigma}\left(1-\frac{z}{r}\right)dz \qquad \begin{cases} N_{xx} = \int_{-\frac{h}{2}}^{+\frac{h}{2}} \sigma_{xx}\left(1-\frac{z}{r_y}\right)dz \\ N_{yy} = \int_{-\frac{h}{2}}^{+\frac{h}{2}} \sigma_{yy}\left(1-\frac{z}{r_x}\right)dz \\ N_{xy} = \int_{-\frac{h}{2}}^{+\frac{h}{2}} \sigma_{xy}\left(1-\frac{z}{r_y}\right)dz \\ N_{yx} = \int_{-\frac{h}{2}}^{+\frac{h}{2}} \sigma_{xy}\left(1-\frac{z}{r_x}\right)dz \end{cases}$$

Bending Moments

$$M = \int_{-\frac{h}{2}}^{+\frac{h}{2}} \boldsymbol{\sigma} z\left(1-\frac{z}{r}\right)dz \qquad \begin{cases} M_{xx} = \int_{-\frac{h}{2}}^{+\frac{h}{2}} \sigma_{xx} z\left(1-\frac{z}{r_y}\right)dz \\ M_{yy} = \int_{-\frac{h}{2}}^{+\frac{h}{2}} \sigma_{yy} z\left(1-\frac{z}{r_x}\right)dz \\ M_{xy} = -\int_{-\frac{h}{2}}^{+\frac{h}{2}} \sigma_{xy} z\left(1-\frac{z}{r_y}\right)dz \\ M_{yx} = \int_{-\frac{h}{2}}^{+\frac{h}{2}} \sigma_{xy} z\left(1-\frac{z}{r_x}\right)dz \end{cases} \tag{3.52}$$

Transverse Shear Forces

$$Q = \int_{-\frac{h}{2}}^{+\frac{h}{2}} \boldsymbol{\tau}\left(1-\frac{z}{r}\right)dz \qquad \begin{cases} Q_x = \int_{-\frac{h}{2}}^{+\frac{h}{2}} \tau_{xz}\left(1-\frac{z}{r_y}\right)dz \\ Q_y = \int_{-\frac{h}{2}}^{+\frac{h}{2}} \tau_{yz}\left(1-\frac{z}{r_x}\right)dz \end{cases}$$

3.4.1.2 Assumptions

For the purpose of simplification, a number of assumptions are considered:

Thin shell: If the terms z/r_x and z/r_y are neglected when they appear with unity, and with $\tau_{xy} = \tau yx$ then

$$N_{xy} = N_{yx} \tag{3.53-a}$$

$$M_{xy} = -M_{yx} \tag{3.53-b}$$

Small-Deflection: changes in geometry will not affect the static equilibrium.

Linear Elastic Behavior: linear relationships between stress and strain (or moment and curvature).

Conservative System: Points on lines normal to the middle surface before deformation remain on lines normal to the middle surface after deformation.

Neglect Shear Deformations: Radial shears Q_x and Q_y will not be considered.

3.4.2 Derivation of Governing Differential Equation

Based on preliminary definitions/assumptions, we can now derive a general shell theory through the following steps:

(1) Determine the **equilibrium** of forces and moments on a differential element (5 equations, 8 unknowns).

(2) Establish the **strain-displacement** relationships (6 equations, 3 unknowns).

(3) Establish a **stress-strain relationship** by assuming a set of elastic properties (3 equations, 6 unknowns).

(4) Transform the the force-strain relationships into **force-displacement** equations (6 equations 3 unknowns).

(5) Obtain a **complete formulation** by combining the force-displacement equations with the equilibrium equations (11 equations with 11 unknowns).

3.4.2.1 Equilibrium

Considering the differential element of a shell, Fig. 3.7, we now consider the 6 equations of static equilibrium

$$\begin{aligned} \Sigma F_x &= 0 \quad \Sigma M_x = 0 \\ \Sigma F_y &= 0 \quad \Sigma M_y = 0 \\ \Sigma F_z &= 0 \quad \Sigma M_z = 0 \end{aligned} \tag{3.54}$$

In shell theory we usually neglect M_z because τ_{xz} and τ_{yz} are neglected. So we have to satisfy 5 equations of equilibrium, Eq. 3.52, in terms of 8 generalized forces, Eq. 3.54.

Equilibrium	Forces
$\Sigma F_x, \Sigma F_y, \Sigma F_z, \Sigma M_x, \Sigma M_y$	$N_x, N_y, N_{xy}, Q_x, Q_y, M_x, M_y, M_{xy}$

(a) $\Sigma F_x = 0$**:**

We will consider the contribution of each term separately, and then combine all components together to form the completed equilibrium equation. Contributions from the stress resultants, N_{xx}, N_{yy}, N_{xy}, N_{yx}, two radial shear forces, Q_x, Q_y, and the external pressures will be considered. The stress couples attribute no force component in the x direction. Each component will be determined by multiplying the stress resultant, Fig. 3.9, by the length of the element side on which it acts.

From Fig. 3.7, a difference in geometry of the differential element can be noted. The sides of the element which intersect the origin have curved lengths of $a_x d\alpha_x$ and $a_y d\alpha_y$, whereas the opposing edges have increased lengths of $(a_x + \frac{\partial a_x}{\partial \alpha_y})d\alpha_x$ and $(a_y + \frac{\partial a_y}{\partial \alpha_x})d\alpha_y$.

Contribution from N_x**:**

$$\Sigma F_x^{N_x} = -N_x a_y d\alpha_y + \left(N_x + \frac{\partial N_x}{\partial \alpha_x} d\alpha_x\right)\left(a_y + \frac{\partial \alpha_y}{d\alpha_x} d\alpha_x\right) d\alpha_y \tag{3.55-a}$$

$$= N_x \frac{\partial \alpha_y}{\partial \alpha_x} d\alpha_x d\alpha_y + a_y \frac{\partial N_x}{\partial \alpha_x} d\alpha_x d\alpha_y + \underbrace{\frac{\partial N_x}{\partial \alpha_x} d\alpha_x \frac{\partial a_y}{\partial \alpha_x} d\alpha_x d\alpha_y}_{2^{nd} \text{ order effect}} \tag{3.55-b}$$

By combining the first two terms and eliminating the third due to second order effects

$$\Sigma F_x^{N_x} = \frac{\partial (N_x a_y)}{\partial \alpha_x} d\alpha_x d\alpha_y \tag{3.56}$$

Contribution from N_y: First we note that in general N_y does not act perpendicular to the x axis but at some angle

$$\Delta_x = \frac{(\partial a_y/\partial \alpha_x) d\alpha_x d\alpha_y}{a_x d\alpha_x} \tag{3.57-a}$$

$$= \frac{\partial a_y}{\partial \alpha_x}\frac{d\alpha_y}{a_x} \tag{3.57-b}$$

thus in the x direction, the component of the total force $N_y a_x d\alpha_x$ is

$$\Sigma F_x^{N_y} = -N_y a_x d\alpha_x \frac{\partial a_y}{\partial \alpha_x}\frac{d\alpha_y}{a_x} \tag{3.58-a}$$

$$= -N_y \frac{\partial a_y}{\partial \alpha_x} d\alpha_x d\alpha_y \tag{3.58-b}$$

Contribution from N_{xy}: As for $N_x y$, this force also has a non perpendicular component and is determined along the angle Δ_y:

$$\Delta_y = \frac{(\partial a_x/\partial \alpha_y) d\alpha_y d\alpha_x}{a_y d\alpha_y} \tag{3.59-a}$$

$$= \frac{\partial a_x}{\partial \alpha_y}\frac{d\alpha_x}{a_y} \tag{3.59-b}$$

and the component of the total force $N_{xy} a_y d\alpha_y$ is

$$\Sigma F_x^{N_{xy}} = N_{xy} a_y d\alpha_y \frac{\partial a_x}{\partial \alpha_y}\frac{d\alpha_x}{a_y} \tag{3.60-a}$$

$$= N_{xy} \frac{\partial a_x}{\partial \alpha_y} d\alpha_y d\alpha_x \tag{3.60-b}$$

Contribution from N_{yx}: is similar to the one of N_x, Eq. 3.56

$$\Sigma F_x^{N_{yx}} = -N_{yx} a_x d\alpha_x + \left(N_{yx} + \frac{\partial N_{yx}}{\partial \alpha_y} d\alpha_y\right)\left(a_x + \frac{\partial a_x}{\partial \alpha_y} d\alpha_y\right) d\alpha_x \tag{3.61-a}$$

$$= \frac{\partial (N_{yx} a_x)}{\partial \alpha_y} d\alpha_x d\alpha_y \tag{3.61-b}$$

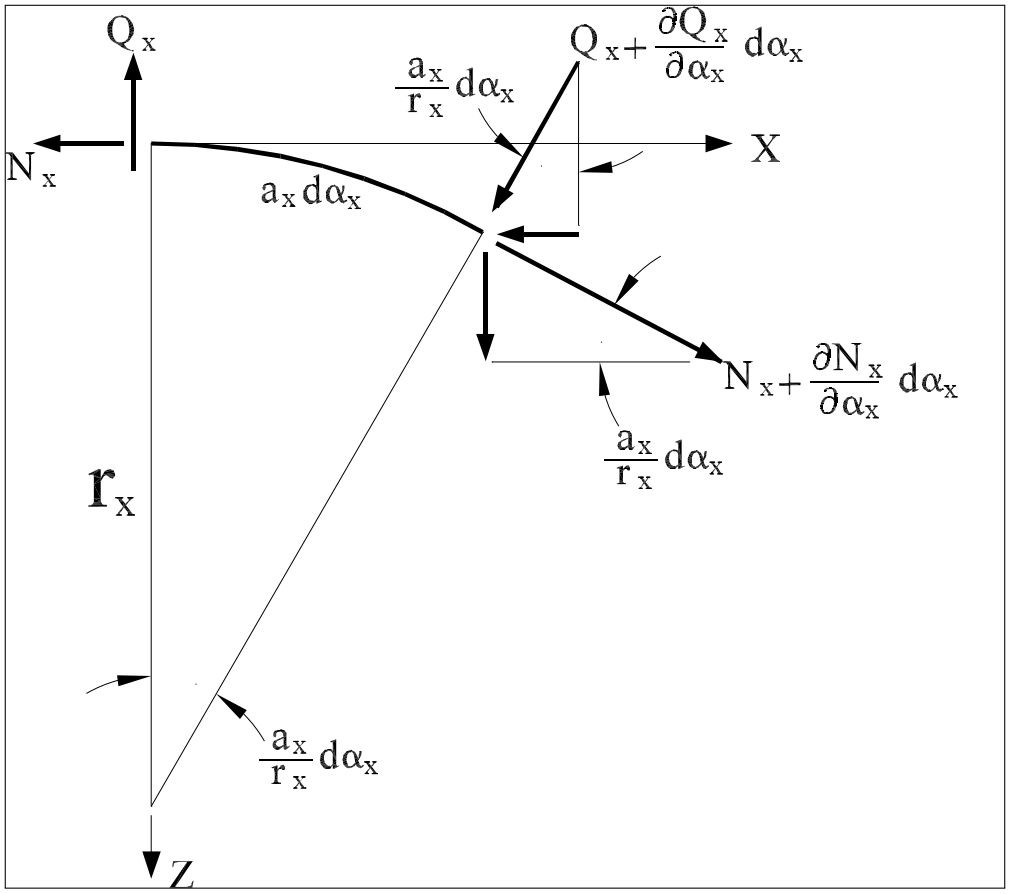

Figure 3.11: Differential Shell Element, Q_x Stress Resultants, (Billington, 1965)

Contribution from Q_x: The horizontal component of the total force on the sloping side, Fig. 3.11, is

$$\Sigma F_x^{Q_x} = -\left(Q_x + \frac{\partial Q_x}{\partial \alpha_x} d\alpha_x\right)\left(a_y + \frac{\partial a_y}{\partial \alpha_x} d\alpha_x\right) d\alpha_y \frac{a_x}{r_x} d\alpha_x \tag{3.62}$$

where $d\alpha_x \simeq \sin d\alpha_x$. We note that Q_x has no x component on the negative side. Neglecting higher order terms, this reduces to

$$\Sigma F_x^{Q_x} = -Q_x a_y d\alpha_y \frac{a_x}{r_x} d\alpha_x \tag{3.63}$$

Contribution from Q_y: The stress resultant will contribute to the equilibrium in the x direction only if a_x and a_y are not principle radii of curvature. In Fig. 3.12 the differential element with curvatures, which result in a total distance of $z_x + z_y + z_{xy}$ at the corner opposite to

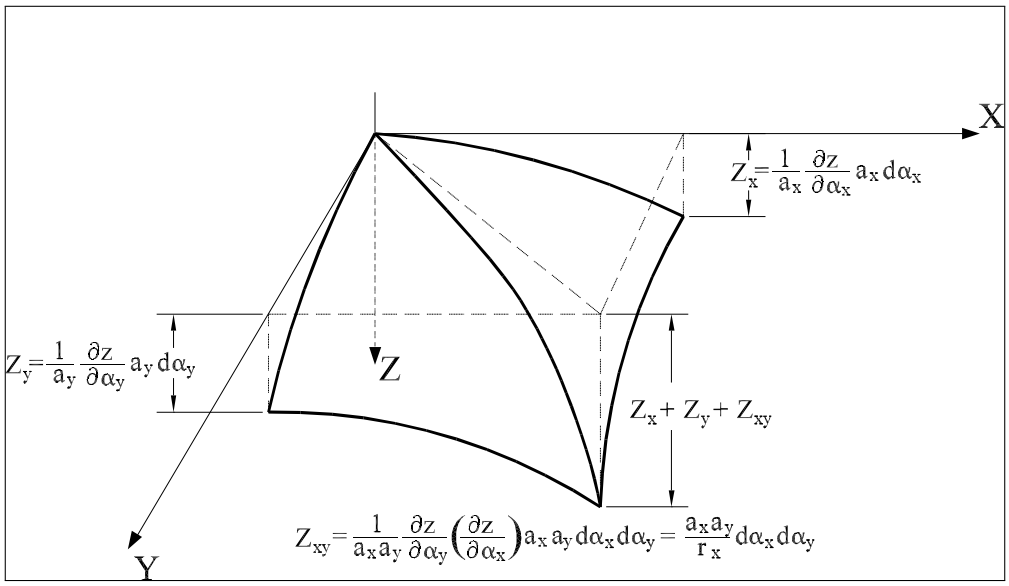

Figure 3.12: Differential Shell Element, Principal Curvatures, (Billington, 1965)

the origin, is shown. z_x and z_y are due to the slopes $\partial z/\partial \alpha_x$ and $\partial z/\partial \alpha_y$. The change in slope results in

$$z_{xy} = \frac{1}{a_x a_y}\frac{\partial^2 z}{\partial \alpha_x \partial \alpha_y} a_x a_y d\alpha_x d\alpha_y \tag{3.64-a}$$

$$= \frac{a_x a_y}{r_{xy}} d\alpha_x d\alpha_y \tag{3.64-b}$$

where

$$\frac{1}{r_{xy}} = \frac{1}{a_x a_y} \frac{\partial^2 z}{\partial \alpha_x \partial \alpha_y} \tag{3.65}$$

and corresponds to the twist of the surface with respect to the x and y axes. Hence, the slope of Q_y is

$$\frac{z_{xy}}{a_x d\alpha_x} = \frac{a_y d\alpha_y}{r_{xy}} \tag{3.66}$$

and the total component of Q_y in the x direction is

$$\Sigma F_x^{Q_y} = \left(Q_y + \frac{\partial Q_y}{\partial \alpha_x} d\alpha_x\right)\left(a_x + \frac{\partial a_x}{\partial \alpha_y} d\alpha_y\right) d\alpha_x \frac{a_y}{r_{xy}} d\alpha_y \tag{3.67-a}$$

$$= Q_y a_x d\alpha_x \frac{a_y d\alpha_y}{r_{xy}} \tag{3.67-b}$$

This expression vanishes where the element is bounded by lines of principal curvature r_x and r_y, $z_{xy} = 0$, the twist $r_{xy} = \infty$.

Contribution from the external load: Assumed to be a pressure with components p_x, p_y and p_z acting on the differential element of an area $a_x d\alpha_x a_y d\alpha_y$:

$$\Sigma F_x^p = p_x a_x d\alpha_x a_y d\alpha_y \tag{3.68}$$

Finally, we can now combine the x components of N_x, N_y, N_{xy}, N_{yx}, Q_x, Q_y and the load from Eqs. 3.56, 3.58-b, 3.60-b, 3.61-b, 3.63, 3.67-b, and 3.68. After cancelling the common multipliers $d\alpha_x d\alpha_y$, we obtain

$$\frac{\partial(N_x a_y)}{\partial \alpha_x} - N_y \frac{\partial a_y}{\partial \alpha_x} + N_{xy} \frac{\partial a_x}{\partial \alpha_y} + \frac{\partial(N_{yx} a_x)}{\partial \alpha_y} - Q_y \frac{a_x a_y}{r_{xy}} - Q_x a_y \frac{a_x}{r_x} + p_x a_x a_y = 0 \tag{3.69}$$

(b) $\Sigma F_y = 0$**:**

This second equation is exactly the same as the one corresponding to $\Sigma F_x = 0$ except that we switch the x and y terms yielding

$$\frac{\partial(N_y a_x)}{\partial \alpha_y} - N_x \frac{\partial a_x}{\partial \alpha_y} + N_{yx} \frac{\partial a_y}{\partial \alpha_x} + \frac{\partial(N_{xy} a_y)}{\partial \alpha_x} - Q_x \frac{a_y a_x}{r_{yx}} - Q_y a_x \frac{a_y}{r_y} + p_y a_x a_y = 0 \tag{3.70}$$

(c) $\Sigma F_z = 0$**:**

The z direction is always defined to be perpendicular to the middle surface; hence it is always in the direction of principal radii of curvature, Fig. 3.11. Thus the assumption for small angles can be made that $\sin\theta \simeq \theta$.

Similar to $\Sigma F_x = 0$, contributions from the stress resultants, N_{xx}, N_{yy}, N_{xy}, N_{yx}, two radial shear forces, Q_x, Q_y, and the external pressures will be considered. The stress couples attribute no force component in the z direction. Each component will be determined by multiplying the stress resultant, Fig. 3.9, or radial shear force, Fig. 3.11, by the length of the element side on which it acts.

Contribution from N_x:

$$\Sigma F_z^{N_x} = N_x a_y d\alpha_y \underbrace{\frac{a_x}{r_x} d\alpha_x}_{\sin\theta \simeq \theta} + 2^{nd} \text{ order terms} \tag{3.71}$$

All of the following expressions will be similar to the layout of the N_x formulation by altering the x and y variables.

Contribution from N_y:

$$\Sigma F_z^{N_y} = N_y a_x d\alpha_x \frac{a_y}{r_y} d\alpha_y \tag{3.72}$$

Contribution from N_{xy}:

$$\Sigma F_z^{N_{xy}} = N_{xy} a_y d\alpha_y \frac{a_x}{r_{xy}} d\alpha_x \tag{3.73}$$

Contribution from N_{yx}:

$$\Sigma F_z^{N_{yx}} = N_{yx} a_x d\alpha_x \frac{a_y}{r_{xy}} d\alpha_y \tag{3.74}$$

Contribution from Q_x:

$$\Sigma F_z^{Q_x} = -Q_x a_y d\alpha_y + \left(Q_x + \frac{\partial Q_x}{\partial \alpha_x} d\alpha_x\right) \underbrace{\cos\left(\frac{a_x}{r_x} d\alpha_x\right)}_{\simeq 1} \left(a_y + \frac{\partial a_y}{\partial \alpha_x} d\alpha_x\right) d\alpha_y \tag{3.75-a}$$

$$= \frac{\partial (Q_x a_y)}{\partial \alpha_x} d\alpha_x d\alpha_y \tag{3.75-b}$$

Contribution from Q_y: By analogy to Q_x

$$\Sigma F_z^{Q_y} = \frac{\partial(Q_y a_x)}{\partial \alpha_y} d\alpha_y d\alpha_x \tag{3.76}$$

Contribution from the external load: From Eq. 3.68

$$\Sigma F_z^p = p_z a_x d\alpha_x a_y d\alpha_y \tag{3.77}$$

Finally, we can now combine the z components of N_x, N_y, N_{xy}, N_{yx}, Q_x, Q_y and the load from Eq. 3.71, 3.72, 3.73, 3.74, 3.75-b, 3.76, and 3.77 respectively. Again after canceling the common multipliers $d\alpha_x d\alpha_y$, we obtain

$$\frac{\partial(Q_x a_y)}{\partial \alpha_x} + \frac{\partial(Q_y a_x)}{\partial \alpha_y} + N_x \frac{a_x}{r_x} a_y + N_{xy} \frac{a_x}{r_{xy}} a_y + N_{yx} \frac{a_y}{r_{xy}} a_x + N_y \frac{a_y}{r_y} a_x + p_z a_x a_y = 0 \tag{3.78}$$

(d) $\Sigma M_x = 0$:

The solutions for moments have components which are similar to the ones of forces seen above, exhibiting differences primarily with the contributors. No contributions are from the stress resultants and only one radial shear forces, Q_y, is considered. However, now the stress couples, M_x, M_y, M_{xy}, M_{yx}, attribute force components in the x, y, and z directions. Each component will be determined by multiplying the stress couples, Fig. 3.10, or radial shear force, Fig. 3.11, by the length of the element side on which it acts.

Contribution from M_x: Has a component about the x axis which is analogous to the one of N_x in the y direction (Eq. 3.56 with x and y reverted)

$$\Sigma M_x^{M_x} = M_x a_y d\alpha_y \frac{\partial a_x}{\partial \alpha_y} \frac{d\alpha_x}{a_y} \tag{3.79-a}$$

$$= M_x \frac{\partial a_x}{\partial \alpha_y} d\alpha_y d\alpha_x \tag{3.79-b}$$

Contribution from M_y: As in Eq. 3.56, and with reference to Fig. 3.10

$$\Sigma M_x^{M_y} = M_y a_x d\alpha_x - \left(M_y + \frac{\partial M_y}{\partial \alpha_y} d\alpha_y \right) \left(a_x + \frac{\partial a_x}{d\alpha_y} d\alpha_y \right) d\alpha_x \tag{3.80-a}$$

$$= -\frac{\partial(M_y a_x)}{\partial \alpha_y} d\alpha_y d\alpha_x \tag{3.80-b}$$

Contribution from M_{xy}: is analogous to Eq. 3.80-b

$$\Sigma M_x^{M_{xy}} = -M_{xy}a_y d\alpha_y + \left(M_{xy} + \frac{\partial M_{xy}}{\partial \alpha_x} d\alpha_x\right)\left(a_y + \frac{\partial a_y}{d\alpha_x} d\alpha_x\right) d\alpha_y \quad (3.81\text{-a})$$

$$= \frac{\partial (M_{xy}a_y)}{\partial \alpha_x} d\alpha_x d\alpha_y \quad (3.81\text{-b})$$

Contribution from M_{yx}:

$$\Sigma M_x^{M_{yx}} = -M_{yx}a_x d\alpha_x \frac{\partial a_y}{\partial \alpha_x}\frac{d\alpha_y}{a_x} \quad (3.82\text{-a})$$

$$= -M_{yx}\frac{\partial a_y}{\partial \alpha_x} d\alpha_x d\alpha_y \quad (3.82\text{-b})$$

Contribution from Q_y:

$$\Sigma M_x^{Q_y} = Q_y a_x d\alpha_x a_y d\alpha_y \quad (3.83)$$

Finally, we can now combine the effect of all the components M_x, M_y, M_{xy}, M_{yx}, and Q_y Eq. 3.79-b, 3.80-b, 3.81-b, 3.82-b and 3.83 respectively. After canceling the common multipliers $d\alpha_x d\alpha_y$, we obtain

$$-\frac{\partial (M_y a_x)}{\partial \alpha_y} + M_x \frac{\partial a_x}{\partial \alpha_y} - M_{yx}\frac{\partial a_y}{\partial \alpha_x} + \frac{\partial (M_{xy}a_y)}{\partial \alpha_x} + Q_y a_x a_y = 0 \quad (3.84)$$

(e) $\Sigma M_y = 0$:

Moments about the y axis give the same expression as in Eq. 3.84 except that the x and y subscripts flip, and the sign of the twisting-stress couples are reversed.

$$-\frac{\partial (M_x a_y)}{\partial \alpha_x} + M_y \frac{\partial a_y}{\partial \alpha_x} + M_{xy}\frac{\partial a_x}{\partial \alpha_y} - \frac{\partial (M_{yx}a_x)}{\partial \alpha_y} + Q_x a_x a_y = 0 \quad (3.85)$$

(f) Complete Set of Equilibrium Equations:

The 5 equilibrium equations, Eq. 3.69, 3.70, 3.78, 3.84 and 3.85 are summarized below

$$\begin{aligned}
\Sigma F_x &= \frac{\partial}{\partial\alpha_x}(N_x a_y) - N_y\frac{\partial a_y}{\partial\alpha_x} + N_{xy}\frac{\partial a_x}{\partial\alpha_y} + \frac{\partial}{\partial\alpha_y}(N_{yx}a_x) - Q_y\frac{a_x a_y}{r_{xy}} - Q_x a_y\frac{a_x}{r_x} + p_x a_x a_y = 0\\
\Sigma F_y &= \frac{\partial}{\partial\alpha_y}(N_y a_x) - N_x\frac{\partial a_x}{\partial\alpha_y} + N_{yx}\frac{\partial a_y}{\partial\alpha_x} + \frac{\partial}{\partial\alpha_x}(N_{xy}a_y) - Q_x\frac{a_y a_x}{r_{yx}} - Q_y a_x\frac{a_y}{r_y} + p_y a_x a_y = 0\\
\Sigma F_z &= \frac{\partial}{\partial\alpha_x}(Q_x a_y) + \frac{\partial}{\partial\alpha_y}(Q_y a_x) + N_x\frac{a_x}{r_x}a_y + N_{xy}\frac{a_x}{r_{xy}}a_y + N_{yx}\frac{a_y}{r_{xy}}a_x + N_y\frac{a_y}{r_y}a_x + p_z a_x a_y = 0\\
\Sigma M_x &= -\frac{\partial}{\partial\alpha_y}(M_y a_x) + M_x\frac{\partial a_x}{\partial\alpha_y} - M_{yx}\frac{\partial a_y}{\partial\alpha_x} + \frac{\partial}{\partial\alpha_x}(M_{xy}a_y) + Q_y a_x a_y = 0\\
\Sigma M_y &= -\frac{\partial}{\partial\alpha_x}(M_x a_y) + M_y\frac{\partial a_y}{\partial\alpha_x} + M_{xy}\frac{\partial a_x}{\partial\alpha_y} - \frac{\partial}{\partial\alpha_y}(M_{yx}a_x) + Q_x a_x a_y = 0
\end{aligned} \tag{3.86}$$

3.4.2.2 Compatibility

(a) ε_{x0}**:**

The strain-displacement relations will next be derived with reference to Fig. 3.13. The linear

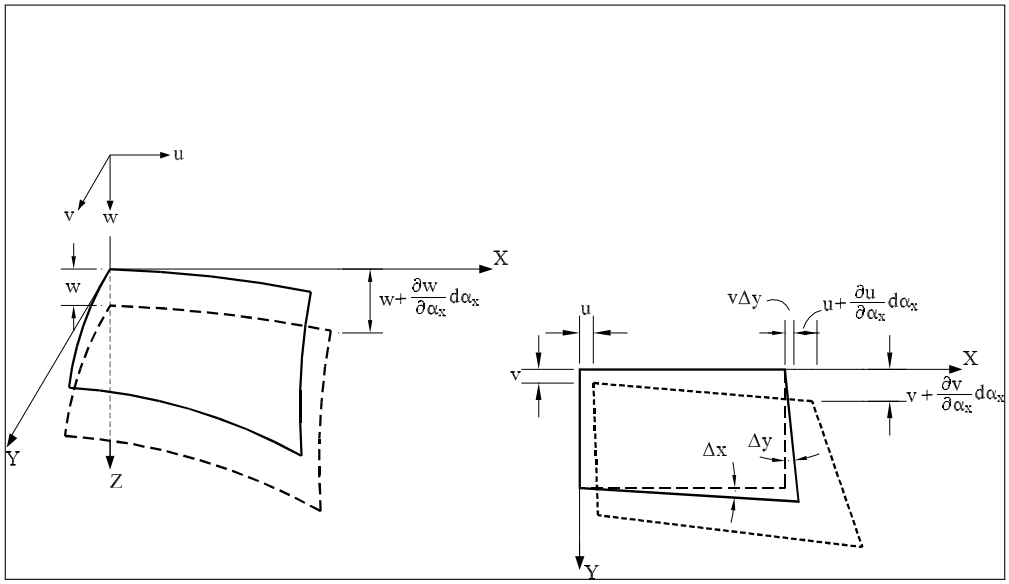

Figure 3.13: Differential Shell Element, Initial and Deformed State, (Billington, 1965)

element of length $a_x d\alpha_x$ undergoes three changes in length:

Axial extension x axis of $\frac{\partial u}{\partial\alpha_x}d\alpha_x$

Lateral extension y: The original undeformed shape of the differential element is not rectangular (as a result of $d\alpha_x$ and $d\alpha_y$), and the angle between the positive y side and the vertical is (Eq. 3.59-b) $\Delta_y = \frac{\partial a_x}{\partial \alpha_y}\frac{d\alpha_x}{a_y}$ (rather than 0); Thus, a translation along the y axis, will result in a translation along the x axis equal to $v\Delta_y$.

Decrease in radius of curvature: $-w\frac{a_x}{r_x}d\alpha_x$

Summing all those terms, and dividing by the original length $a_x d\alpha_x$ yields

$$\varepsilon_{x0} = \frac{1}{a_x}\frac{\partial u}{\partial \alpha_x} + \frac{v}{a_x a_y}\frac{\partial a_x}{\partial \alpha_y} - \frac{w}{r_x} \tag{3.87}$$

where the 0 subscript indicates that the middle surface is being considered.

(b) ε_{y0}:

The strain of the middle surface along the y axis, by analogy, is obtained by reversing the x and y variables along with v and u in the preceding equation.

$$\varepsilon_{y0} = \frac{1}{a_y}\frac{\partial v}{\partial \alpha_y} + \frac{u}{a_x a_y}\frac{\partial a_y}{\partial \alpha_x} - \frac{w}{r_y} \tag{3.88}$$

(c) γ_{xy0}:

The shearing strain, representing the total angular change between $a_y d\alpha_y$ and $a_x d\alpha_x$, is also somewhat complex, and its three components will be derived separately.

Difference in displacements: For the v term, Fig. 3.13, we have $(v + \frac{\partial v}{\partial \alpha_x}d\alpha_x) - v$. If we divide by the elemental length, $a_x d\alpha_x$, and repeat the same operation for the u displacement, we obtain:

$$\gamma^I_{xy0} = \frac{1}{a_x}\frac{\partial v}{\partial \alpha_x} + \frac{1}{a_y}\frac{\partial u}{\partial \alpha_y} \tag{3.89}$$

Increase in length of positive sides: We start by determining Δs, Fig. 3.14

$$\Delta s = \left(u + \frac{\partial u}{\partial \alpha_x}d\alpha_x\right)\Delta_y \tag{3.90}$$

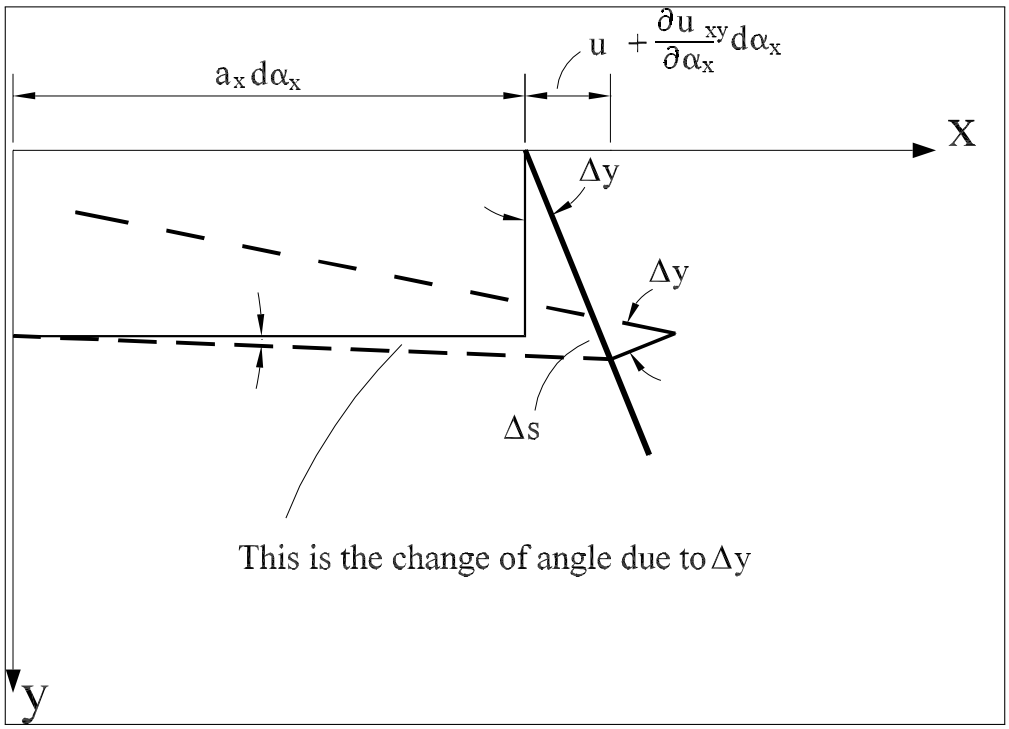

Figure 3.14: Differential Shell Element, Initial and Deformed State; Shear Strain Caused by Increase in Length of Positive Sides, (Billington, 1965)

where Δ_y was derived in Eq. 3.59-b as

$$\Delta_y = \frac{\partial a_x}{\partial \alpha_y} \frac{d\alpha_x}{a_y} \tag{3.91}$$

hence,

$$\Delta s = \left(u + \frac{\partial u}{\partial \alpha_x} d\alpha_x \right) \frac{\partial a_x}{\partial \alpha_y} \frac{d\alpha_x}{a_y} \tag{3.92-a}$$

$$= u \frac{\partial a_x}{\partial \alpha_y} \frac{d\alpha_x}{a_y} + \underbrace{\frac{\partial u}{\partial \alpha_x} d\alpha_x \frac{\partial a_x}{\partial \alpha_y} \frac{d\alpha_x}{a_y}}_{\text{Higher order term}} \tag{3.92-b}$$

By dividing Δs by the element length, $a_x d\alpha_x$ and repeating the same operation for the other side, we obtain

$$\gamma^{II}_{xy0} = -\frac{u}{a_x a_y} \frac{\partial a_x}{\partial \alpha_y} - \frac{v}{a_x a_y} \frac{\partial a_y}{\partial \alpha_x} \tag{3.93}$$

where the negative sign reflects the fact that the angle between the $x = 0$ and $y = 0$ faces has decreased (originally was a right angle).

Twist of Surfaces: With reference to Fig. 3.15, we have

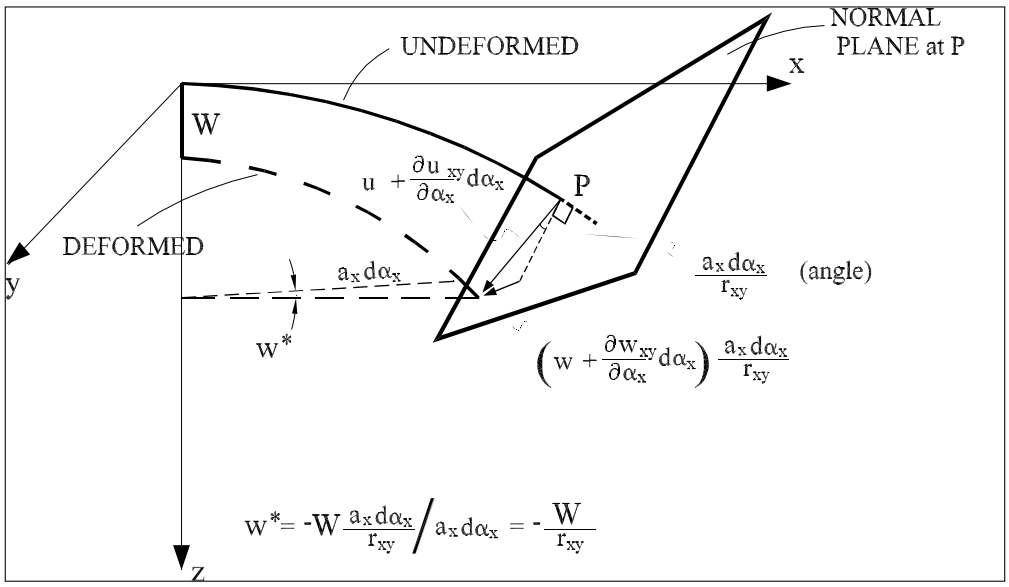

Figure 3.15: Differential Shell Element, Initial and Deformed State; Shear Strain Caused by Twist of Surface, (Billington, 1965)

$$w^* = -w\frac{a_x d\alpha_x}{r_{xy}} \tag{3.94}$$

Dividing by original length $a_x d\alpha_x$ and recognizing that we have a similar term for the plane $x = 0$, we obtain

$$\gamma^{III}_{xy0} = -2\frac{w}{r_{xy}} \tag{3.95}$$

Thus, summing all three components, Eq. 3.89, 3.93 and 3.95, we obtain

$$\gamma_{xy0} = \underbrace{\frac{1}{a_x}\frac{\partial v}{\partial \alpha_x} + \frac{1}{a_y}\frac{\partial u}{\partial \alpha_y}}_{} \underbrace{- \frac{u}{a_x a_y}\frac{\partial a_x}{\partial \alpha_y} - \frac{v}{a_x a_y}\frac{\partial a_y}{\partial \alpha_x}}_{} \underbrace{- 2\frac{w}{r_{xy}}}_{} \tag{3.96}$$

(d) Changes in Curvature: Considering the $x - z$ plane, Fig. 3.16, and assuming $w = 0$,

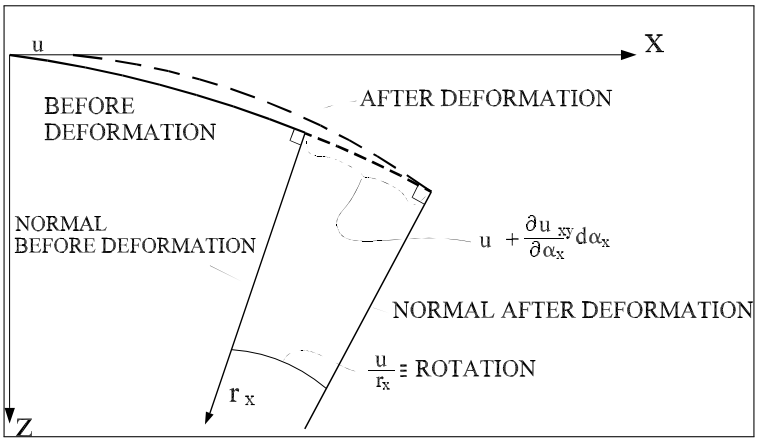

Figure 3.16: Differential Shell Element, Initial and Deformed State; Rotation, (Billington, 1965)

the normals to the differential element on the positive face before and after deformation make an angle $\frac{u}{r_x}$. The conventional term due to transverse displacement is $\frac{\partial w}{\partial s_{\alpha_x}} = \frac{\partial w}{a_x \partial \alpha_x}$. Finally accounting also for the twisting term we obtain

$$\phi_x = \frac{u}{r_x} + \frac{\partial w}{a_x \partial \alpha_x} + \frac{v}{r_{xy}} \tag{3.97}$$

Similarly we obtain

$$\phi_y = \frac{v}{r_y} + \frac{\partial w}{a_y \partial \alpha_y} + \frac{u}{r_{xy}} \tag{3.98}$$

The change in curvature will thus be equal to the change in rotation $\partial\phi_x$ per arc length $a_x\partial\alpha_x$

$$\chi_x = \frac{1}{a_x}\frac{\partial\phi_x}{\partial\alpha_x} \tag{3.99}$$

Furthermore, due to the non parallel sides of the element, because of the changing values of a_x and a_y, the rotation ϕ_y in the y direction will produce a component in the x direction.

$$\frac{\phi_y\Delta_y}{a_x\partial\alpha_x} = \frac{\phi_y}{a_xa_y}\frac{\partial a_x}{\partial\alpha_y} \tag{3.100}$$

Hence the complete expressions for changes in curvature become

$$\chi_x = \frac{1}{a_x}\frac{\partial\phi_x}{\partial\alpha_x} + \frac{\phi_y}{a_xa_y}\frac{\partial a_x}{\partial\alpha_y} \tag{3.101-a}$$

$$\chi_y = \frac{1}{a_y}\frac{\partial\phi_y}{\partial\alpha_y} + \frac{\phi_x}{a_ya_x}\frac{\partial a_y}{\partial\alpha_x} \tag{3.101-b}$$

$$2\chi_{xy} = \frac{1}{a_y}\frac{\partial\phi_x}{\partial\alpha_y} + +\frac{1}{a_x}\frac{\partial\phi_y}{\partial\alpha_x} - \frac{\phi_x}{a_xa_y}\frac{\partial a_x}{\partial\alpha_y} - \frac{\phi_y}{a_ya_x}\frac{\partial a_y}{\partial\alpha_x} \tag{3.101-c}$$

Summary:

We now summarize all six strain expressions in terms of the three unknown displacements, Eq. 3.87, 3.88, 3.96 and the preceding set, we have

$$\begin{aligned}
\varepsilon_{x0} &= \tfrac{1}{a_x}\tfrac{\partial u}{\partial\alpha_x} + \tfrac{v}{a_xa_y}\tfrac{\partial a_x}{\partial\alpha_y} - \tfrac{w}{r_x} \\
\varepsilon_{y0} &= \tfrac{1}{a_y}\tfrac{\partial v}{\partial\alpha_y} + \tfrac{u}{a_xa_y}\tfrac{\partial a_y}{\partial\alpha_x} - \tfrac{w}{r_y} \\
\gamma_{xy0} &= \tfrac{1}{a_x}\tfrac{\partial v}{\partial\alpha_x} + \tfrac{1}{a_y}\tfrac{\partial u}{\partial\alpha_y} - \tfrac{u}{a_xa_y}\tfrac{\partial a_x}{\partial\alpha_y} - \tfrac{v}{a_xa_y}\tfrac{\partial a_y}{\partial\alpha_x} - 2\tfrac{w}{r_{xy}} \\
\chi_x &= \tfrac{1}{a_x}\tfrac{\partial\phi_x}{\partial\alpha_x} + \tfrac{\phi_y}{a_xa_y}\tfrac{\partial a_x}{\partial\alpha_y} \\
\chi_y &= \tfrac{1}{a_y}\tfrac{\partial\phi_y}{\partial\alpha_y} + \tfrac{\phi_x}{a_ya_x}\tfrac{\partial a_y}{\partial\alpha_x} \\
2\chi_{xy} &= \tfrac{1}{a_y}\tfrac{\partial\phi_x}{\partial\alpha_y} + \tfrac{1}{a_x}\tfrac{\partial\phi_y}{\partial\alpha_x} - \tfrac{\phi_x}{a_xa_y}\tfrac{\partial a_x}{\partial\alpha_y} - \tfrac{\phi_y}{a_ya_x}\tfrac{\partial a_y}{\partial\alpha_x}
\end{aligned} \tag{3.102}$$

where

$$\begin{aligned}
\phi_x &= \tfrac{u}{r_x} + \tfrac{\partial w}{a_x\partial\alpha_x} + \tfrac{v}{r_{xy}} \\
\phi_y &= \tfrac{v}{r_y} + \tfrac{\partial w}{a_y\partial\alpha_y} + \tfrac{u}{r_{xy}}
\end{aligned} \tag{3.103}$$

3.4.2.3 Stress-Strain

The strain ε_x at a distance z from the middle surface, Fig. 3.17,

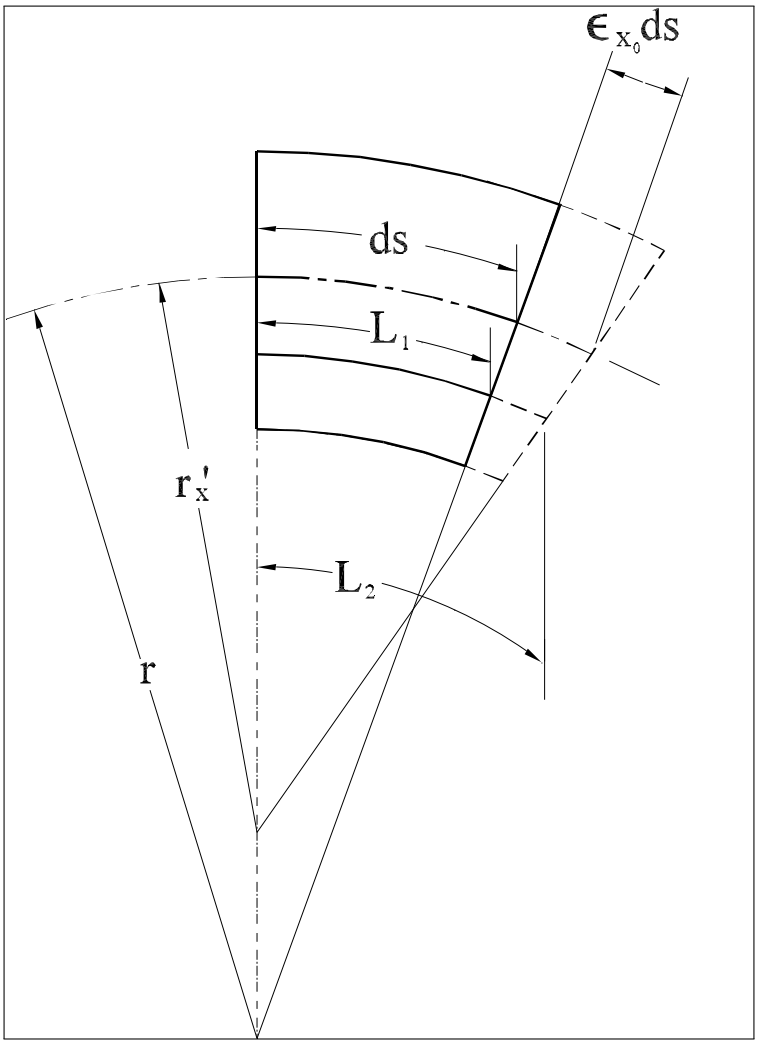

Figure 3.17: Middle surface of differential element, (Billington, 1965)

is composed of an axial component ε_{x0} caused by extension of the middle surface, and another

caused by bending.

$$\varepsilon_x = \frac{L_2 - L_1}{L1} \tag{3.104-a}$$

$$L_1 = ds\left(1 - \frac{z}{r_x}\right) \tag{3.104-b}$$

$$L_2 = ds(1+\varepsilon_{x0})\left(1 - \frac{z}{r'_x}\right) \tag{3.104-c}$$

$$\varepsilon_x = \frac{(1+\varepsilon_{x0})(1 - z/r'_x) - (1 - z/r_x)}{1 - z/r_x} \tag{3.104-d}$$

$$= \frac{1 - z/r'_x + \varepsilon_{x0}(1 - z/r'_x) - 1 + z/r_x}{1 - z/r_x} \tag{3.104-e}$$

we can drop the small term z/r'_x and z/r_x when they appear with unity,

$$\varepsilon_x = \varepsilon_{x0} - z\left(\frac{1}{r'_x} - \frac{1}{r_x}\right) \tag{3.105}$$

Again χ, referring to the change in curvature, we find

$$\varepsilon_x = \varepsilon_{x0} - z\chi_x \tag{3.106-a}$$

$$\varepsilon_y = \varepsilon_{y0} - z\chi_y \tag{3.106-b}$$

$$\gamma_{xy} = \gamma_{xy0} - 2z\chi_{xy} \tag{3.106-c}$$

At this point, we will no longer ignore the material properties of the system. In order to derive the stress-strain relationship, we will assume that we have a linear elastic, isotropic and homogeneous material. Since we have already assumed $\sigma_z = 0$, we have a plane stress condition and from mechanics of materials:

$$\sigma_x = \frac{E}{1-\nu^2}(\varepsilon_x + \nu\varepsilon_y) \tag{3.107-a}$$

$$\sigma_y = \frac{E}{1-\nu^2}(\varepsilon_y + \nu\varepsilon_x) \tag{3.107-b}$$

$$\tau_{xy} = G\gamma_{xy} \tag{3.107-c}$$

where the modulus of rigidity, $G = \frac{E}{2(1+\nu)}$.

Substituting the actual expressions for the strains, Eqs. 3.106-a, 3.106-b, and 3.106-c, we

obtain

$$\sigma_x = \frac{E}{1-\nu^2}[(\varepsilon_{x0} + \nu\varepsilon_{y0} - z(\chi_x + \nu\chi_y)] \quad (3.108\text{-a})$$

$$\sigma_y = \frac{E}{1-\nu^2}[(\varepsilon_{y0} + \nu\varepsilon_{x0} - z(\chi_y + \nu\chi_x)] \quad (3.108\text{-b})$$

$$\tau_{xy} = G(\gamma_{xy0} - 2z\chi_{xy}) \quad (3.108\text{-c})$$

Substituting the previous set of equations into the expressions for the force-stress relations, Eq. 3.52, integrating over h and neglecting the z/r_x and z/r_y terms when they appear next to unity, we obtain

$$N_x = K(\varepsilon_{x0} + \nu\varepsilon_{y0}) \quad (3.109\text{-a})$$

$$N_y = K(\varepsilon_{y0} + \nu\varepsilon_{x0}) \quad (3.109\text{-b})$$

$$N_{xy} = N_{yx0} = Gh\gamma_{xy0} \quad (3.109\text{-c})$$

$$M_x = -D(\chi_x + \nu\chi_y) \quad (3.109\text{-d})$$

$$M_y = -D(\chi_y + \nu\chi_x) \quad (3.109\text{-e})$$

$$M_{xy} = -M_{yx} = \frac{Gh^3}{6}\chi_{xy} = D(1-\nu)\chi_{xy} \quad (3.109\text{-f})$$

where

$$K = \frac{Eh}{1-\nu^2} \quad (3.110\text{-a})$$

$$D = \frac{Eh^3}{12(1-\nu^2)} \quad (3.110\text{-b})$$

K is axial rigidity and D the flexural rigidity, corresponding to EA and EI for the equivalent one dimensional problem. We note that K and D are larger than the corresponding one-dimensional constants by a factor $1-\nu^2$ which represents the increase in rigidity caused by restriction on lateral strains.

3.4.2.4 Final Equations

We now substitute the axial and flexural strains given by Eq. 3.102 into Eqs. 3.109-a through 3.109-f to obtain

$$\begin{aligned}
N_x &= K\left[\frac{1}{a_x}\frac{\partial u}{\partial \alpha_x} + \frac{v}{a_x a_y}\frac{\partial a_x}{\partial \alpha_y} - \frac{w}{r_x} + \nu\left(\frac{1}{a_y}\frac{\partial v}{\partial \alpha_y} + \frac{u}{a_x a_y}\frac{\partial a_y}{\partial \alpha_x} - \frac{w}{r_y}\right)\right] \\
N_y &= K\left[\frac{1}{a_y}\frac{\partial v}{\partial \alpha_y} + \frac{u}{a_x a_y}\frac{\partial a_y}{\partial \alpha_x} - \frac{w}{r_y} + \nu\left(\frac{1}{a_x}\frac{\partial u}{\partial \alpha_x} + \frac{v}{a_x a_y}\frac{\partial a_x}{\partial \alpha_y} - \frac{w}{r_x}\right)\right] \\
N_{xy} &= N_{yx} = Gh\left(\frac{1}{a_x}\frac{\partial v}{\partial \alpha_x} + \frac{1}{a_y}\frac{\partial u}{\partial \alpha_y} - \frac{u}{a_x a_y}\frac{\partial a_x}{\partial \alpha_y} - \frac{v}{a_x a_y}\frac{\partial a_y}{\partial \alpha_x} - \frac{2w}{r_{xy}}\right) \\
M_x &= -D\left[\frac{1}{a_x}\frac{\partial \phi_x}{\partial \alpha_x} + \frac{\phi_y}{a_x a_y}\frac{\partial a_x}{\partial \alpha_y} + \nu\left(\frac{1}{a_y}\frac{\partial \phi_y}{\partial \alpha_y} + \frac{\phi_x}{a_x a_y}\frac{\partial a_y}{\partial \alpha_x}\right)\right] \\
M_y &= -D\left[\frac{1}{a_y}\frac{\partial \phi_y}{\partial \alpha_y} + \frac{\phi_x}{a_x a_y}\frac{\partial a_y}{\partial \alpha_x} + \nu\left(\frac{1}{a_x}\frac{\partial \phi_x}{\partial \alpha_x} + \frac{\phi_y}{a_x a_y}\frac{\partial a_x}{\partial \alpha_y}\right)\right] \\
M_{xy} &= -M_{yx} = \frac{D(1-\nu)}{2}\left(\frac{1}{a_y}\frac{\partial \phi_x}{\partial \alpha_y} + \frac{1}{a_x}\frac{\partial \phi_y}{\partial \alpha_x} - \frac{\phi_x}{a_x a_y}\frac{\partial a_x}{\partial \alpha_y} - \frac{\phi_y}{a_x a_y}\frac{\partial a_y}{\partial \alpha_x}\right)
\end{aligned} \tag{3.111}$$

where we recall that from Eq. 3.97

$$\phi_x = \frac{u}{r_x} + \frac{\partial w}{a_x \partial \alpha_x} + \frac{v}{r_{xy}} \tag{3.112-a}$$

$$\phi_y = \frac{v}{r_y} + \frac{\partial w}{a_y \partial \alpha_y} + \frac{u}{r_{xy}} \tag{3.112-b}$$

These six equations contain three stress resultants (N_x, N_y, and N_{xy}), three stress couples (M_x, M_y, and M_{xy}) and three displacements (u, v and w). The five equations of equilibrium, Eq. 3.86, in turn contain eight unknowns: five stress resultants (N_x, N_y, N_{xy}, Q_x and Q_y), and three stress couples (M_x, M_y, and M_{xy}). When those two sets of equations are comnined together, we have a total of 11 equations with 11 unknowns (N_x, N_y, N_{xy}, Q_x, Q_y, M_x, M_y, and M_{xy}, u, v and w). Thus the problem is properly defined and a complete solution is possible.

3.4.2.5 Summary

Table 3.2 summarizes some of the major equations governing thin shells.

3.4.3 Simplifications

The derivation of the analysis discussed in the previous section (11 equations - 11 unknowns) can be used to solve the stresses and displacements for any type of thin elastic shell. However,

Kinematic

$$\underbrace{\begin{Bmatrix} \epsilon_{x0} \\ \epsilon_{y0} \\ \gamma_{xy0} \end{Bmatrix}}_{\boldsymbol{\varepsilon}} = \underbrace{\frac{1}{a_x a_y} \begin{bmatrix} a_y \frac{\partial}{\partial \alpha_x} & \frac{\partial a_x}{\partial \alpha_y} & -\frac{a_x a_y}{r_x} \\ \frac{\partial a_y}{\partial \alpha_x} & a_x \frac{\partial}{\partial \alpha_y} & -\frac{a_x a_y}{r_y} \\ a_x \frac{\partial}{\partial \alpha_y} - \frac{\partial a_x}{\partial \alpha_y} & a_y \frac{\partial}{\partial \alpha_x} - \frac{\partial a_y}{\partial \alpha)_x} & -\frac{2 a_x a_y}{r_{xy}} \end{bmatrix}}_{\mathbf{L}} \underbrace{\begin{Bmatrix} u \\ v \\ w \end{Bmatrix}}_{\mathbf{u}}$$

$$\underbrace{\begin{Bmatrix} \chi_{xx} \\ \chi_{yy} \\ 2\chi_{xy} \end{Bmatrix}}_{\boldsymbol{\chi}} = \underbrace{\frac{1}{a_x a_y} \begin{bmatrix} a_y \frac{\partial}{\partial \alpha_x} & \frac{\partial a_x}{\partial \alpha_y} \\ \frac{\partial a_y}{\partial \alpha_x} & a_x \frac{\partial}{\partial \alpha_y} \\ a_x \frac{\partial}{\partial \alpha_y} - \frac{\partial a_x}{\partial \alpha_y} & a_y \frac{\partial}{\partial \alpha_x} - \frac{\partial a_y}{\partial \alpha_x} \end{bmatrix}}_{\mathbf{L}} \underbrace{\begin{Bmatrix} \theta_{xx} \\ \theta_{yy} \end{Bmatrix}}_{\boldsymbol{\theta}}$$

Equilibrium

$$\underbrace{\begin{bmatrix} \frac{\partial}{\partial \alpha_x}(a_y) & -\frac{\partial a_y}{\partial \alpha_x} & \frac{\partial a_x}{\partial \alpha_x} + \frac{\partial}{\partial \alpha_y}(a_x) & 0 & 0 & 0 \\ -\frac{\partial a_x}{\partial \alpha_y} & \frac{\partial}{\partial \alpha_y}(a_x) & \frac{\partial a_y}{\partial \alpha_x} + \frac{\partial}{\partial \alpha_x}(a_y) & 0 & 0 & 0 \\ \frac{a_x}{r_x} a_y & \frac{a_y}{r_y} a_x & \frac{a_x}{r_{xy}} a_y + \frac{a_y}{r_{xy}} a_x & 0 & 0 & 0 \\ 0 & 0 & 0 & \frac{\partial a_x}{\partial \alpha_y} & -\frac{\partial}{\partial \alpha_y}(a_x) & \frac{\partial}{\partial \alpha_x}(a_y) - \frac{\partial a_y}{\partial \alpha_x} \\ 0 & 0 & 0 & -\frac{\partial}{\partial \alpha_x}(a_y) & \frac{\partial a_y}{\partial \alpha_x} & \frac{\partial a_x}{\partial \alpha_y} - \frac{\partial}{\partial \alpha_y}(a_x) \end{bmatrix}}_{\mathbf{L}^T} \underbrace{\begin{Bmatrix} N_{xx} \\ N_{yy} \\ N_{xy} \\ M_{xx} \\ M_{yy} \\ M_{xy} \end{Bmatrix}}_{\mathbf{M}} + a_x a_y \underbrace{\begin{bmatrix} 1 & 0 & 0 & -\frac{1}{r_x} & -\frac{1}{r_{xy}} \\ 0 & 1 & 0 & -\frac{1}{r_{xy}} & -\frac{1}{r_y} \\ 0 & 0 & 1 & \frac{\partial}{\partial \alpha_x}(a_y) & \frac{\partial}{\partial \alpha_y}(a_x) \\ 0 & 0 & 0 & 0 & 1 \\ 0 & 0 & 0 & 1 & 0 \end{bmatrix}}_{\mathbf{b}} \underbrace{\begin{Bmatrix} P_{xx} \\ P_{yy} \\ P_{zz} \\ Q_{xx} \\ Q_{yy} \end{Bmatrix}}_{\rho} = 0$$

Constitutive

$$\underbrace{\begin{Bmatrix} \sigma_{xx} \\ \sigma_{yy} \\ \tau_{xy} \end{Bmatrix}}_{\boldsymbol{\sigma}} = \beta \underbrace{\begin{bmatrix} 1 & \nu & 0 & -z & -z\nu & 0 \\ \nu & 1 & 0 & -z\nu & -z & 0 \\ 0 & 0 & \frac{1}{\beta} & 0 & 0 & \frac{-2z}{\beta} \end{bmatrix}}_{\mathbf{D}} \underbrace{\begin{Bmatrix} \epsilon_{xx0} \\ \epsilon_{yy0} \\ \gamma_{xy0} \\ \chi_{xx} \\ \chi_{yy} \\ \chi_{xy} \end{Bmatrix}}_{\boldsymbol{\kappa}}$$

$$\beta = \frac{E}{1-\nu^2}$$

Table 3.2: Summary of major governing equations in thin shells

even an analysis of this sort can be extremely complicated for even the simplest thin shell systems. Thus, shell design has often utilized two types of simplifications to ease the analysis.

The first type of simplification is of the mathematical formulations. Often we assume or prove certain terms of relative unimportance and remove these terms from the equation of interest. This has already been performed in Sec. 3.4.2 by neglecting the terms z/r when they appear with unity, along with the assumption of plane stress, $\sigma_z = 0$. The purpose of this simplification is to reduce the number of terms while still obtaining a reasonable mathematical solution.

The second type of simplification is of the physical formulations. Often we can assume a specific structural action to ease the analysis. This assumption can be used to replace the shell system with an equivalent simpler structure. This new, simpler structure is then utilized for analysis of the complex one.

These simplifications are desirable for RC design where precise analysis is not justified due to a lack of construction accuracy. Even so, it is vital for the designer to understand the real structural action obtained only through the physical features of the system and the corresponding mathematical formulation.

Two simplified theories of analysis are considered, the theory of shallow shells and membrane theory, and will be presented in the sections to follow.

3.4.4 Shallow Shells

Shallow shells is the first of two simplified shell theories we will review. The following will utilize both simplifications of mathematical and physical system formulations discussed in the previous section.

3.4.4.1 Assumptions

Shallow shell theory will utilize the following assumptions:

(1) The shell's slope is small compared to some reference plane (often the horizontal plane for roofs).

(2) The surface curvature is small.

(3) The shell boundaries are such that the surface loads are carried by in-plane stress resultants (N_x, N_y and N_{xy}). Therefore the transverse deflections will be much greater than the in-plane deflections.

(4) The changes in curvature of the surface are small.

3.4.4.2 Application of Assumptions

We will now apply these assumptions to Eqs. 3.86 and 3.111. Assumption 1 allows us to neglect the radial component of loading. From assumption 2, the terms containing Q in the first two of Eq. 3.86 and N in the third of Eq. 3.86 are small. This also applies to the terms with w in the first three of Eq. 3.111 and the u and v terms in the last three of 3.111. However, we cannot just drop these terms without first considering the third assumption.

Assumption 3 relates the shell to a flat arch, which, under uniform loading, the axial stress and vertical displacements control. Meaning, the small transverse components of the in-plane stress resultants, in the third of Eq. 3.86, are not negligible in comparing the change in the transverse shear resultant.

Combining assumptions 2 and 3 together, we can drop Q from the first two terms of Eq. 3.86 but not N from the third. From Eq. 3.111 we are allowed to drop the effect of in-plane displacements (u and v terms) on stress couples but not the effect of displacement (w terms) on in-plane stress resultants. Assumption 4 allows us to take a_x and a_y as constants.

Eqs. 3.86 and 3.111 can be rewritten as:

$$\frac{1}{a_x}\frac{\partial N_x}{\partial \alpha_x} + \frac{1}{a_y}\frac{\partial N_{yx}}{\partial \alpha_y} + p_x = 0 \tag{3.113-a}$$

$$\frac{1}{a_y}\frac{\partial N_y}{\partial \alpha_y} + \frac{1}{a_x}\frac{\partial N_{xy}}{\partial \alpha_x} + p_y = 0 \tag{3.113-b}$$

$$\frac{1}{a_x}\frac{\partial Q_x}{\partial \alpha_x} + \frac{1}{a_y}\frac{\partial Q_y}{\partial \alpha_y} + \frac{N_x}{r_x} + \frac{2N_{xy}}{r_{xy}} + \frac{N_y}{r_y} + p_z = 0 \tag{3.113-c}$$

$$-\frac{1}{a_y}\frac{\partial M_y}{\partial \alpha_y} + \frac{1}{a_x}\frac{\partial M_{xy}}{\partial \alpha_x} + Q_y = 0 \tag{3.113-d}$$

$$-\frac{1}{a_x}\frac{\partial M_x}{\partial \alpha_x} - \frac{1}{a_y}\frac{\partial M_{yx}}{\partial \alpha_y} + Q_x = 0 \tag{3.113-e}$$

$$N_x = K\left[\frac{1}{a_x}\frac{\partial u}{\partial \alpha_x} - \frac{w}{r_x} + \nu\left(\frac{1}{a_y}\frac{\partial v}{\partial \alpha_y} - \frac{w}{r_y}\right)\right] \tag{3.113-f}$$

$$N_y = K\left[\frac{1}{a_y}\frac{\partial v}{\partial \alpha_y} - \frac{w}{r_y} + \nu\left(\frac{1}{a_x}\frac{\partial u}{\partial \alpha_x} - \frac{w}{r_x}\right)\right] \tag{3.113-g}$$

$$N_{xy} = N_{yx} = Gh\left(\frac{1}{a_x}\frac{\partial v}{\partial \alpha_x} + \frac{1}{a_y}\frac{\partial u}{\partial \alpha_y} - \frac{2w}{r_{xy}}\right) \tag{3.113-h}$$

$$M_x = -D\left(\frac{1}{a_x^2}\frac{\partial^2 w}{\partial \alpha_x^2} + \nu\frac{1}{a_y^2}\frac{\partial^2 w}{\partial \alpha_y^2}\right) \tag{3.113-i}$$

$$M_y = -D\left(\frac{1}{a_y^2}\frac{\partial^2 w}{\partial \alpha_y^2} + \nu\frac{1}{a_x^2}\frac{\partial^2 w}{\partial \alpha_x^2}\right) \tag{3.113-j}$$

$$M_{xy} = -M_{yx} = D(1-\nu)\left(\frac{1}{a_x a_y}\frac{\partial^2 w}{\partial \alpha_x \partial \alpha_y}\right) \tag{3.113-k}$$

We observe that we have separate deep-beam and slab equations, paired by the N terms in Eq. 3.113-c and the w terms in 3.113-f through 3.113-h. Eqs. 3.113-a and 3.113-b are expressions for a plate loaded in its plane (deep-beam equations). Eqs. 3.113-f through 3.113-h are also deep-beam equations except for the w terms. Eqs. 3.113-i through 3.113-k are expressions for a laterally loaded plate (bent slab). Eqs. 3.113-c through 3.113-e are also slab equations except for the N terms in 3.113-c.

3.4.4.3 Deep Beam Equation

We will now combine the above expressions into a single shallow shell expression. But first, we must derive the deep beam and slab equations. From Eqs. 3.113-f, 3.113-g and 3.113-h

$$N_x - \nu N_y = K(1-\nu^2)\left(\frac{1}{a_x}\frac{\partial u}{\partial \alpha_x} - \frac{w}{r_x}\right) \tag{3.114-a}$$

$$N_y - \nu N_x = K(1-\nu^2)\left(\frac{1}{a_y}\frac{\partial v}{\partial \alpha_y} - \frac{w}{r_y}\right) \tag{3.114-b}$$

$$2(1+\nu)N_{xy} = K(1-\nu^2)\left(\frac{1}{a_x}\frac{\partial v}{\partial \alpha_x} + \frac{1}{a_y}\frac{\partial u}{\partial \alpha_y} - \frac{2w}{r_{xy}}\right) \tag{3.114-c}$$

Differentiated twice and combined, we obtain

$$\begin{aligned}&\frac{1}{a_y^2}\frac{\partial^2(N_x-\nu N_y)}{\partial \alpha_y^2} - \frac{2(1+\nu)}{a_x a_y}\frac{\partial^2 N_{xy}}{\partial \alpha_x \partial \alpha_y} + \frac{1}{a_x^2}\frac{\partial^2(N_y-\nu N_x)}{\partial \alpha_x^2} \\ &= -K(1-\nu^2)\left[\frac{1}{a_x^2}\frac{\partial^2}{\partial \alpha_x^2}\left(\frac{w}{r_y}\right) - \frac{2}{a_x a_y}\frac{\partial^2}{\partial \alpha_x \partial \alpha_y}\left(\frac{w}{r_{xy}}\right) + \frac{1}{a_y^2}\frac{\partial^2}{\partial \alpha_y^2}\left(\frac{w}{r_x}\right)\right]\end{aligned} \tag{3.115}$$

When r_x, r_y and r_{xy} are assumed constant, we set

$$\Delta_R^2 w = \left(\frac{1}{r_y a_x^2}\frac{\partial^2}{\partial \alpha_x^2} - \frac{2}{r_{xy} a_x a_y}\frac{\partial^2}{\partial \alpha_x \partial \alpha_y} + \frac{1}{r_x a_y^2}\frac{\partial^2}{\partial \alpha_y^2}\right) w \tag{3.116}$$

Replacing the stress resultants with the following stress functions

$$N_x = \frac{1}{a_y^2}\frac{\partial^2 F}{\partial \alpha_y^2} - \int p_x a_x d\alpha_x \tag{3.117-a}$$

$$N_y = \frac{1}{a_x^2}\frac{\partial^2 F}{\partial \alpha_x^2} - \int p_y a_y d\alpha_y \tag{3.117-b}$$

$$N_{xy} = -\frac{1}{a_x a_y}\frac{\partial^2 F}{\partial \alpha_x \partial \alpha_y} \tag{3.117-c}$$

and substituting into Eq. 3.115, we arrive at our differential equation for deep beams

$$\Delta^4 F + K(1-\nu^2)\Delta_R^2 w = \int \frac{1}{a_y^2}\frac{\partial^2 p_x}{\partial \alpha_y^2} a_x d\alpha_x + \int \frac{1}{a_x^2}\frac{\partial^2 p_y}{\partial \alpha_x^2} a_y d\alpha_y - \nu\frac{1}{a_x}\frac{\partial p_x}{\partial \alpha_x} - \nu\frac{1}{a_y}\frac{\partial p_y}{\partial \alpha_y} \tag{3.118}$$

where

$$\Delta^4 F = \left(\frac{1}{a_x^4}\frac{\partial^4}{\partial \alpha_x^4} + \frac{2}{a_x^2 a_y^2}\frac{\partial^4}{\partial \alpha_x^2 \partial \alpha_y^2} + \frac{1}{a_y^4}\frac{\partial^4}{\partial \alpha_y^4}\right) F \tag{3.119}$$

If $r_x = r_y = r_{xy} = \infty$, $a_x d\alpha_x = dx$, and $a_y d\alpha_y = dy$, and $p_x = p_y = 0$, Eq. 3.118 reduces to

$$\Delta^4 F = 0 \tag{3.120}$$

3.4.4.4 Slab Equation

In deriving the slab equation, we will first substitute the values of Q_x and Q_y from Eqs. 3.113-d and 3.113-e into Eq. 3.113-c to create the combined equation

$$\frac{1}{a_x^2}\frac{\partial^2 M_x}{\partial \alpha_x^2} - 2\frac{1}{a_x a_y}\frac{\partial^2 M_{xy}}{\partial \alpha_x \partial \alpha_y} + \frac{1}{a_y^2}\frac{\partial^2 M_y}{\partial \alpha_y^2} + \frac{N_x}{r_x} + \frac{2N_{xy}}{r_{xy}} + \frac{N_y}{r_y} + p_z = 0 \tag{3.121}$$

We next substitute Eqs. 3.113-i, 3.113-j and 3.113-k into 3.121 to obtain

$$-\Delta^4 w + \frac{1}{D}\left(\frac{N_x}{r_x} + \frac{2N_{xy}}{r_{xy}} + \frac{N_y}{r_y}\right) = -\frac{p_z}{D} \tag{3.122}$$

Once again, we will insert the stress functions of Eqs. 3.117-a, 3.117-b and 3.117-c into our differential equation 3.122 to generate the bent slab differential equation

$$\Delta^4 w - \frac{1}{D}\Delta_R^2 F = \frac{p_z}{D} - \frac{1}{D}\left(\frac{1}{r_x}\int p_x a_x d\alpha_x + \frac{1}{r_y}\int p_y a_y d\alpha_y\right) \tag{3.123}$$

If $r_x = r_y = r_{xy} = \infty$, Eq. 3.123 reduces to

$$\Delta^4 w = \frac{p_z}{D} \tag{3.124}$$

3.4.4.5 Equation for Shallow Shells

The differential equations of deep beam (3.118) and bent slab (3.123) are required to solve the problem of shallow shells. The simultaneous differential equations can be rewritten in the form of

$$\Delta^4 F + K(1-\nu^2)\Delta_R^2 w = f(p) \tag{3.125}$$

$$\Delta^4 w - \frac{1}{D}\Delta_R^2 F = f'(p) \tag{3.126}$$

where $f(p)$ and $f'(p)$ are the right sides of Eqs. 3.118 and 3.123. If we operate on Eq. 3.125 by Δ^4 and on Eq. 3.126 by $K(1-\nu^2)\Delta_R^2$, and combine we obtain

$$\Delta^8 F + \frac{12(1-\nu^2}{h^2}\Delta_R^4 F = \Delta^4 f(p) + K(1-\nu^2)\Delta_R^2 f' p \tag{3.127}$$

However, if we operate on Eq. 3.125 by $(1/D)\Delta_R^2$ and on Eq. 3.126 by Δ^4 and combine, we obtain the solution for shallow shells

$$\Delta^8 w + \frac{12(1-\nu^2)}{h^2}\Delta_R^4 w = \frac{1}{D}\Delta_R^2 f(p) + \Delta^4 f'(p) \tag{3.128}$$

3.4.5 Membrane Theory

Membrane theory is the second simplified method we will review. However, we will focus more on the assumptions and theory than the methodology.

3.4.5.1 Assumptions

Membrane theory will utilize the following assumptions:

(1) All bending in the shell is neglected. Therefore Eq. 3.86 becomes

$$\begin{aligned} \frac{\partial(N'_x a_y)}{\partial\alpha_x} - N'_y\frac{\partial a_y}{\partial\alpha_x} + N'_{xy}\frac{\partial a_x}{\partial\alpha_y} + \frac{\partial(N'_{yx}a_x)}{\partial\alpha_y} + p_x a_x a_y = 0 \\ \frac{\partial(N'_y a_x)}{\partial\alpha_y} - N'_x\frac{\partial a_x}{\partial\alpha_y} + N'_{yx}\frac{\partial a_y}{\partial\alpha_x} + \frac{\partial(N'_{xy}a_y)}{\partial\alpha_x} + p_y a_x a_y = 0 \\ \frac{N'_x}{r_x} + \frac{N'_{xy}}{r_{xy}} + \frac{N'_{yx}}{r_{xy}} + \frac{N'_y}{r_y} + p_z = 0 \end{aligned} \tag{3.129}$$

(2) Since we assume $N_{xy} = N_{yx}$, the three equations above only have three unknowns N'_x, N'_y and $N'_{xy} = N'_{yx}$. The prime marks indicate the values are approximate.

(3) All membrane stresses act in the plane of the shell.

3.4.5.2 Theory

The membrane theory can provide a reasonable design basis if the following conditions are fullfilled:

(1) The displacement due to membrane stress resultants does not increase shell bending substantially. Previous assumptions state that all bending in the shell is neglected.

(2) A uniform load distribution must be seen over entire shell surface.

(3) The boundaries can supply the forces and permit the displacements required by the membrane stress resultants.

Usually membrane theory is insufficient but may be found useful for hemispherical roofs or cylindrical tanks.

3.4.6 Classification

Thin shells can be classified into three main categories. The basis of this classification comes from gaussian curvature. Synclastic shells are those of positive gaussian curvature and are formed by two families of curves both with the same direction. Singly curved shells are those of zero gaussian curvature and are formed by one family of curves. Finally, anticlastic shells are those of negative curvature and are formed by tow families of curves of opposite direction.

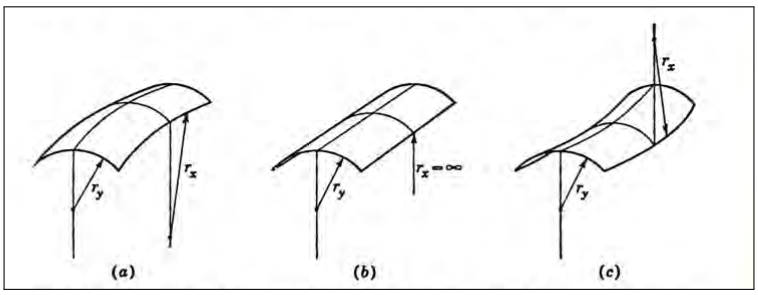

Figure 3.18: (a) Shell of positive gaussian curvature. (b) Shell of zero gaussian curvature. (c) Shell of negative gaussian curvature, (Billington, 1965)

The main property difference between the three categories is the propagation of edge effects into the shells. In synclastic shells, the edge effects often damp rapidly and are restricted to a narrow near edge zone. This property allows for valid use of the membrane theory throughout the entire shell except at the boundaries. In singly curved shells, the edge effects are damped similar to the synclastic shell, but propagate farther into the shell away from the edge. In anticlastic shells, the damping is much smaller than the other two allowing boundary effects to control over majority

of the shell.

Another type of classification defines the shell systems as either rotational or translational. Domes and tanks are often classified as rotational systems, while cylindrical barrels, elliptical paraboloids and hyperbolic paraboloids are considered translational.

3.4.7 Conclusion

We have now introduced the derivations of the differential equations of a beam and plate subject to flexure, along with the discussion of shells. Building up from the basics of a beam, we progressed to the plate, and finally began the discussion of thin shells.

Now that we fully understand thin shells and have derived some of the basic differential equations, we can now shift our focus to the actual analysis of a system. In the upcoming section, we will begin our discussion on circular cylindrical shells, including an in depth discussion of the analysis and design.

Chapter 4

Analysis of Circular Cylindrical Shells

4.1 Introduction

This chapter focuses on the analysis of a circular cylindrical shell using both the theories of shallow shells and membrane theory. The analysis focuses exclusively on a simply supported shell with edge beams. The stress resultants, stress couples, and displacements are first derived via membrane theory, and repeated utilizing the theory of shallow shells. Given the results from both shallow shells and membrane theory, a discussion comparing the two theories and the results follows.

The chapter continues with the methodology of bending theory. In this section, our eighth order differential equation is derived and solved to determine all eight arbitrary constants. These constants can then be substituted into the equations for the stress resultants, couples, and displacements. Given the finalized stresses and displacements, the chapter concludes with the addition of the edge beam and the derivation of the equation of compatibility required to combine the shell and beam. Both the vertical and horizontal beam cases are discussed.

4.2 Circular Cylindrical Shell

Circular cylindrical shells or barrel vaults are often "defined as a curved slab...cut from a full cylinder" (Billington, 1965). The slab is curved in only one direction and thus may be classified as a singly curved shell as discussed in the previous chapter. The shell consists of two straight longitudinal edges and two curved transverse edges. The basic structure and shape of the shell can

be seen in the Figs. 4.1 and 4.2.

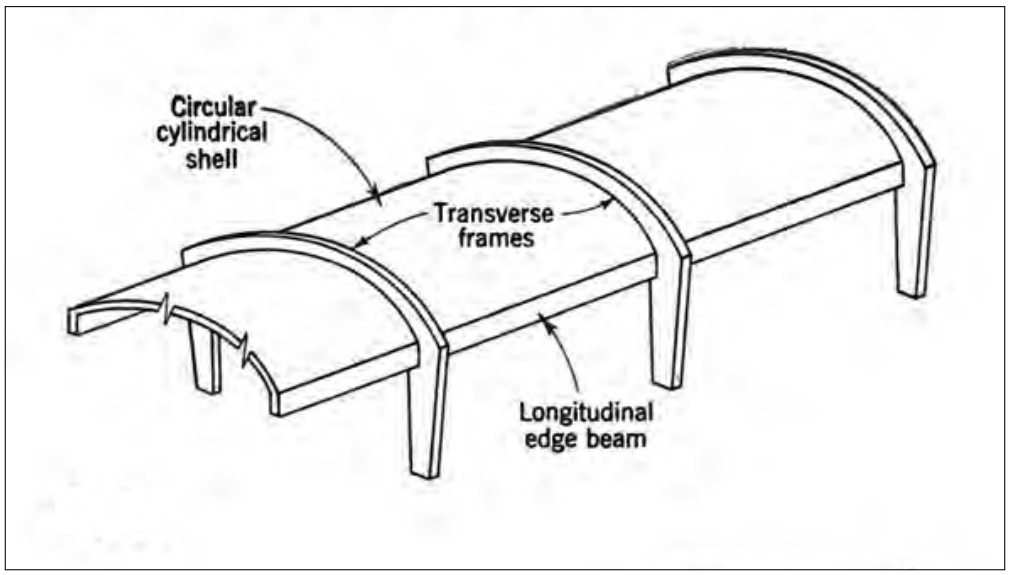

Figure 4.1: Circular Cylindrical Shell Structure,(Billington, 1965)

Three categories are available for describing cylindrical shells. The class is dependent upon the ratio of transverse radius and longitudinal length, r/L. The ratio categories can vary depending upon the source. Common classification consists of long, intermediate and short.

4.3 Simply Supported Shell

The analysis of the circular cylindrical shell will be conducted for the case of a simply supported shell with all boundary conditions along the straight longitudinal edge satisfied. The procedure for analysis focuses on four key items and are as follows:

Primary System : This is obtained by reducing the general theory to membrane theory. Through membrane theory, the surface loads are resisted solely by stress resultants.

Errors : These correspond to the incompatible edge effects, or forces required by membrane theory at the free edges.

Corrections : Line loads (unit edge effects) are applied along the free edges.

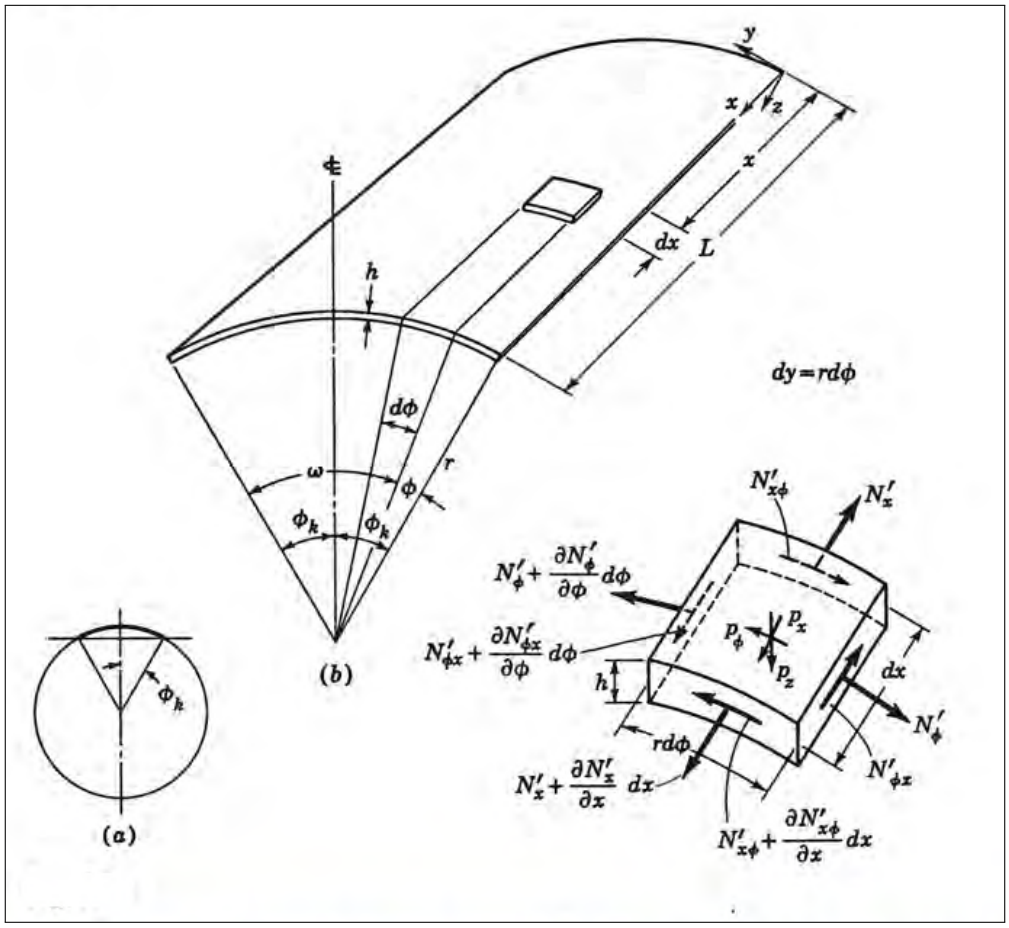

Figure 4.2: Typical Cylindrical Shell Section, (Billington, 1965)

Compatibility : Equilibrium can be achieved by determining the number of corrections required to remove the errors of membrane theory. In our example, we will set the line loads equal to the membrane stress resultants along the free edge.

4.3.1 Membrane Theory

Prior to examining a full analysis conducted through shallow shells, we will first examine the membrane theory. However, we will only focus on the derivations of the stress resultants and displacements.

4.3.1.1 Stress Resultants

The general stress resultants are derived from Eq. 3.129. The equations reduce to

$$\begin{aligned} \frac{\partial N'_\theta}{\partial \theta} + r\frac{\partial N'_{y\theta}}{\partial y} + p_\theta r = 0 \\ r\frac{\partial N'_y}{\partial y} + \frac{\partial N'_{\theta y}}{\partial \theta} + p_y r = 0 \\ \frac{N'_\theta}{r} + p_z = 0 \end{aligned} \tag{4.1}$$

with the following circular cylindrical shell definitions:

$$\begin{aligned} &\alpha_x = \theta \quad a_x = r \quad r_x = r \quad N'_{xy} = N'_{\theta y} \\ &\alpha_y = y \quad a_y = 1 \quad r_y = \infty \quad N'_x = N'_\theta \end{aligned} \tag{4.2}$$

where r is a constant. The equations of 4.1 are rewritten to the form of

$$\begin{aligned} N'_\phi &= -p_z r \\ N'_{x\phi} &= -\tfrac{1}{r}\int \frac{\partial N'_\phi}{\partial \phi} dx - \int p_\phi dx + f_1(\phi) \\ N'_x &= -\tfrac{1}{r}\int \frac{\partial N'_{\phi x}}{\partial \phi} dx - \int p_x dx + f_2(\phi) \end{aligned} \tag{4.3}$$

when the following definitions are prescribed:

$$\begin{aligned} &\alpha_x = x \quad a_x = 1 \quad r_x = \infty \quad r_{xy} = \infty \quad N'_{xy} = N'_{x\phi} \\ &\alpha_y = \phi \quad a_y = r \quad r_y = r \quad N'_y = N'_\phi \quad p_y = p_\phi \end{aligned} \tag{4.4}$$

where r is a constant and ϕ is measured from the longitudinal edge.

The stress resultant expressions are now written in the form of three equations with three unknowns N'_ϕ, N'_x and $N'_{x\phi} = N'_{\phi x}$ and the primary system is established. It must be noted, as per the errors stage of the analysis, that longitudinal edge reactions must equal the membrane values of N'_ϕ and $N'_{x\phi}$ in order for the membrane theory to produce the correct internal stress resultants. However, at the free edges of the shell, these reactions are zero.

The required edge reaction forces can be seen in Fig. 4.3(a). In order to account for the lack of free edge reaction forces, we must apply corrections or line loads, Fig. 4.3(b). In order to find the true resultant reactions and achieve equilibrium, line loads $T_L = -N'_\phi$ and $S_L = -N'_{x\phi}$ must be applied.

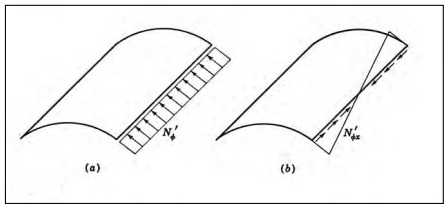

(a) Required Edge Reactions, (Billington, 1965)

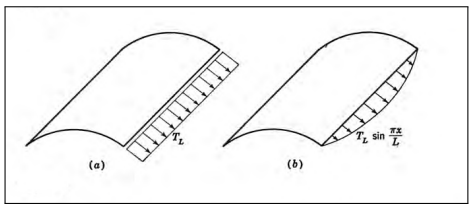

(b) Applied Line Load, (Billington, 1965)

Bending Theory must be considered to determine the displacements and internal forces produced from the line loads in the corrections phase of the analysis. For simplicity, uniformly distributed line loads can be assumed as a sum of partial loads and represented by a Fourier series.

$$(T_L)_x = \frac{4}{\pi} T_L \sum_{n=1,3,5\ldots}^{\infty} \frac{1}{n} \sin \frac{n\pi x}{L} \tag{4.5}$$

The first three terms of the series are plotted and can be seen in Fig. 4.3. The three waves together closely assimilate a uniform load. The first term is often considered sufficient for long shells. However, short shells often require the addition of the second term. This methodology will be discussed in more detail in Sec. 4.3.2.

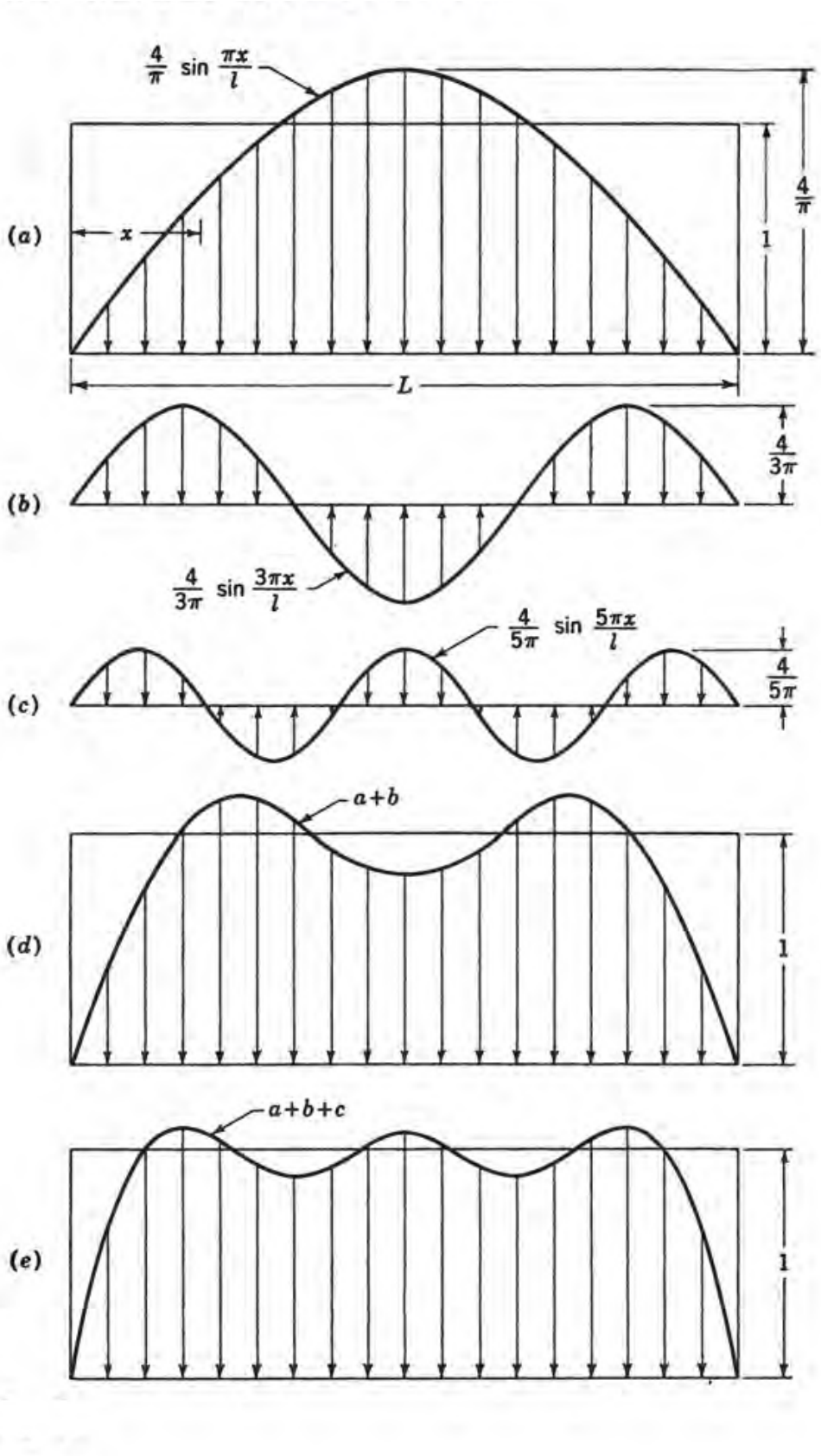

Figure 4.3: Sine Series Plot, (Billington, 1965)

4.3.1.2 Displacements

The derivation of the displacement equations from membrane theory requires recalling the middle surface strains from Sec. 3.4.2.2 (Eqs. 3.87, 3.88 and 3.89). Utilizing the circular cylindrical shell definitions (4.4), the strains can be rewritten as

$$\begin{aligned} \epsilon_x &= \tfrac{\partial u}{\partial x} \\ \epsilon_y = \epsilon_\phi &= \tfrac{\partial v}{r\partial \phi} - \tfrac{w}{r} \\ \gamma_{x\phi} &= \tfrac{\partial v}{\partial x} + \tfrac{\partial u}{r\partial \phi} \end{aligned} \tag{4.6}$$

The strains may be rewritten once more to accommodate membrane stress resultants

$$\begin{aligned} \epsilon_x = \tfrac{\partial u}{\partial x} &= \tfrac{1}{Eh}\left(N'_x - \nu N'_\phi\right) \\ \epsilon_y = \epsilon_\phi = \tfrac{\partial v}{r\partial \phi} - \tfrac{w}{r} &= \tfrac{1}{Eh}\left(N'_\phi - \nu N'_x\right) \\ \gamma_{x\phi} = \tfrac{\partial v}{\partial x} + \tfrac{\partial u}{r\partial \phi} &= \tfrac{2(1+\nu)}{Eh} N'_{x\phi} \end{aligned} \tag{4.7}$$

Since ν has minimal impact on the deformations, it is neglected to simplify the displacement equations. The first term of Eq. 4.7 is solved for the longitudinal displacement

$$u = \frac{1}{Eh}\int N'_x dx + f_3(\phi) \tag{4.8}$$

The third term is solved for the tangential displacement equation

$$v = -\frac{1}{r}\int \frac{\partial u}{\partial \phi} dx + \frac{2}{Eh}\int N'_{x\phi} dx + f_4(\phi) \tag{4.9}$$

and the radial displacement is obtained from the second

$$w = \frac{\partial v}{\partial \phi} - \frac{rN'_\phi}{Eh} \tag{4.10}$$

In order to determine the vertical and horizontal displacements, the following relations must be considered.

$$\begin{aligned} \Delta_V &= -v\sin(\phi_k - \phi) + w\cos(\phi_k - \phi) \\ \Delta_H &= v\cos(\phi_k - \phi) + w\sin(\phi_k - \phi) \end{aligned} \tag{4.11}$$

where Δ_V can be written in the form of

$$\Delta_V = \frac{L^4}{r^3 hE}\left\{pr\left[\left(\frac{2r}{\pi L}\right)^2 + \frac{2}{\pi^4} + \left(\frac{r}{L}\right)^4 \cos^2(\phi_k - \phi)\right]\right\}\sin kx \tag{4.12}$$

and Δ_H is

$$\Delta_H = \frac{pr^2}{Eh}\sin(\phi_k - \phi)\cos(\phi_k - \phi)\sin kx \tag{4.13}$$

where Δ_V is positive for downward displacement and Δ_H is positive for inward displacement.

4.3.2 Theory of Shallow Shells

Before performing the analysis through the theory of shallow shells, we must first rederive the equations of the stress resultants and couples along with the equations of equilibrium to accommodate the properties of the circular cylindrical shell. The equations of equilibrium (3.86) were previously derived for shallow shell theory in Sec. 3.4.4. Utilizing the definition for a cylindrical shell (4.4), the equations of equilibrium become

$$\begin{aligned}
\tfrac{\partial N_x}{\partial x}r + \tfrac{\partial_{\phi x}}{\partial \phi} + p_x r &= 0 \\
\tfrac{\partial N_\phi}{\partial \phi} + \tfrac{\partial N_{x\phi}}{\partial x}r - Q_\phi + p_\phi r &= 0 \\
\tfrac{\partial Q_x}{\partial x}r + \tfrac{\partial Q_\phi}{\partial \phi} + N_\phi + p_x r &= 0 \\
-\tfrac{\partial M_\phi}{\partial \phi} + \tfrac{\partial M_{x\phi}}{\partial x}r + Q_\phi r &= 0 \\
-\tfrac{\partial M_x}{\partial x}r - \tfrac{\partial M_{\phi x}}{\partial \phi} + Q_x r &= 0
\end{aligned} \tag{4.14}$$

The stress resultants and stress couples, Eq. 3.111, were also previously derived in Sec. 3.4.4. Once again, the equations are modified to account for the cylindrical shell properties

$$\begin{aligned}
N_x &= Eh\tfrac{\partial u}{\partial x} \\
N_\phi &= Eh\left(\tfrac{\partial v}{r\partial \phi} - \tfrac{w}{r}\right) \\
N_{x\phi} = N_{\phi x} &= \tfrac{Eh}{2}\left(\tfrac{\partial v}{\partial x} + \tfrac{\partial u}{r\partial \phi}\right) \\
M_x &= -\tfrac{Eh^3}{12}\tfrac{\partial^2 w}{\partial x^2} \\
M_\phi &= -\tfrac{Eh^3}{12}\left(\tfrac{\partial v}{r^2\partial \phi} + \tfrac{\partial^2 w}{r^2\partial \phi^2}\right) \\
M_{x\phi} = -M_{\phi x} &= \tfrac{Eh^3}{12}\left(\tfrac{\partial v}{2r\partial x} + \tfrac{\partial^2 w}{r\partial x\partial \phi}\right)
\end{aligned} \tag{4.15}$$

where

$$\phi_x = \frac{\partial w}{\partial x} \quad \phi_y = \frac{v}{r} + \frac{\partial w}{r\partial \phi} \quad \nu = 0$$

Now that we have rederived all 11 equations, we can begin the derivation of the single eighth-order partial differential equation using the theory of shallow shells. We will ultimately reduce the 11 equations to one equation with one unknown.

We will first recall the assumptions for shallow shells presented in Sec. 3.4.4.1. All stress couples must be expressed in terms of the radial displacement. This is achieved by neglecting the terms with v in Eq. 4.15

$$\begin{aligned} M_x &= -\frac{Eh^3}{12}\frac{\partial^2 w}{\partial x^2} \\ M_\phi &= -\frac{Eh^3}{12}\left(\frac{\partial^2 w}{r^2\partial \phi^2}\right) \\ M_{x\phi} &= -M_{\phi x} = \frac{Eh^3}{12}\left(\frac{\partial^2 w}{r\partial x \partial \phi}\right) \end{aligned} \tag{4.16}$$

We will next rewrite the radial shear stress resultants from Eq. 4.14 in terms of w

$$\begin{aligned} Q_\phi &= -\frac{Eh^3}{12}\left(\frac{\partial^3 w}{r^3\partial \phi^3} + \frac{\partial^3 w}{r\partial x^2 \partial \phi}\right) \\ Q_x &= -\frac{Eh^3}{12}\left(\frac{\partial^3 w}{\partial x^3} + \frac{\partial^3 w}{r^2\partial x \partial \phi^2}\right) \end{aligned} \tag{4.17}$$

where h and r are constants. All other stress resultants can now be written in terms of w by substituting Eq. 4.17 into the third equation of 4.14, obtaining

$$N_\phi = \frac{Eh^3}{12}\left(r\frac{\partial^4 w}{\partial x^4} + \frac{2}{r}\frac{\partial^4 w}{\partial x^2 \partial \phi^2} + \frac{1}{r^3}\frac{\partial^4 w}{\partial \phi^4}\right) - p_z r \tag{4.18}$$

In turn, we substitute N_ϕ into the second equation of 4.14. If we drop Q_ϕ, due to the assumption 2, we obtain

$$\frac{\partial N_{x\phi}}{\partial x} = -\frac{Eh^3}{12}\left(\frac{\partial^5 w}{\partial x^4 \partial \phi} + \frac{2}{r^2}\frac{\partial^5 w}{\partial x^2 \partial \phi^3} + \frac{1}{r^4}\frac{\partial^5 w}{\partial \phi^5}\right) + \frac{\partial p_z}{\partial \phi} - p_\phi \tag{4.19}$$

Finally, the first equation of 4.14 is differentiated with respect to x

$$\frac{\partial^2 N_x}{\partial x^2} = -\frac{1}{r}\frac{\partial^2 N_{\phi x}}{\partial \phi \partial x} - \frac{\partial p_x}{\partial x} \tag{4.20}$$

By differentiating Eq. 4.19 with respect to ϕ and substituting the new derived term

$$\frac{\partial^2 N_{\phi x}}{\partial \phi \partial x} \tag{4.21}$$

into Eq. 4.20, we obtain

$$\frac{\partial^2 N_x}{\partial x^2} = \frac{Eh^3}{12}\left[\frac{1}{r}\frac{\partial^6 w}{\partial x^4 \partial \phi^2} + \frac{2}{r^3}\frac{\partial^6 w}{\partial x^2 \partial \phi^4} + \frac{1}{r^5}\frac{\partial^6 w}{\partial \phi^6}\right] - \frac{\partial^2 p_z}{r\partial \phi^2} + \frac{\partial p_\phi}{r\partial \phi} - \frac{\partial p_x}{\partial x} \tag{4.22}$$

Now that we have rederived our stress couples and stress resultants in terms of radial displacements, we begin the formation our compatibility equation with the remaining stress resultants of Eq. 4.15. The first three equations are rearranged to the form of

$$\begin{aligned} \tfrac{\partial u}{\partial x} &= \tfrac{1}{Eh} N_x \\ \tfrac{\partial v}{\partial \phi} &= \tfrac{r}{Eh} N_\phi + w \\ N_{x\phi} &= \tfrac{Eh}{2}\left(\tfrac{\partial v}{\partial x} + \tfrac{1}{r}\tfrac{\partial u}{\partial \phi}\right) \end{aligned} \tag{4.23}$$

Once again, we differentiate to obtain common terms

$$\begin{aligned} \tfrac{\partial^5 u}{\partial x^3 \partial \phi^2} &= \tfrac{1}{Eh}\tfrac{\partial^4 N_x}{\partial x^2 \partial \phi^2} \\ \tfrac{\partial^5 v}{\partial x^4 \partial \phi} &= \tfrac{r}{Eh}\tfrac{\partial^4 N_\phi}{\partial x^4} + \tfrac{\partial^4 w}{\partial x^4} \\ \tfrac{\partial^4 N_{x\phi}}{\partial x^3 \partial \phi} &= \tfrac{Eh}{2}\left(\tfrac{\partial^5 v}{\partial x^4 \partial \phi} + \tfrac{1}{r}\tfrac{\partial^5 u}{\partial x^3 \partial \phi^2}\right) \end{aligned} \tag{4.24}$$

and substitute to obtain one equation of compatibility

$$\frac{\partial^4 N_{x\phi}}{\partial x^3 \partial \phi} = \frac{1}{2}\left(r\frac{\partial^4 N_\phi}{\partial x^4} + \frac{1}{r}\frac{\partial^4 N_x}{\partial x^2 \partial \phi^2}\right) + \frac{Eh}{2}\frac{\partial^4 w}{\partial x^4} \tag{4.25}$$

The stress resultants derived in Eqs. 4.18, 4.19 and 4.22 are now substituted into the newly derived compatibility equation (Eq. 4.25).

$$\begin{aligned} &\frac{r^2}{2}\frac{\partial^8 w}{\partial x^8} + \frac{\partial^8 w}{\partial x^6 \partial \phi^2} + \frac{1}{2r^2}\frac{\partial^8 w}{\partial x^4 \partial \phi^4} + \frac{1}{2r^2}\frac{\partial^8 w}{\partial x^4 \partial \phi^4} + \frac{1}{r^4}\frac{\partial^8 w}{\partial x^2 \partial \phi^6} + \frac{1}{2r^6}\frac{\partial^8 w}{\partial \phi^8} + \frac{\partial^8 w}{\partial x^6 \partial \phi^2} \\ &\quad + \frac{2}{r^2}\frac{\partial^8 w}{\partial x^4 \partial \phi^4} + \frac{1}{r^4}\frac{\partial^8 w}{\partial x^2 \partial \phi^6} + \frac{6}{h^2}\frac{\partial^4 w}{\partial x^4} = \frac{12}{Eh^3}\left(\frac{r^2}{2}\frac{\partial^4 p_z}{\partial x^4}\right. \\ &\quad \left. + \frac{1}{2r^2}\frac{\partial^4 p_z}{\partial \phi^4} - \frac{1}{2r^2}\frac{\partial^3 p_\phi}{\partial \phi^3} + \frac{1}{2r}\frac{\partial^3 p_x}{\partial x \partial \phi^2} + \frac{\partial^4 p_z}{\partial x^2 \partial \phi^2} - \frac{\partial^3 p_\phi}{\partial x^2 \partial \phi}\right) \end{aligned} \tag{4.26}$$

After simplification, we arrive at the eighth order partial differential equation.

$$r^2\left(\frac{\partial^2}{\partial x^2}+\frac{\partial^2}{r^2\partial\phi^2}\right)^4 w+\frac{12}{h^2}\frac{\partial^4 w}{\partial x^4}=\frac{12}{Eh^3}\left[r^2\left(\frac{\partial^2}{\partial x^2}+\frac{\partial^2}{r^2\partial\phi^2}\right)^2 p_z-2\frac{\partial^3 p_\phi}{\partial x^2\partial\phi}-\frac{1}{r^2}\frac{\partial^3 p_\phi}{\partial\phi^3}+\frac{1}{r}\frac{\partial^3 p_x}{\partial x\partial\phi^2}\right] \tag{4.27}$$

If we recall our previously derived equation for shallow shells, Eq. 3.128, our new equation is of the same form when ν equals zero.

$$\Delta^8 w+\frac{12(1-\nu^2)}{h^2}\Delta_R^4 w=\frac{1}{D}\Delta_R^2 f(p)+\Delta^4 f'(p) \tag{4.28}$$

where, for circular cylindrical shells,

$$\begin{aligned}
&\Delta_R^4 w=\tfrac{\partial^4 w}{r^2\partial x^4}\\
&\Delta^8 w=\left(\tfrac{\partial^2}{\partial x^2}+\tfrac{\partial^2}{r^2\partial\phi^2}\right)^4 w\\
&f(p)=\tfrac{1}{r^2}\int\tfrac{\partial^2 p_x}{\partial\phi^2}dx+r\int\tfrac{\partial^2 p_\phi}{\partial x^2}d\phi\\
&f'(p)=\tfrac{p_z}{D}-\tfrac{1}{D}\int p_\phi d\phi
\end{aligned} \tag{4.29}$$

4.3.3 Shallow Shells vs. Membrane Theory

Now that we have reviewed the analysis methods of the theory of shallow shells and membrane theory, we will briefly discuss the difference between the two methodologies and the results.

4.3.3.1 Methodology

Membrane theory is an approximate method that is often practiced to avoid the more rigorous approach of shallow shells. Membrane theory allows for the computation of the stress resultants and displacements without the use of bending, since all bending in the shell is neglected. The theory also assumes that all membrane stresses act in the plane of the shell. This is similar to the theory of shallow shells which requires the surface loads to be carried by the in-plane stresses. However, contrary to membrane theory, the theory of shallow shells accounts for bending within the shell. The theory assumes that the shell's surface curvature, along with the change in curvature, is small but is still required for analysis purposes.

4.3.3.2 Results

We will now view two examples, first with membrane theory, and second with the theory of shallow shells, to compare the results of both methods.

Membrane Theory : Lets first consider the stress resultants derived from membrane theory given a uniform shell load $p = (4/\pi)p_d$. The loading components are as follows:

$$p_z = p\cos(\phi_k - \phi)\sin kx \quad p_\phi = p\sin(\phi_k - \phi)\sin kx \quad p_x = 0$$

where $k = n\pi/L$ and $n = 1$. Substituting into Eq. 4.3 we obtain the stress resultant

$$N'_\phi = -pr\cos(\phi_k - \phi)\sin kx \tag{4.30}$$

When we substitute N'_ϕ into the second term of Eq. 4.3 we obtain

$$N'_{x\phi} = -\frac{1}{r}\int \frac{\partial[-pr\cos(\phi_k - \phi)\sin kx]}{\partial\phi}dx + \int p\sin(\phi_k - \phi)\sin kx dx + f_1(\phi) \tag{4.31}$$

After differentiation and integration, $N'_{x\phi}$ becomes

$$N'_{x\phi} = 2\frac{p}{k}\sin(\phi_k - \phi)\cos kx + f_1(\phi) \tag{4.32}$$

where for a simply supported shell $f_1(\phi) = 0$.

We will next substitute the newly derived term into the third term of Eq. 4.3. Again through differentiation and integration we obtain

$$N'_x = -2\frac{p}{k^2 r}\cos(\phi_k - \phi)\sin kx + f_2(\phi) \tag{4.33}$$

where for a simply supported beam $N'_x = 0$ at $x = 0$ and $x = L$. $f_2(\phi)$ can be computed as zero and dropped from the above equation.

Next we will derive the displacements from membrane theory using the above derived stress resultants and Eqs. 4.8, 4.10, and 4.9.

After substitution, we find

$$\begin{aligned} u &= \tfrac{2}{EH}\tfrac{p}{k^3 r}\cos(\phi_k-\phi)\cos kx \\ v &= \tfrac{2}{EH}\tfrac{p}{k^4 r^2}\left(1+2k^2r^2\right)\sin(\phi_k-\phi)\sin kx \\ w &= \tfrac{2}{EH}\tfrac{pk^4}{r^2}\left(1+2k^2r^2+\tfrac{r^4k^4}{2}\right)\cos(\phi_k-\phi)\sin kx \end{aligned} \tag{4.34}$$

Theory of Shallow Shells : The loading components will be the same as those used for membrane theory.

$$p_z = p\cos(\phi_k-\phi)\sin kx \quad p_\phi = p\sin(\phi_k-\phi)\sin kx \quad p_x = 0$$

Using the right side of the partial differential equation (Eq. 4.27), we determine the particular solution.

$$\begin{aligned} &\frac{12}{Eh^3}\Big[r^2k^4p\cos(\phi_k-\phi)\sin kx + 2p(-\cos(\phi_k-\phi))(-\sin kx)k^2 + \\ &\frac{1}{r^2}p\sin kx\cos(\phi_k-\phi) - 2k^2p\cos\phi_k(-\sin kx) - \frac{1}{r^2}p\sin kx(- \\ &\cos(\phi_k-\phi))\Big]\frac{12}{Eh^3}\left(r^2k^4+4k^2+\frac{2}{r^2}\right)p\cos(\phi_k-\phi)\sin kx \end{aligned} \tag{4.35}$$

The particular solution is determined as

$$w = Cp\cos(\phi_k-\phi)\sin kx \tag{4.36}$$

When substituted into the left side of the partial differential equation, we find

$$\begin{aligned} &r^2\left(\tfrac{\partial^2}{\partial x^2}+\tfrac{\partial^2}{r^2\partial\phi^2}\right)^4 Cp\cos(\phi_k-\phi)\sin kx + \tfrac{12}{h^2}\tfrac{\partial^4[Cp\cos(\phi_k-\phi)\sin kx]}{\partial x^4} \\ &r^2\left(k^2+\tfrac{1}{r^2}\right)^4 Cp\cos(\phi_k-\phi)\sin kx + \tfrac{12}{h^2}k^4Cp\cos(\phi_k-\phi)\sin kx \end{aligned} \tag{4.37}$$

Equating the left and right hand sides of the equation, we solve for the constant C of our particular solution

$$C = \frac{1}{Eh}\left[\frac{r^2k^4+4k^2+2/r^2}{(r^2h^2/12)(k^2+1/r^2)^4+k^4}\right] \tag{4.38}$$

Substituting into Eq. 4.36, we compute w at any point in terms of the load and dimensions of the shell. The stress couples, stress resultants and displacement are obtained by substituting w into Eq. 4.16 through Eq. 4.24.

4.3.3.3 Comparison

It is helpful to compare the results of the membrane theory to that of shallow shells. The results are presented in the table below.

Membrane Theory	Theory of Shallow Shells
Stress Couples	
$M'_\phi = 0$	$M_\phi = \frac{Eh^3}{12r^2} pC\cos(\phi_k)\sin kx$
$M'_{x\phi} = 0$	$M_{x\phi} = \frac{Eh^3}{12r} kpC\sin(\phi_k)\cos kx$
$M'_x = 0$	$M_x = \frac{Eh^3}{12} k^2 pC\cos(\phi_k)\sin kx$
Stress Resultants	
$N'_\phi = -pr\cos(\phi_k)\sin kx$	$N_\phi = -pr(1-2P)\cos(\phi_k)\sin kx$
$N'_{x\phi} = 2\frac{p}{k}\sin(\phi_k)\cos kx$	$N_{x\phi} = 2\frac{p}{k}(1-P)\sin(\phi_k)\cos kx$
$N'_x = -\frac{2p}{k^2 r}\cos(\phi_k)\sin kx$	$N_x = -\frac{2p}{k^2 r}(1-P)\cos(\phi_k)\sin kx$
Displacements	
$u = \frac{2}{Eh}\frac{p}{k^3 r}\cos(\phi_k)\cos kx$	$u = \frac{2}{Eh}\frac{p}{k^3 r}(1-P)\cos(\phi_k)\cos kx$
$v = \frac{2}{Eh}\frac{p}{k^4 r^2}(1+2k^2r^2)\sin(\phi_k)\sin kx$	$v = \frac{2}{Eh}\frac{p}{k^4 r^2}(1+2k^2r^2)(1-P)\sin(\phi_k)\sin kx$
$w = \frac{2}{Eh}\frac{p}{k^4 r^2}\left(1+2k^2r^2+\frac{r^4k^4}{2}\right)\cos(\phi_k)\sin kx$	$w = \frac{2}{Eh}\frac{p}{k^4 r^2}\left[(1+2k^2r^2)(1-P)-\frac{r^4k^4}{2}(1-2P)\right]\cos(\phi_k)\sin kx$

Table 4.1: Comparison of Analysis Results

Note that the displacement computed via the particular solution can be rewritten as

$$\begin{aligned} u &= u'(1-P) \\ v &= v'(1-P) \\ w &= w'\frac{1}{B+1} \end{aligned} \tag{4.39}$$

where

$$\begin{aligned} P &= \frac{Eh^3}{24r^4}(1+2k^2r^2+k^4r^4)C \\ B &= \frac{h^2}{12r^6k^4}(k^2r^2+1)^4 \end{aligned} \tag{4.40}$$

and from the comparison table, $\phi_k = (\phi_k - \phi)$. P and B are used to measure the accuracy of the membrane approach compared to the shallow shell method.

Let us consider the following variables:

$$\begin{aligned} h &= 3 \text{ in} = 0.25 \text{ ft} & \frac{h}{r} &= \frac{1}{106} \\ r &= 26.6 \text{ ft} & \frac{r}{L} &= 0.4 \\ L &= 66.5 \text{ ft} & k &= \frac{\pi}{L} \\ \phi_k &= 45\,\text{deg} & E &= 4.32\text{x}10^5 \text{ ksf} \end{aligned}$$

The long shell example allows the use of membrane theory in comparison to the theory of shallow shells based on the following values:

$$\begin{aligned} C &= 0.0284 \text{ ft}^3/\text{kip} \\ P &= 0.00011 \\ B &= 0.000131 \end{aligned} \tag{4.41}$$

Now lets consider the case of a short shell where

$$\begin{aligned} h &= 4 \text{ in} = 0.33 \text{ ft} & \frac{h}{r} &= \frac{1}{420} \\ r &= 140 \text{ ft} & \frac{r}{L} &= 4.67 \\ L &= 30 \text{ ft} & \phi_k &= 45 \deg \\ E &= 4.32\text{x}10^5 \text{ ksf} \end{aligned}$$

The results of the short shell case are still reasonable and would allow the use of membrane theory.

$$\begin{aligned} C &= 0.135 \text{ ft}^3/\text{kip} \\ P &= 0.011 \\ B &= 0.024 \end{aligned} \tag{4.42}$$

Even though membrane theory may seem like the easy choice to avoid the rigorous eighth order differential equation, it can only provide reasonable results if it meets certain criteria. First, the displacement results must not increase the shell bending substantially since the methodology neglects all shell bending. Next, the loading on the shell must be uniform over the entire surface. Finally, the boundaries must supply the forces and permit the displacements required by the theory. Often membrane theory is not permitted for design use, but in the case of a circular cylindrical shall, it appears useful to accelerate the design process.

4.3.4 Bending Theory

After determination of the primary system and errors by either membrane theory or the theory of shallow shells, we continue the analysis by determining the displacements and internal forces produced from the line loads in the corrections phase of the analysis. We must first determine

the homogeneous solution to our general formulation. In this case, we will view the eighth order differential equation derived from the theory of shallow shells (4.27).

From the left side of the equation, the homogeneous equation is written as

$$r^2\left(\frac{\partial^2}{\partial x^2}+\frac{\partial^2}{r^2\partial\phi^2}\right)^4 w+\frac{12}{h^2}\frac{\partial^4 w}{\partial x^4}=0 \tag{4.43}$$

The solution has the form of

$$w=\sum_{n=1,3,\ldots}^{\infty} A_m \exp^{M\phi}\sin kx \tag{4.44}$$

where A_m and M represent eight arbitrary constants and eight roots. The constants are based upon the longitudinal boundary conditions while the roots are based solely on the dimensions of the shell.

The roots are computed by substituting Eq. 4.44 into Eq. 4.43

$$\begin{aligned} &r^2 A_m \exp^{M\phi}\sin kx\left(-k^2+\tfrac{M^2}{r^2}\right)^4+\tfrac{12}{h^2}k^4 A_m \exp^{M\phi}\sin kx=0\\ &\left(M^2-k^2r^2\right)^4 A_m \exp^{M\phi}\sin kx+\tfrac{12r^6k^4}{h^2}=0 \end{aligned} \tag{4.45}$$

In substituting

$$Q^8=3(kr)^4\left(\frac{r}{h}\right)^2 \tag{4.46}$$

we obtain

$$\left(M^2-(kr)^2\right)^4 A_m \exp^{M\phi}\sin kx+4Q^8 A_m \exp^{M\phi}\sin kx=0 \tag{4.47}$$

which can be rewritten as

$$\left[\frac{M^2-(kr)^2}{\sqrt{2}Q^2}\right]^4+1=0 \tag{4.48}$$

With one additional substitution,

$$\gamma=\left(\frac{kr}{Q}\right)^2 \tag{4.49}$$

Eq. 4.48 becomes

$$\frac{M^2}{Q^2}-\gamma=\sqrt[4]{-1}\sqrt{2} \tag{4.50}$$

We are now left with the imaginary term $\sqrt[4]{-1}$ that is rewritten as

$$\sqrt[4]{-1}=\sqrt{\pm i} \tag{4.51}$$

where $i = \sqrt{-1}$. A complex number is written as

$$z = x + iy = \mathrm{Re}^{i\theta} \tag{4.52}$$

When $x = 0$, $y = 1$, and $r = \sqrt{x^2 + y^2} = 1$ the complex number becomes

$$i = e^{i\theta} \tag{4.53}$$

where, from Euler's equation,

$$e^{i\theta} = \cos\theta + i\sin\theta \tag{4.54}$$

and $\theta = \pi/2$ forming the complex relation of

$$i = e^{i\pi/2} \tag{4.55}$$

Now that we have derived the complex relation, we compute

$$\begin{aligned} \sqrt{i} &= (i)^{\frac{1}{2}} = e^{i\pi/4} \\ e^{i\pi/4} &= \cos\pi/4 + i\sin\pi/4 \\ e^{i\pi/4} &= \tfrac{1}{\sqrt{2}} + i\tfrac{1}{\sqrt{2}} \end{aligned} \tag{4.56}$$

If we substitute Eq. 4.56 into Eq. 4.50, we find our eight roots

$$\begin{aligned} M_1 &= \pm(\alpha_1 \pm i\beta_1) \\ M_2 &= \pm(\alpha_1' \pm i\beta_1') \end{aligned} \tag{4.57}$$

where

$$\begin{aligned} \alpha_1 &= Q\sqrt{\tfrac{\sqrt{(1+\gamma)^2+1}+(1+\gamma)}{2}} = Qm_1 \\ \beta_1 &= Q\sqrt{\tfrac{\sqrt{(1+\gamma)^2+1}-(1+\gamma)}{2}} = Qn_1 \\ \alpha_1' &= Q\sqrt{\tfrac{\sqrt{(1-\gamma)^2+1}-(1-\gamma)}{2}} = Qm_2 \\ \beta_1' &= Q\sqrt{\tfrac{\sqrt{(1-\gamma)^2+1}+(1-\gamma)}{2}} = Qn_2 \end{aligned} \tag{4.58}$$

We next determine the eight arbitrary constants, A_m, by expanding upon Eq. 4.44.

$$w = \begin{bmatrix} A_1 e^{(\alpha_1+i\beta_1)\phi} & A_2 e^{(\alpha_1-i\beta_1)\phi} \\ A_3 e^{(\alpha_1'+i\beta_1')\phi} & A_4 e^{(\alpha_1'-i\beta_1')\phi} \\ A_5 e^{-(\alpha_1+i\beta_1)\phi} & A_6 e^{-(\alpha_1-i\beta_1)\phi} \\ A_7 e^{-(\alpha_1'+i\beta_1')\phi} & A_8 e^{-(\alpha_1'-i\beta_1')\phi} \end{bmatrix} \sin kx \tag{4.59}$$

As noted before from Euler's equation

$$e^{\pm i\beta_1\phi} = \cos\beta_1\phi \pm i\sin\beta_1\phi \tag{4.60}$$

allowing the first row of our matrix to be rewritten as

$$[(A_1 + A_2)\cos\beta_1\phi + i(A_1 - A_2)\sin\beta_1\phi]\exp^{\alpha_1\phi} \tag{4.61}$$

where A_1 and A_2 must be complex conjugate constants in order for w to be real.

$$A_1 + A_2 = 2a \quad A_1 - A_2 = i2b \tag{4.62}$$

and rewritten in the form of

$$A_1 = a + ib \quad A_2 = a - ib \tag{4.63}$$

We now substitute the constants back into Eq. 4.61 to simplify.

$$2(a\cos\beta_1\phi - b\sin\beta_1\phi)\exp^{\alpha_1\phi} \tag{4.64}$$

When we compare the above expression with the first term of Eq. 4.59

$$A_1\exp^{(\alpha_1+i\beta_1)\phi} = [a\cos\beta_1\phi - b\sin\beta_1\phi + i(b\cos\beta_1\phi + a\sin\beta_1\phi)]\exp^{\alpha_1\phi} \tag{4.65}$$

we notice it is twice the real part, $2\mathrm{Re}\left(A_1\exp^{M_1\phi}\right)$, meaning

$$w = 2\mathrm{Re}\begin{bmatrix} A_1\exp^{M_1\phi} & + & A_3\exp^{M_2\phi} \\ A_5\exp^{-M_1\phi} & + & A_7\exp^{-M_2\phi} \end{bmatrix}\sin kx \tag{4.66}$$

Thus, the partial derivatives of w is easily attained and applied to Eqs. 4.16, 4.17, 4.18, 4.19 and 4.20 to obtain the stress resultants and couples in terms of A_m. As an example, we will view the term M_ϕ.

$$M_\phi = -\tfrac{Eh^3}{12r^2}\tfrac{\partial^2 w}{\partial\phi^2}$$

$$M_\phi = -\tfrac{Eh^3}{12r^2} * 2R\begin{pmatrix} A_1M_1^2e^{M_1\phi} + A_3M_2^2e^{M_2\phi} \\ A_5M_1^2e^{-M_1\phi} + A_7M_2^2e^{-M_2\phi} \end{pmatrix}\sin kx$$

The A_m terms are rewritten in the form of the eight arbitrary constants as in Eq. 4.63

$$\begin{aligned} A_1 &= a + ib \quad A_3 = c + id \\ A_5 &= e + if \quad A_7 = g + ih \end{aligned} \tag{4.67}$$

and M_ϕ is rewritten as

$$M_\phi = -\frac{Eh^3}{6r^2} R \begin{bmatrix} (a+ib)M_1^2(\cos\beta_1\phi + i\sin\beta_1\phi)e^{\alpha_1\phi} \\ (c+id)M_2^2(\cos\beta_1'\phi + i\sin\beta_1'\phi)e^{\alpha_1'\phi} \\ (e+if)M_1^2(\cos\beta_1\phi - i\sin\beta_1\phi)e^{-\alpha_1\phi} \\ (g+ih)M_2^2(\cos\beta_1'\phi - i\sin\beta_1'\phi)e^{-\alpha_1'\phi} \end{bmatrix} \sin kx \tag{4.68}$$

After expansion, substitution of M_n and dropping the imaginary terms, we attain the resulting stress couple in terms of eight unknowns.

$$M_\phi = -\frac{Eh^3}{6r^2} Q^2 \begin{pmatrix} \langle [a(1+\gamma) - b]\cos\beta_1\phi - [a + b(1+\gamma)]\sin\beta_1\phi \rangle e^{\alpha_1\phi} \\ \langle [c(\gamma-1) - d]\cos\beta_1'\phi - [c + d(\gamma-1)]\sin\beta_1'\phi \rangle e^{\alpha_1'\phi} \\ \langle [e(1+\gamma) -]\cos\beta_1\phi + [e + f(1+\gamma)]\sin\beta_1\phi \rangle e^{-\alpha_1\phi} \\ \langle [g(\gamma-1) - h]\cos\beta_1'\phi - [g + h(\gamma-1)]\sin\beta_1'\phi \rangle e^{-\alpha_1\phi} \end{pmatrix} \sin kx \tag{4.69}$$

In the case of a symmetrical shell, the unknowns are reduced to four, given $a = e$, $b = f$, $c = g$, and $d = h$. Next we replace the exponential terms with their hyperbolic counterpart

$$\begin{aligned} \exp^{\alpha\phi} &= \cosh\alpha\phi + \sinh\alpha\phi \\ \exp^{-\alpha\phi} &= \cosh\alpha\phi + \sinh\alpha\phi \end{aligned} \tag{4.70}$$

to obtain the stress resultant and couple in its final form.

$$M_\phi = -\frac{Eh^3}{3r^2} Q^2 \begin{Bmatrix} [a(1+\gamma) - b]\cos\beta_1\phi\cosh\alpha_1\phi - [a + b(1+\gamma)]\sin\beta_1\phi\sinh\alpha_1\phi \\ [c(\gamma-1) - d]\cos\beta_1'\phi\cosh\alpha_1'\phi - [c + d(\gamma-1)]\sin\beta_1'\phi\sinh\alpha_1'\phi \end{Bmatrix} sinkx \tag{4.71}$$

This process is repeated to solve all eight functions, M_ϕ, M_x, $M_{x\phi}$, Q_x, Q_ϕ, N_ϕ, N_x, and $N_{x\phi}$.

The next step is to solve for the edge effects due to line loads. The effects can be obtained by setting three boundary conditions equal to zero and the fourth equal to one. We then have four equation and four unknowns which are solved simultaneously for the four arbitrary constants a, b, c and d. For the unsymmetrical cases, we solve eight simultaneous equations for eight unknowns. In order to solve for the displacements, the newly solved arbitrary constants are substituted directly into u, v, and w.

4.3.5 Edge Beams

The purpose of the edge beam is to stiffen the shell edge and, along with the shell, carry flexural stresses. Two types of edge beams will be reviewed in the analysis of the shell, vertical and horizontal edge beams, seen in Figs. 4.4 and 4.5. Vertical beams see extensive use in long shells where longitudinal bending controls the design. Whereas horizontal beams are used primarily in short shells where transverse arching controls.

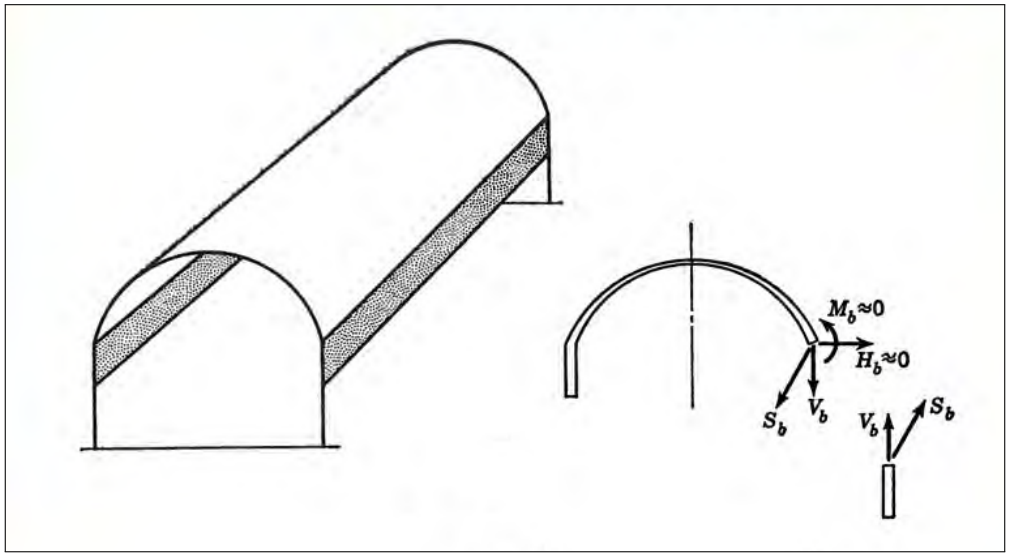

Figure 4.4: Shell with Vertical Edge Beams, (Billington, 1965)

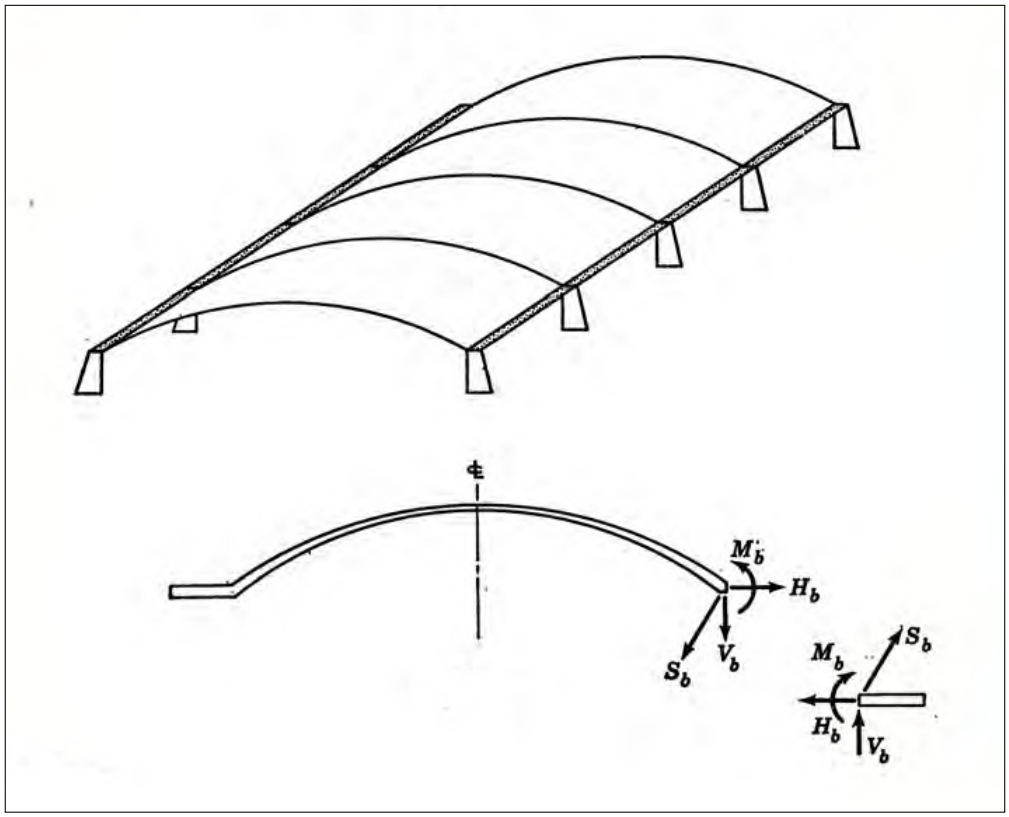

Figure 4.5: Shell with Horizontal Edge Beams, (Billington, 1965)

The analysis for both beams follows the typical four steps:

Primary System : The surface loads are supported by a shell containing free edges. Also at the free edges, edge members consisting of simple beams carrying their own dead weight are present.

Errors : Two errors are presented by the primary system of the shell and edge members. First, the difference in the vertical deflections of the shell free edge and the edge beam, $D_{10}^S + D_{10}^B$. Next, the difference in the longitudinal stresses in the shell edge and the top of the edge beam, $f_{20}^S + f_{20}^B$.

Corrections : A vertical force, V_b, and shearing force, S_b are applied at the edge beam as seen in Fig. 4.6. V_b acts upward on the shell and downward on the beam reducing the vertical

deflection and longitudinal stresses in the shell. It is assumed positive when acting downward on the shell and upward on the beam. S_b acts inward on the shell and outward on the beam reducing the vertical deflection and longitudinal stresses in the shell. It is assumed positive when acting outward on the shell and inward on the beam.

Compatibility : Two compatibility equations are applied. Vertical displacement is restored by Eq. 4.72

$$X_1\left(D_{11}^S + D_{11}^B\right) + X_2\left(D_{12}^S + D_{12}^B\right) + D_{10}^S + D_{10}^B = 0 \tag{4.72}$$

Longitudinal stresses are restored by Eq. 4.73

$$X_1\left(f_{21}^S + f_{21}^B\right) + X_2\left(f_{22}^S + f_{22}^B\right) + f_{20}^S + f_{20}^B = 0 \tag{4.73}$$

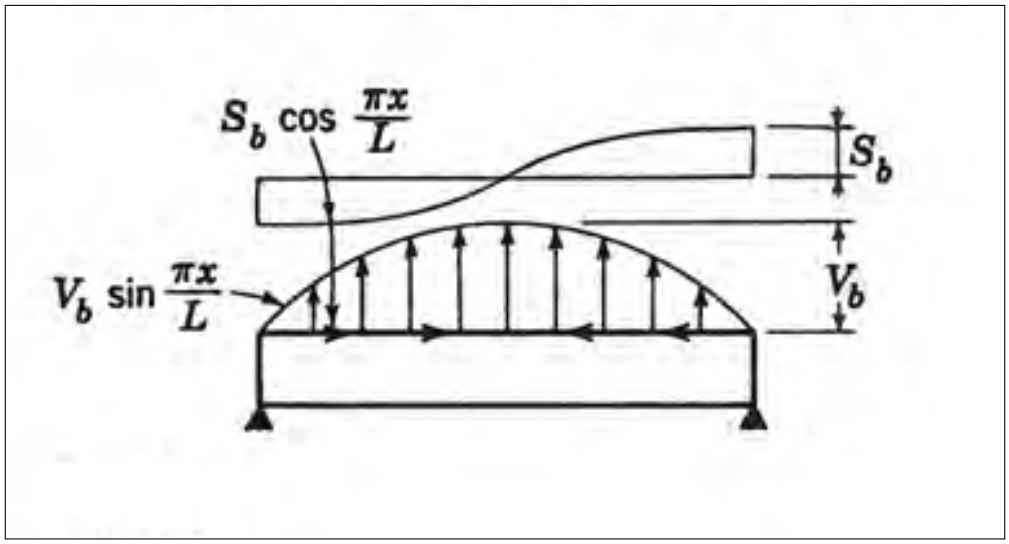

Figure 4.6: Corrective Line Loads Applied at Edge Members, (Billington, 1965)

4.3.5.1 Vertical Edge Beams

Let us first review the vertical edge beam. For free edge analysis, discussed previously, corrective line loads T_L and S_L are applied so that the free edge forces equal zero. The purpose of the vertical edge beam is to resist vertical movement and longitudinal edge strain (N_x/Eh). If

the beam is slender, it is assumed that negligible resistance to rotation and horizontal translation is offered. This means that the edge forces are no longer zero and unknown edge forces of V_b and S_b must be applied. The determination of these values depends on the properties of the edge beam and its capacity to resist vertical deflection and longitudinal edge strain.

The values of the shell displacements and stresses were discussed previously in Sec. 4.3 via membrane theory and th theory of shallow shells. The values of edge beam displacements and stresses are computed by the ordinary flexural theory as follows.

4.3.5.2 Ordinary Flexural Theory

Since the shell line loads are represented by Fourier series, the same representation must be required for the edge beam loading in order to achieve compatibility with the shell over the longitudinal length's entirety. The ordinary flexural theory utilizes the following relationships:

$$\begin{aligned} EI\frac{d^4y}{dx^4} &= w_x = \text{loading} \\ EI\frac{d^3y}{dx^3} &= -S_x = \text{shear} \\ EI\frac{d^2y}{dx^2} &= -M_x = \text{moment} \\ \frac{dy}{dx} &= -\int_0^L \frac{M_x}{EI}dx + f_1(x) = \theta = \text{slope} \\ y &= -\int_0^L \int \frac{M_x}{EI}dx + \int_0^L f_1(x)dx + f_2(x) = \text{deflection} \end{aligned} \tag{4.74}$$

The shear, moment, slope, and deflection are all solved by a known loading case and basic integration. Since the load on the beam is assumed as $V_b \sin\frac{n\pi x}{L}$ the loading equation takes the form of

$$\frac{\partial^4\delta}{\partial x^4} = \frac{V_b}{EI}\sin\frac{n\pi x}{L} \tag{4.75}$$

Integrating the previous, we derive the moment equation

$$M = \frac{\partial^2\delta}{\partial x^2} = -\frac{V_b}{EI}\left(\frac{L}{n\pi}\right)^2 \sin\frac{n\pi x}{L} \tag{4.76}$$

and the displacement

$$\delta = \frac{V_b}{EI}\left(\frac{L}{n\pi}\right)^4 \sin\frac{n\pi x}{L} \tag{4.77}$$

The longitudinal stress at the top of the beam are computed as

$$f_t = \frac{M}{Z_t} \tag{4.78}$$

With a known shearing force, $S_b \cos\frac{n\pi x}{L}$, a resultant thrust at the edge of the beam is produced at any distance x from the beam support.

$$T = -\int_0^x S_b \cos\frac{n\pi x}{L} dx = -S_b \frac{L}{n\pi}\sin\frac{n\pi x}{L} \tag{4.79}$$

A bending moment Te and a normal load T result from the thrust. The vertical deflection is computed from Eq. 4.74, with $f_1(x) = f_2(x) = 0$ and the longitudinal stress at the top of the beam is recomputed as

$$f_t = \frac{T}{A} + \frac{Te}{Z_t} \tag{4.80}$$

4.3.5.3 Matrix Analysis

For a rectangular cross section, the previously discussed equations can be written in matrix form. When $I = bd^3/12$, $Z = bd^2/6$ and $e = d/2$, the equations are summarized as seen below.

For $V_b = 1$:

$$\begin{aligned} D_{11}^B &= \tfrac{L^4}{Ebd^3}\tfrac{12}{\pi^4 n^4}\sin kx \\ f_{21}^B &= -\tfrac{L^2}{bd^2}\tfrac{6}{\pi^2 n^2}\sin kx \end{aligned} \tag{4.81}$$

For $S_b = 1$:

$$\begin{aligned} D_{12}^B &= -\tfrac{L^3}{Ebd^2}\tfrac{6}{\pi^3 n^3}\sin kx \\ f_{22}^B &= \tfrac{L}{bd}\tfrac{4}{\pi n}\sin kx \end{aligned} \tag{4.82}$$

The beam displacement and stress due to full loads on the beam alone can be found from Eqs. 4.81 and 4.82. Utilizing Fourier series representation for the vertical uniform load

$$(w_{B+L})_x = -\frac{4}{\pi} w_{B+L} \sum_{n=1,3,5\ldots}^{\infty} \frac{1}{n}\sin kx \tag{4.83}$$

we derive

$$\begin{aligned} D_{10}^{B} &= -\tfrac{4}{\pi} w_{B+L} \tfrac{L^4}{Ebd^3} \tfrac{0.12319}{n^4} \sin kx \\ f_{20}^{B} &= \tfrac{4}{\pi} w_{B+L} \tfrac{L^2}{bd^2} \tfrac{0.60793}{n^2} \sin kx \end{aligned} \tag{4.84}$$

4.3.5.4 Horizontal Edge Beams

The process for analyzing a horizontal edge beam is nearly identical to that of the vertical beam. H_b replaces the V_b values in Eq. 4.74 and the matrix equations. The d and b terms of Eqs. 4.81 and 4.82 are reversed representing the beam width and depth. Similar to the vertical beam, it is assumed to have negligible rotational and transverse stiffness.

The primary difference is found in the addition of a vertical load V_{B+L} and a bending moment M_{B+L} at the shell edge.

$$\begin{aligned} V_{B+L} &= w_{B+L} d \\ M_{B+L} &= w_{B+L} \tfrac{d^2}{2} \end{aligned} \tag{4.85}$$

In addition, the horizontal edge beam is assumed to carry its own load as a cantilever of span d, and not a beam of length L.

4.3.6 Prestressing

The purpose of prestressing within the edge beam is to allow a reduction in the size of the beam. We will once again follow our four step analysis procedure and is as follows:

Primary System : The primary system consists of two separate items. The first is the shell carrying no load with free edges. The second is the edge beam analyzed as a simple beam subject to the prestressing load.

Errors : Two errors are presented by the primary systems of the shell and edge members. First, the difference in the vertical deflections of the shell free edge and the beam. Second, the difference in the longitudinal stresses in the shell edge and the top of the edge beam. For both cases, zero deflection will occur at the shell edge since the shell structure is unloaded.

Corrections : A vertical force, V_b, and shearing force, S_b are applied at the edge beam as seen in Sec. 4.3.5. V_b acts upward on the shell and downward on the beam reducing the vertical deflection and longitudinal stresses in the shell. It is assumed positive when acting downward on the shell and upward on the beam. S_b acts inward on the shell and outward on the beam reducing the vertical deflection and longitudinal stresses in the shell. It is assumed positive when acting outward on the shell and inward on the beam.

Compatibility : The compatibility equations are the same as those given for Sec. 4.3.5 with the exception of the error terms derived in Eq. 4.84.

The new error terms are derived from Eqs. 4.81 and 4.82. If the edge beam is considered as a simple beam, a parabolic reinforcing profile causes a vertical upward deflection and a longitudinal stress at the top of the edge beam.

$$\begin{aligned} D_{10}^B &= -\int_0^L \int \frac{M_F}{EI} dx dx + \int_0^L f_1(x) dx + f_2(x) \\ f_{20}^B &= \frac{F}{A} - \frac{M_F}{Z_t} \end{aligned} \tag{4.86}$$

where M_F is the bending moment due to eccentricity of the tendon profile.

The deflections and stresses caused by this bending moment are computed throughout the member except at the supports were the bending moment is assumed zero. The equivalent uniform load is then used to compute the deflections and stresses.

$$w_e = \frac{8Fe_c}{L^2} \tag{4.87}$$

The loading is once again represented by the Fourier series:

$$(w_e)_x = \frac{4}{\pi} w_e \sum_{n=1,3,5...}^{\infty} \frac{1}{n} \sin kx \tag{4.88}$$

If the edge beam is of a rectangular cross section, Eq. 4.86 is rewritten in the form of

$$\begin{aligned} D_{10}^B &= \tfrac{4}{\pi} \tfrac{8Fe_c}{L^2} \tfrac{L^4}{Ebd^3} \tfrac{0.12319}{n^4} \sin kx \\ f_{20}^B &= \tfrac{4}{\pi} \tfrac{F}{bd} \sin kx - \tfrac{4}{\pi} \tfrac{8Fe_c}{L^2} \tfrac{L^2}{bd^2} (0.60793) \sin kx \end{aligned} \tag{4.89}$$

where the first term F/A uses on the first term of Fourier series.

Note that the values of V_b^F and S_b^F can by determined be inputting the values of Eq. 4.89 in the compatibility equations (4.72) and (4.73).

4.4 Conclusion

In this chapter, we focused on the analysis of the shell structure, first through membrane theory, and second through the theory of shallow shells. We concluded by viewing the analysis of the edge beams and the required reinforcement.

Chapter 5

Circular Cylindrical Shell Design Tool

5.1 Introduction

Chapter five discusses the development of a design tool to aid in future cylindrical shell design along with a brief preliminary design. The code utilizes the theory of shallow shells in the determination of the stresses and displacements and is presented in the appendix of the thesis (7). A discussion of the code and results is presented followed by a reinforcement section and the equations for required steel within the shell and beam. An example structure is presented for validation of the code.

5.1.1 Preliminary Design Example

The structure that will be utilized for this example is a warehouse complex located in Pennsylvania. For purposes of this design, the structure will used to validate the results since the structure has been previously studied using the theory of shallow shells. We will design a single barrel from the warehouse assuming restraint from the longitudinal edge beam.

Figure 5.1: Pennsylvania Warehouse Complex, (Billington, 1965)

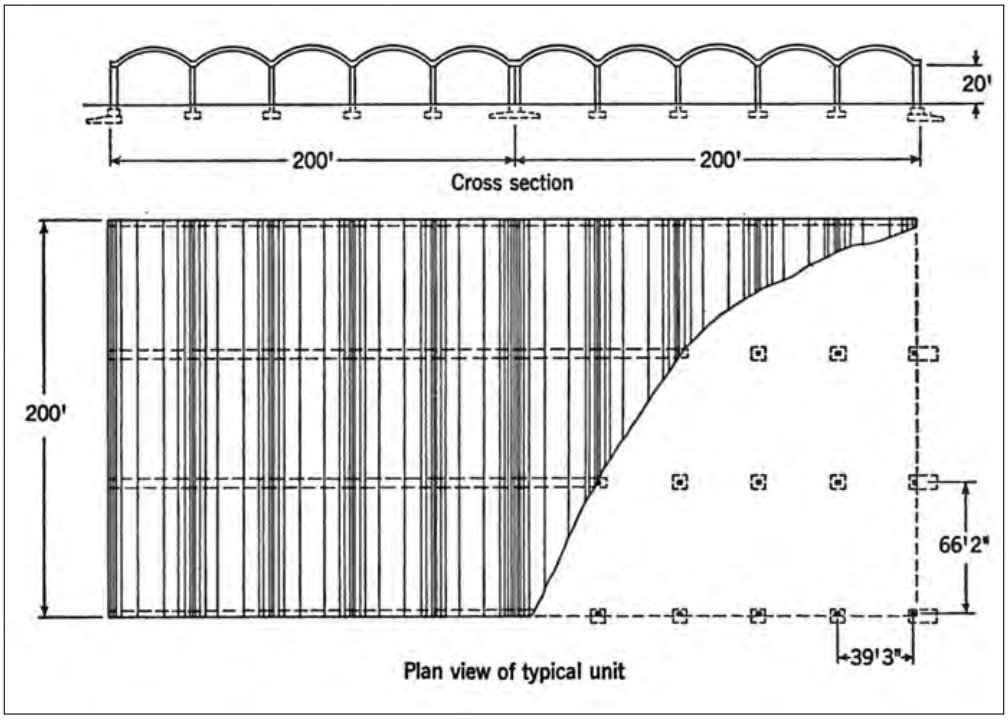

Figure 5.2: Pennsylvania Warehouse Roof Layout, (Billington, 1965)

The structure of interest can be seen in Fig. 5.1. The warehouse roof consists of 15 barrels

covering 40,000 ft^2 (see Fig. 5.2). The complex totals 16 separate units (240 barrels)covering 640,000 ft^2.

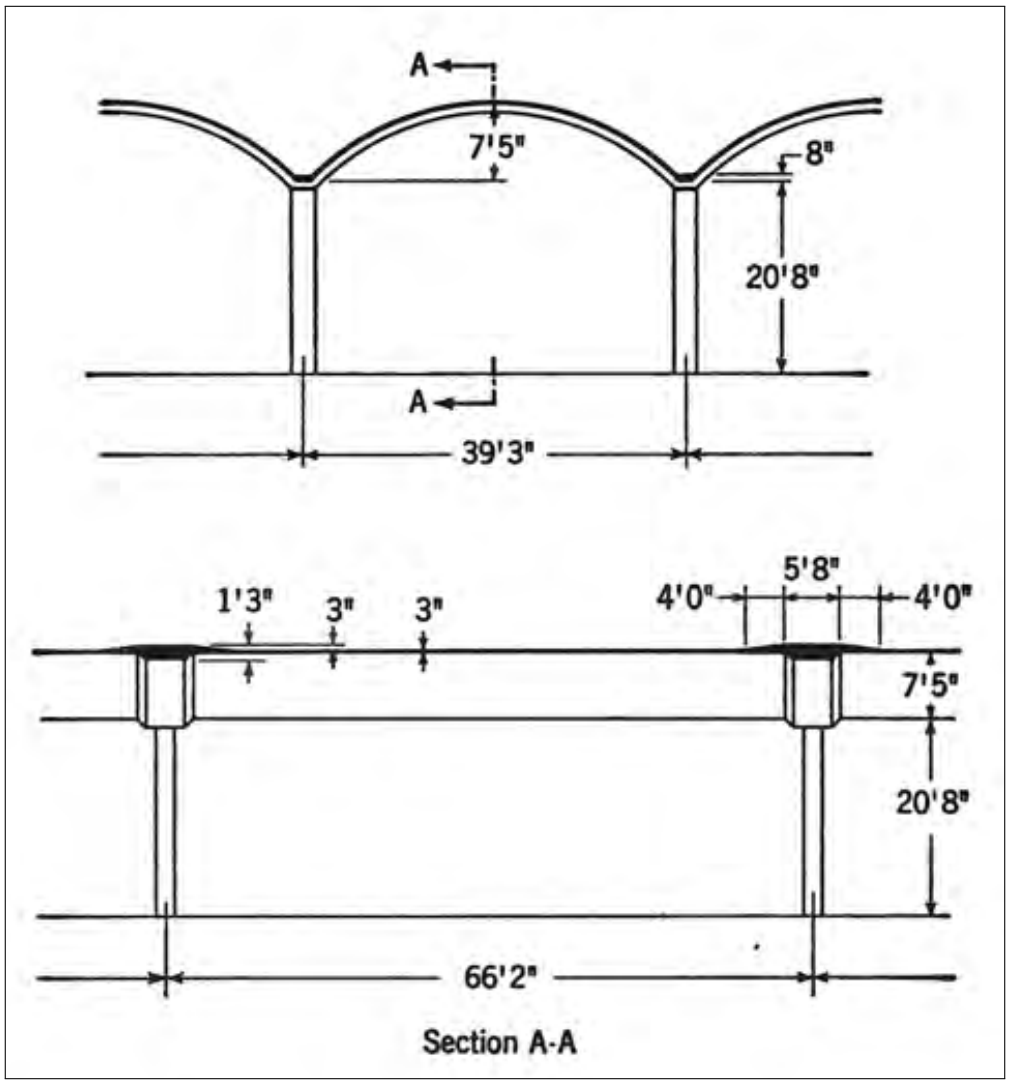

Figure 5.3: Single Barrel used for Design, (Billington, 1965)

We will consider the column height and spacing fixed for the design and given in Fig. 5.3. The barrels are oriented in the direction of the long span with a shell thickness, h, of 3 in. The shell will contain a minimum of three layers of reinforcement. Wire fabric will be used top and bottom with main bars running in between. The cover over the fabric will be no less than $\frac{3}{8}$ in.

assuming $\frac{1}{2}$ in. thick fabric. The bars will be no greater than $\frac{3}{4}$ in. in diameter.

The curvature of the barrel will be initially assumed based upon the ease of construction and material costs. If the shell is classified as semicircular, the roof will carry low stresses but contain a surface area of 1.5 time greater than the actual covered surface increasing material costs greatly. Also, the concrete would be very difficult to place near the springing where the slope is nearly vertical. The desirable slope should be no greater than 45deg. However, with the ease of construction comes the increase in stresses. For this design, we will use a slope of $\phi_k = 45\,\text{deg}$ with a radius of $r = 26.6$ ft.

The loads considered for the design are as follows:

Shell Dead Load	40
Roofing and Mechanical Equipment	10
Live Load (snow)	30
Total:	80

Even though the snow load often requires further thought due to drifting, for simplicity, we will consider all three loads to be uniformly distributed over the surface of the shell. Note that all predefined variables are selected as initial values and may be modified as required to benefit the analysis.

5.2 Matlab

The matlab program presented in the appendix 7 is utilized to design a reinforced concrete circular cylindrical shell. The program allows the user to design a simply supported shell with longitudinal edge beams. The code is based on the theory of shallow shells along with the analysis methods discussed in the previous chapter. Following the method laid out in Sec. 3.4.4, the program first defines the principle system by computing the moment, M_ϕ, shear, $N_{\phi x}$, and the radial and longitudinal forces, N_ϕ and N_x.

The program is relatively simple to use and understand. The user will input a few values based on given dimensions, properties and loads for the shell of interest. Once the values are the

selected the program can be ran. By the default, the moment, shear, and radial and longitudinal forces are computed for the edge of the shell at midspan. This can be easily adjusted by paging to the final section of code entitled, Shell Forces. Here the user can select a new angle ϕ (distance from longitudinal edge, rad) and new length x (distance from transverse edge, ft), depending upon the specific location of interest. Other locations of interest would include the crown along with the end and quarter span points.

First, the design of the shell will be discussed below.

5.2.1 Cylindrical Shell Roof

The preliminary design of the shell structure is the first task that must be accomplished in the design of the barrel vault. The matlab program follows the design process laid out by the theory of shallow shells. The initial inputs for the program were determined in Sec. 5.1.1 and will be the basis for our initial sizing of the structure.

The program requires the inputs of basic shell dimensions and the loading. Dimension inputs include the shell length, radius, height, and the slope at the springing. The external and self weight loads must also be considered. The program analyzes a uniformly distributed load over the surface of the shell, similar to self weight. Points loads are not considered and outside the capabilities of the code.

Once the basic dimension and load parameters have been input, the next step is to define the shell constants, k, γ and Q.

$$\begin{aligned} k &= \tfrac{n*\pi}{L} \\ \gamma &= \tfrac{rk}{\sqrt[4]{3}}\sqrt{\tfrac{h}{r}} \\ Q &= \sqrt[8]{3}\sqrt[4]{\frac{r}{h}}\sqrt{rk} \end{aligned} \tag{5.1}$$

where $n = 1$ due to the close approximation of a uniform load from the first equation of fourier series.

We will next define the roots and powers from Eq. 4.58. This will be necessary for the definition of our trigonometric and hyperbolic multiples, required for determining our arbitrary

constants. The determination of the multiples is dependent on the location ϕ within the shell. The ϕ will be measured from the crown with negative taken as the clockwise direction of rotation.

The final step is to solve the series of simultaneous equations consisting of four equations and four unknowns. The equations for consideration will be M_ϕ, as seen in Eq. 4.71, N_ϕ, Q'_ϕ, and $N_{\phi x}$. The derivation of the latter three variables will follow the same process as M_ϕ seen in Sec. 4.3.4. Now that we have four equations and four unknowns, the final requirement is the shell edge conditions. In order to solve the simultaneous equations, we will set the longitudinal edge force N_ϕ equal to the corrective line load T_L.

$$T_L = -\frac{4}{\pi} pr \cos(\phi_k - \phi) \sin kx$$

and the shear force $N_{\phi x}$ equal to the line load S_L.

$$S_L = -\frac{4}{\pi} pr \times \frac{2}{rk} \sin(\phi_k - \phi) \cos kx$$

The remaining forces will be set to zero and the simultaneous equations are solved for a, b, c and d. The newly solved arbitrary constants are next substituted back into the equations of interest to solve for the stress resultants, stress couples, and displacements.

As proof for validation, the results compiled by the matlab program match those presented in Table 6-5 (Billington, 1965). The program allows for the adjustment of ϕ and x to locate the moment, shear, and axial forces throughout the entire shell. These results, however, are only preliminary since they do not take into consideration the edge beam the shell is supported by. The next part of the design will consider the edge beam.

5.2.2 Edge Beam

Now that we have established the primary system of the shell roof and the results, we can analyze the edge beams. It is important that all internal forces and displacements are know to size the edge beam. Once again for proof of validation, we will use the size chosen for the design of the Pennsylvania warehouse. The warehouse beam design can be seen below in Fig. 5.4.

The program requires the inputs of basic shell dimensions, edge beam dimensions, edge beam properties, steel properties and the loading. In addition, since the program is yet optimized, the user must input the longitudinal stress resultant, N_x, determined by the Shell code. Also the constants from ASCE Manual 31 Tables 2A and 2B must be inputted.

Shell dimension inputs include the shell length, radius, height, and the slope at the springing. The external and self weight loads must also be considered. The program analyzes a uniformly distributed load over the surface of the shell, similar to self weight. Points loads are not considered and outside the capabilities of the code. Edge beam dimension and property inputs include the beam width and depth along with the density of the concrete in use. The final property input is the steel yield stress.

We will follow the analysis discussed previously in Sec. 4.3.5. Since the edge beam is considered as a simple beam separate from the shell, the displacements and internal forces of the edge beam will be computed separately. However, in order to join the two systems, an equation of compatibility, consisting of two simultaneous equations, must be solved to determine the correction forces V_b and S_b. Similar to the shell corrective line loads, T_L and S_L, the edge beam must also attribute corrective values to the forces computed on the shell. After applying the correction forces, the final stress resultants and couples are determined

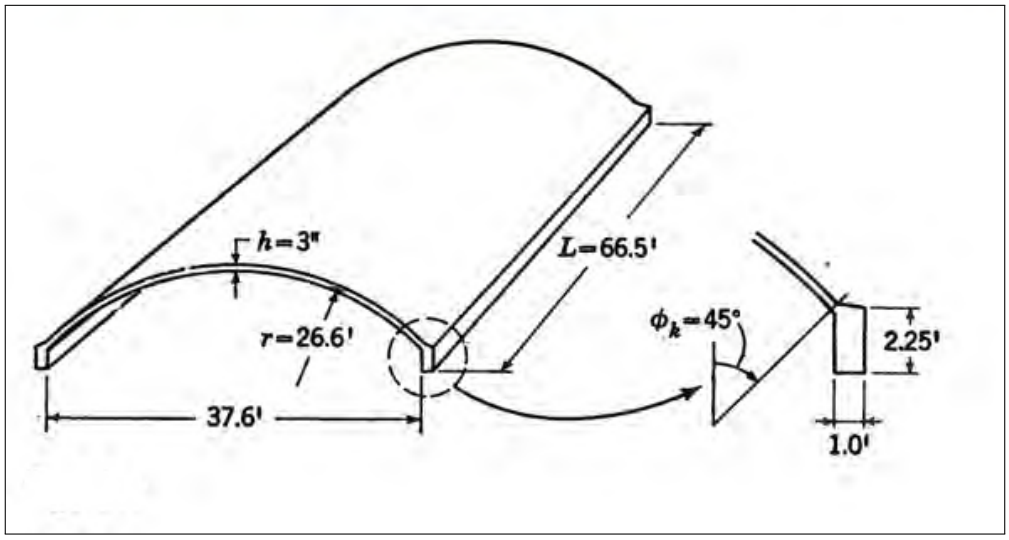

Figure 5.4: Pennsylvania Warehouse Roof Edge Beam Dimensions, (Billington, 1965)

For simplicity, the compatibility equation can be written in matrix form

$$\begin{bmatrix} B_{11}+S_{11} & B_{12}+S_{12} \\ B_{21}+S_{21} & B_{22}+S_{22} \end{bmatrix} \begin{Bmatrix} V_b \\ S_b \end{Bmatrix} = \begin{Bmatrix} FB_{11}+FS_{11} \\ FB_{21}+FS_{21} \end{Bmatrix} \tag{5.2}$$

The values for $B_{:,:}$ have been previously derived in 4.3.5. The values of $S_{:,:}$, however, require the ASCE Manual no. 31 (Whitney, 1952). The required coefficients can be taken directly out of the tables within for the following equations:

$$\begin{aligned} S_{11} &= \tfrac{L^4}{r^3hE} C \sin(kx) \\ S_{12} &= \tfrac{L^4}{r^3hE} C \sin(kx) \\ S_{21} &= \tfrac{L^2}{r^2h} C \sin(kx) \\ S_{22} &= \tfrac{L^2}{r^2h} C \sin(kx) \end{aligned} \tag{5.3}$$

where C is the constant selected from Tables 2A and 2B (Whitney, 1952). The final values required are FB and FS. The values of FB have also been computed previously in Sec. 4.3.5. FS can be computed by the shell values calculated by the Shell Design Matlab code. FB will require the displacements v and w along with the longitudinal stress resultant N_x.

$$\begin{aligned} FS_{11} &= -v\sin(\phi_k - \phi) + w\cos(\phi_k - \phi) \\ FS_{21} &= \frac{N_x}{h} \end{aligned} \tag{5.4}$$

With all variables known, the values of V_b and S_b can be determined. The final internal shell values are computed by the summation of stress resultant or couple determined by the Shell Design code along with $C * Vb$ and $C * Sb$ where once again C is a constant taken from Table 2A (Whitney, 1952).

5.2.2.1 Reinforcement

The final step of the preliminary design is to add reinforcement to the slab and beam. Even though concrete can resist tensile stresses up to about 0.1 of its compressive strength, steel is required to resist the tensile forces. The computation of reinforcement requires the finalized stress resultants and couples calculated by the Edge Beam code.

The first step is to determine the principal stresses:

$$\begin{aligned} N_1 &= \frac{N_x + N_\phi}{2} + \sqrt{N_{x\phi}^2 + \left(\frac{N_x - N_\phi}{2}\right)^2} \\ N_2 &= \frac{N_x + N_\phi}{2} - \sqrt{N_{x\phi}^2 + \left(\frac{N_x - N_\phi}{2}\right)^2} \end{aligned} \tag{5.5}$$

and the plane on which the first principal acts

$$\tan 2\theta = \frac{-2N_{x\phi}}{N_x - N_\phi} \tag{5.6}$$

where θ is measured counter clockwise from the face on which T_x acts. The second principle stress will act at a right angle to the first.

The shell reinforcement will first be considered. The required area of steel, A_s, can be determined by the general formulation

$$A_s = \frac{N_1}{f_s} \tag{5.7}$$

For the presented design example at $\phi = 0$, $N_1 = 82.988$ kip/ft and $f_s = 20$ ksi (depends on type of steel in use), requiring an $A_s = 4.149\ in^2/ft$. The steel requirement can be computed throughout

the entire shell by altering ϕ and solving for N_1 from the newly computed stress resultants and couples.

The final shell requirement will be the bending steel. Bending reinforcement is required over the center half of the shell as this is where the maximum moment and thrust occur. In computing the bending reinforcement, the thrust N_ϕ can be neglected

$$A_s = \frac{M_\phi \times 12}{f_s \times 7/8 \times d_s} \tag{5.8}$$

where d_s is the depth of steel.

The edge beam reinforcement will now be considered. At the midspan of the the beam, all tension is concentrated in the edge beam. Therefore the total tension is

$$T = \left[\frac{N_1 + 8.32}{2} - 8.32\right] \times d \tag{5.9}$$

and the required steel can be computed as

$$A_s = \frac{T}{f_s} \tag{5.10}$$

The minimum steel requirement must be met throughout the shell and edge beam

$$\begin{aligned} a_{min1} &= 0.35 \times \text{area of concrete (tensile zone)} \\ a_{min2} &= 0.18 \times \text{area of concrete (shell)} \end{aligned} \tag{5.11}$$

5.3 Discussion

Even though the purpose of this analysis was to develop a preliminary design using only hand derived equation, it was found that it is not entirely possible. In developing the Shell Design code, the theory of shallow shells was used in its entirety allowing for a smooth design code based solely on hand derived equations. The difficulty, however, came when designing the edge beam. The design requires variables for compatibility to join the shell and beam. The edge beam values were easily computed utilizing the ordinary theory of flexure. However, the compatibility constants required for the slab are not so easily computed. In multiple sources of literature, (Billington,

1965), and (Whitney, 1952), the text refers to the tables found in Whitney (1952) with no answer as to how the constants within those tables have been derived.

Without full knowledge of the source of the constants, the edge beam code can not be fully automated with equations, but rather requires inputs from the tables. With the given table constants, the program does function sufficiently and determines the finalized stress resultants and couples. These values were not only validated by the Billington (1965) publication but also the shell described in example 3 of Whitney (1952). The validation by two different shells proves the code works and is accurate for design.

The current code requires about three minutes to enter the inputs for analysis and run. However, the code would be classified as a beta version and requires cleaning up. I believe by combining the two files and adding an separate input notebook, the program can be completely automated allowing the user to find any value within the shell in under a minute. Even the best structural programs today cannot compute a design in that short of time, mainly due to the time requirement of setting up the model itself.

5.4 Conclusion

In this chapter we applied the theory of shallow shells to develop a design tool to aid in future cylindrical shell analysis. Utilizing the design tool, a brief preliminary design was conducted. The design consisted of two parts, the shell itself and the edge beam with reinforcement.

Chapter 6

Conclusions and Recommendations for Future Studies

6.1 Conclusions

In conclusion, I find that hand calculations have been and will continue to be a useful tool in the design of arches and shells. Methodologies seen throughout history have engaged the designers in basic hand calculations which have been determined as accurate design principles. Each designer used what was given previously to further the practice and enable growth within the sector of arch and shell design.

Through an extensive literature review of historical analysis and design methodologies, an appreciation for hand calculations and the work to derive and ensure accuracy was developed. Within the basis of masonry arch design, principles such as basic geometric design, wedge theory, line of thrust and the ultimate load theorem were discovered and researched to gain basic knowledge on the development of these methods. Furthermore, designers were able to implement these principles for the design of vaults and domes as seen in the case study of St. Peter's Basilica by Poleni.

Only with this basic understanding of the development of these theories can a designer continue onward toward the advanced derivations of shell theories. Similar to the development of the masonry arch theories, equilibrium, compatibility, and stress-strain relations were considered to step through the derivations of a beam and plate in flexure, and ultimately the shell. This process allowed for the development of a differential equation relating transverse displacement to the applied load. In each stage of the derivation, the designer is able to build upon the first, just as the designers of old, always looking to improve upon the current principle.

Next, a vigorous derivation was conducted to develop membrane and shallow shell theories, which are both vital for the design of shells. Both theories utilized the previously derived shell equation, through simplifications specific to circular cylindrical shells. First, the methodology of membrane theory was followed to develop the stress resultant and couples within the shell, along with the displacements.

Building upon previous design principles, the theory of shallow shells expands upon the theory of membranes by no longer neglecting bending but rather conducting an elaborate derivation involving an eighth order differential equation. Solving the homogeneous and particular solutions for the arbitrary constants allow the development of a solution more accurate than membrane theory.

Even though the process of deriving and solving the equations is tedious, once the equations are available, they can be of great use to a skilled programmer in developing working code similar to what I have developed. Not only are the equations easily inputted into a code, they output highly desirable results in a short amount of time. Solely by modifying the inputs, the user can determine the moments, thrusts, and shears throughout the shell. Hand derived equations based on the theory of shallow shells allows for accurate solutions in developing the design of a circular cylindrical shell. Given the time required to clean up and optimize the program, the code can allow for fast solutions without the time required to set up the shell in a structural design program.

This ultimately proves that hand calculations can still be useful for today's engineered world. Rather than running to buy the newest, most expensive structural analysis tool on the market, it can be just as useful, and efficient, to develop your own software that allows the designers to see the basic equations and codes that are utilized in the design.

6.2 Recommendations for Future Work

In conducting the research and development of this thesis, many future work opportunities have come to mind. The first opportunity consists of expanding upon the type of shells and conducting a similar analyses as presented within this thesis. Shell such as hemispherical domes

the hyperbolic parabola are of most interest.

In addition, analyzing additional shell structures presents an opportunity to further an understanding of the limitations of the membrane theory and draw a larger push for the theory of shallow shells. The cylindrical shell case presented within this thesis does not allow for a clear distinction between the two theories since many of the assumptions of membrane theory are met within a cylindrical shell. The comparison of the theory of shallow shells and membrane theory is more easily displayed within complex structures like the hyperbolic parabola.

Third,in keeping with the topic of cylindrical shells, instead of solely viewing a simply supported shell as in this example, the design of a multiple barrel shell would be of interest. Once again, the theory of shallow shells would be utilized in the preliminary design of the structure. Conducting an analysis of multiple barrels will require great attention to detail in the regions of joined barrels and boundary conditions.

Similarly, a shell analysis of the transverse support would be important. Not all shells can be designed as a simply supported shell and require transverse ribs. Researching the design of such supports would be important to the design of cylindrical shells.

However, prior to optimizing the code, an understanding must be gained as to where the coefficients of Whitney (1952) originate. One must fully understand the derivation of these coefficients through the respective free body diagrams and corresponding equations. Though the equations and coefficients of Table 1 were easily derived, Table 2 presented difficulty in understanding the origination and derivation of both the equations and coefficients.

An additional topic of future work would be the development of the cylindrical shell program itself. As stated previously, the code does require some optimization to allow for more efficient use than a structural analysis tool. Code may be added or subtracted to allow for a single program, rather than two, along with an inputs page.

Understanding the underlying mathematical model of a shell and encapsulating the governing equations in a numerical code (as presented within thesis), could ultimately prove to be a more appropriate tool for engineers than the use of the finite element analysis without proper under-

standing of shell behavior. In optimizing the presented code, it may hopefully someday be found useful to designers interested in the lost topic of concrete and masonry shell design.

Bibliography

Benvenuto, E. (1991). An introduction to the history of structural mechanics; Part II: Vaulted structures and elastic systems. Springler-Verlag.

Billington, D. (1965). Thin Shell Concrete Structures. McGraw-Hill, Inc., Princeton University.

Coulomb, C. (1773). *Essai sur une application de maximis & minimis à quelques problèmes de statique relatifs à l'architecture.* *mémoires de l'académie Royale des Sciences*, 7:343–382.

Couplet, C. (1731). *De la poussée des voûtes.* *Mémoires de l'académie Royale des Sciences.*

Couplet, C. (1732). *Seconde partie de l'examen des voûtes.* *mémoires de l'académie Royale des Sciences.*

de la Hire, P. (1679). *Nouveaux éléments des sections coniques, les lieux géometriques.* Chez Andre Prallard, Paris.

de la Hire, P. (1712). *Sur la construction des voûtes dans les édifices.* *mémoires de l'académie Royale des Sciences*, 69.

Derand, F. (1743). *L'architecture des voûtes, ou l'art des traits, et coupes de voûtes.* Chez Andre Cailleau, Paris.

Heyman, J. (1997). The Stone Skeleton: Structural Engineering of Masonry Architecture. Cambridge University Press.

Heyman, J. (1998). Structural analysis; A historical approach. Cambridge University Press.

Huerta, S. (2005). Essays in the history of the theory of structures: In honour of Jacques Heyman. Instituto Juan de Herrera, Madrid.

Krivoshapko, S. N. and Hyeng, C.and Mamieva, I. (2014). Chronology of erection of the earliest reinforced concrete shells. International Journal of Research and Reviews in Applied Sciences, 18(2).

Kurrer, K. (2012). The History of the Theory of Structures: From Arch Analysis to Computational Mechanics. John Wiley & Sons.

López, G. (2006). *Poleni's Manuscripts about the Dome of Saint Peter's.* *Proceedings of the Second International Congress on Construction History*, 2.

Moseley, H. (1839). On the theory of the arch. In Hann, J., editor, The theory , practice and architecture of bridges.

Navier, C. (1826). *Resumé des leçons données à l'école des ponts et chaussées sur l'application de la mécanique à* Dunot, Paris.

Peerdeman, B. (2008). Analysis of thin concrete shells revisited: Opportunities due to innovations in materials and analysis methods. Master's thesis.

Poleni, G. (1748). *Memorie Istoriche della Gran Cupola del Tempio Vaticano, e de danni di essa e de ristoramenti loro, divise in libri cinque*. Stamperia del Seminario, Padova.

Prusinski, K. (2015). Analysis of complex structures. Master's thesis, Department of Civil, Environmental and Architectural Engineering, University of Colorado at Boulder.

Salimbeni, L. (1787). Degli archi e delle volte. Ramanzini, Verona.

Whitney, C. (1952). Design of Cylindrical Shell Roofs. American Society of Civil Engineers, no. 31 edition.

Winkler, E. (1880). *Die Lage der Stützlinie im Gewölbe*. *Deutsche Bauzeitung*, 13:127–130.

Appendix A

Design Code

The following code has been developed via matlab for the preliminary design of the circular cylindrical shell example. The code is discussed in detail within Sec. 5.2.

The shell design code (part one) consists of three sections, the shell design (master copy), 7.1, the shell coefficient function, 7.1.1, and the shell force function, 7.1.2. The edge beam design code (part two) 7.2 consists of only one piece of code computing the final stresses in the beam and shell along with the required reinforcement.

A.1 Shell Design - Part One

The following code is developed for the design of the shell portion of the simply supported cylindrical shell. The code follows the design procedure outlined by the theory of shallow shells and is discussed in Sec. 5.2.1. The purpose of the design tool is to determine the internal forces and displacements within the shell.The shell design code consists of the basic inputs and formulations the the shell dimensioning. The shell coefficient function produces the simultaneous equations required to solve for the arbitrary constants. With known constant values, the shell forces function determines the internal forces and displacement of the shell. The code is presented as follows:

```
close all; fclose all; clear all; clc;
%%Inputs
%Dimensions and Loads
L=66.5; %ft
r=26.6; %ft
h=0.25; %ft
phi_k=45*pi/180; %rad
phi=0; %rad (measured from edge)
```

```
phit=phi  phi_k;
q=.080; %ksf
Phi=phi_k  phi;
dimload.Length=L;
dimload.Radius=r;
dimload.Height=h;
dimload.Phi_k=phi_k;
dimload.Phi=phi;
dimload.Pd=q;

%Shell Constants
n=1;
k= n*pi/L;
gamma=r*k/3^(1/4)*sqrt(h/r);
Q=3^(1/8)*(r/h)^(1/4)*sqrt(r*k);
x=L/2;
E=4.32e5;%ksf
D=E*h^3/12;

Shell.k=k;
Shell.gamma=gamma;
Shell.Q=Q;
Shell.x=x;
Shell.E=E;
Shell.D=D;

%%Roots
%from Eq.4.54
m1=sqrt((sqrt((1+gamma)^2+1)+(1+gamma))/2);
n1=sqrt((sqrt((1+gamma)^2+1) (1+gamma))/2);
m2=sqrt((sqrt((1 gamma)^2+1) (1 gamma))/2);
n2=sqrt((sqrt((1 gamma)^2+1)+(1 gamma))/2);
mn=[m1,n1,m2,n2];
%root powers Eq. 4.55
alpha1=Q*m1;
beta1=Q*n1;
alpha1p=Q*m2;
beta1p=Q*n2;
rp=[alpha1,beta1,alpha1p,beta1p];

Roots.M1=m1;
Roots.N1=n1;
Roots.M2=m2;
Roots.N2=n2;
Roots.Alpha1=alpha1;
Roots.Alpha2=alpha1p;
Roots.Beta1=beta1;
Roots.Beta2=beta1p;

%%Shell Edge Conditions (Fourier Series)
TL=4/pi*q*r*cos(phi_k  phi)*sin(k*x);
```

```
SL=4/pi*q*r*2/(r*k)*sin(phi_k  phi)*cos(k*x);
M_phi=0;
Np_phi= TL;
Qp_phi=0;
Np_xphi= SL;

EdgeLoad.M_phi=M_phi;
EdgeLoad.N_phi=Np_phi;
EdgeLoad.Qp_phi=Qp_phi;
EdgeLoad.N_xphi=Np_xphi;

f=[M_phi;Np_phi;Qp_phi;Np_xphi];

%%Shell Coefficients
%(1)Mphi (2)Mx (3)Qx (4)Nphi (5)Nx (6)u (7)w
%(8)Qphi (9)Nxphi (10)v (11)Mxphi (12)Qphip

%M_phi
SC=1;
F1=shell_coefficients(SC,k,r,phit,rp,mn,Q,gamma, h,x);

%N_phi
SC=4;
F2=shell_coefficients(SC,k,r,phit,rp,mn,Q,gamma,h,x);

%Qphip
SC=12;
F3=shell_coefficients(SC,k,r,phit,rp,mn,Q,gamma,h,x);

%Nxphi
SC=9;
F4=shell_coefficients(SC,k,r,phit,rp,mn,Q,gamma,h,x);
F=[F1;F2;F3;F4];

ShellCoef.M_phi=F1;
ShellCoef.N_phi=F2;
ShellCoef.Qp_phi=F3;
ShellCoef.N_xphi=F4;

constants= F^ 1*f;

%Shell Forces
phi=0; %rad (measured from edge)
phit=phi  phi_k;
x=L/2;
Np_x= 4/pi*2*q/(r*k^2)*cos(phi_k  phi)*sin(k*x);
Np_phi= 4/pi*q*r*cos(phi_k  phi)*sin(k*x);
Np_xphi= 4/pi*q*r*2/(r*k)*sin(phi_k  phi)*cos(k*x);
up=2*q/(E*h*r*k^3)*cos(phi_k  phi)*cos(k*x);
vp= 2*q/(E*h*r^2*k^4)*(1+2*k^2*r^2)*sin(phi_k  phi)*sin(k*x);
wp= 2*q/(E*h*r^2*k^4)*(1+2*k^2*r^2+r^4*k^4/2)*cos(phi_k  phi)*sin(k*x);
```

```
111 %M_phi
112 SC=1;
113 M_phi=shell_forces(SC,k,r,phit,rp,mn,Q,gamma,h,constants,x);
114
115 %M_x
116 SC=2;
117 M_x=shell_forces(SC,k,r,phit,rp,mn,Q,gamma,h,constants,x);
118
119 %M_xphi
120 SC=11;
121 M_xphi=shell_forces(SC,k,r,phit,rp,mn,Q,gamma,h,constants,x);
122
123 %Q_phi
124 SC=8;
125 Q_phi=shell_forces(SC,k,r,phit,rp,mn,Q,gamma,h,constants,x);
126
127 %Q_x
128 SC=3;
129 Q_x=shell_forces(SC,k,r,phit,rp,mn,Q,gamma,h,constants,x);
130
131 %N_phi
132 SC=4;
133 N_phi=shell_forces(SC,k,r,phit,rp,mn,Q,gamma,h,constants,x)+Np_phi;
134
135 %N_x
136 SC=5;
137 N_x=shell_forces(SC,k,r,phit,rp,mn,Q,gamma,h,constants,x)+Np_x;
138
139 %N_xphi
140 SC=9;
141 N_xphi=shell_forces(SC,k,r,phit,rp,mn,Q,gamma,h,constants,x)+Np_xphi;
142
143 %u
144 SC=6;
145 u=shell_forces(SC,k,r,phit,rp,mn,Q,gamma,h,constants,x)+up;
146
147 %v
148 SC=10;
149 v=shell_forces(SC,k,r,phit,rp,mn,Q,gamma,h,constants,x)+vp;
150
151 %w
152 SC=7;
153 w=shell_forces(SC,k,r,phit,rp,mn,Q,gamma,h,constants,x)+wp;
154
155 DV= v*sin(phi_k  phi)+w*cos(phi_k  phi);
156 DH=v*cos(phi_k  phi)+w*sin(phi_k  phi);
157
158 Forces.M_phi=M_phi;
159 Forces.N_phi=N_phi;
160 Forces.N_x=N_x;
161 Forces.N_xphi=N_xphi;
```

```
Displacement.u=u;
Displacement.v=v;
Displacement.w=w;
Displacement.up=up;
Displacement.vp=vp;
Displacement.wp=wp;
```

A.1.1 Shell Coefficients

The shell coefficient function produces the simultaneous equations required to solve for the arbitrary constants. The methodology for deriving coefficients 1 - 11 have been previously discussed in Sec.4.3.4 and seen by the example equation M_ϕ (4.71.

```
%%Shell Coefficients
function Shell=shell_coefficients(SC, k, r, phit, rp, mn, Q, gamma, h,x)

alpha1=rp(1);
beta1=rp(2);
alpha1p=rp(3);
beta1p=rp(4);
m1 = mn(1);
n1 = mn(2);
m2 = mn(3);
n2 = mn(4);

%Trigonometric and Hyperbolic Multiples at Edge
T1=cos(beta1*phit)*cosh(alpha1*phit);
T2=sin(beta1*phit)*sinh(alpha1*phit);
T3=cos(beta1p*phit)*cosh(alpha1p*phit);
T4=sin(beta1p*phit)*sinh(alpha1p*phit);
T5=cos(beta1*phit)*sinh(alpha1*phit);
T6=sin(beta1*phit)*cosh(alpha1*phit);
T7=cos(beta1p*phit)*sinh(alpha1p*phit);
T8=sin(beta1p*phit)*cosh(alpha1p*phit);

%Coefficients
E=4.32e5;
D=E*h^3/12;
%(1) M_phi
R(1) = 2*D/r^2*sin(k*x);
B1(1)=Q^2*(1+gamma);
B2(1)=Q^2;
B3(1)=Q^2*(gamma 1);
B4(1)=Q^2;

%(2) M_x
R(2)=2*D*k^2*sin(k*x);
B1(2)=1;
```

```
B2(2)=0;
B3(2)=1;
B4(2)=0;

%(3) Q_x
R(3) = 2*D*k^3/(gamma)*cos(k*x);
B1(3)=1;
B2(3)=1;
B3(3) = 1;
B4(3)=1;

%(4) N_phi
R(4)=4*D*r*k^4/gamma^2*sin(k*x);
B1(4)=0;
B2(4)=1;
B3(4)=0;
B4(4) = 1;

%(5) N_x
R(5) = 4*D*r*k^4/gamma^3*sin(k*x);
B1(5) = 1;
B2(5)=1+gamma;
B3(5)=1;
B4(5)=1 gamma;

%(6) u
R(6)=4*D*r*k^3/(h*E*gamma^3)*cos(k*x);
B1(6) = 1;
B2(6)=1+gamma;
B3(6)=1;
B4(6)=1 gamma;

%(7) w
R(7)=2*sin(k*x);
B1(7)=1;
B2(7)=0;
B3(7)=1;
B4(7)=0;

%(8) Q_phi
R(8) = 2*D*k^3/(sqrt(gamma))^3*sin(k*x);
B1(8)=m1 n1;
B2(8)=m1+n1;
B3(8) = (m2+n2);
B4(8)=m2 n2;

%(9) N_xphi
R(9)=4*D*r*k^4/(sqrt(gamma))^5*cos(k*x);
B1(9) = n1;
B2(9)=m1;
B3(9)=n2;
```

```
B4(9) = m2;

%(10) v
R(10)=4*D*r*k^3/(E*h*(sqrt(gamma))^7)*sin(k*x);
B1(10)=m1+n1*(1 gamma);
B2(10)=n1  m1*(1 gamma);
B3(10) = m2+n2*(1+gamma);
B4(10) = n2  m2*(1+gamma);

%(11) M_xphi
R(11)=2*D*k/r*cos(k*x);
B1(11)=alpha1;
B2(11)=beta1;
B3(11)=alpha1p;
B4(11)=beta1p;

%Q_phip
R(12) = 2*D*k^3/(sqrt(gamma))^3*sin(k*x);
B1(12)=m1*(1 gamma)  n1;
B2(12)=m1+n1*(1 gamma);
B3(12) = m2*(1+gamma)  n2;
B4(12)=m2  n2*(1+gamma);
%Variables
syms
if SC<8
    A=(B1(SC)*T1    B2(SC)*T2);
    B= B2(SC)*T1    B1(SC)*T2;
    C=B3(SC)*T3    B4(SC)*T4;
    D= B4(SC)*T3    B3(SC)*T4;
else
    A=B1(SC)*T5    B2(SC)*T6;
    B= B2(SC)*T5    B1(SC)*T6;
    C=B3(SC)*T7    B4(SC)*T8;
    D= B4(SC)*T7    B3(SC)*T8;
end
Shell=[A,B,C,D]*2*R(SC);

end
```

A.1.2 Shell Forces

The shell force function follows the procedure of the shell coefficient function with the exception of known A, B, C and D constants. With known constant values, the shell forces function determines the internal forces and displacement of the shell utilizes the same equations developed in Sec.4.3.4 and seen above in 7.1.1.

```
%%Shell Forces
```

```
function F=shell_forces(SC, k, r, phit, rp, mn, Q, gamma, h, constants,x)

a=constants(1);
b=constants(2);
c=constants(3);
d=constants(4);
alpha1=rp(1);
beta1=rp(2);
alpha1p=rp(3);
beta1p=rp(4);
m1 = mn(1);
n1 = mn(2);
m2 = mn(3);
n2 = mn(4);

%Trigonometric and Hyperbolic Multiples at Edge
T1=cos(beta1*phit)*cosh(alpha1*phit);
T2=sin(beta1*phit)*sinh(alpha1*phit);
T3=cos(beta1p*phit)*cosh(alpha1p*phit);
T4=sin(beta1p*phit)*sinh(alpha1p*phit);
T5=cos(beta1*phit)*sinh(alpha1*phit);
T6=sin(beta1*phit)*cosh(alpha1*phit);
T7=cos(beta1p*phit)*sinh(alpha1p*phit);
T8=sin(beta1p*phit)*cosh(alpha1p*phit);

%Coefficients
E=4.32e5;
D=E*h^3/12;

%(1) M_phi
R(1) = 2*D/r^2*sin(k*x);
B1(1)=Q^2*(1+gamma);
B2(1)=Q^2;
B3(1)=Q^2*(gamma 1);
B4(1)=Q^2;

%(2) M_x
R(2)=2*D*k^2*sin(k*x);
B1(2)=1;
B2(2)=0;
B3(2)=1;
B4(2)=0;

%(3) Q_x
R(3) = 2*D*k^3/(gamma)*cos(k*x);
B1(3)=1;
B2(3)=1;
B3(3) = 1;
B4(3)=1;

%(4) N_phi
```

```
R(4)=4*D*r*k^4/gamma^2*sin(k*x);
B1(4)=0;
B2(4)=1;
B3(4)=0;
B4(4)= 1;

%(5) N_x
R(5)= 4*D*r*k^4/gamma^3*sin(k*x);
B1(5)= 1;
B2(5)=1+gamma;
B3(5)=1;
B4(5)=1 gamma;

%(6) u
R(6)=4*D*r*k^3/(h*E*gamma^3)*cos(k*x);
B1(6)= 1;
B2(6)=1+gamma;
B3(6)=1;
B4(6)=1 gamma;

%(7) w
R(7)=2*sin(k*x);
B1(7)=1;
B2(7)=0;
B3(7)=1;
B4(7)=0;

%(8) Q_phi
R(8)= 2*D*k^3/(sqrt(gamma))^3*sin(k*x);
B1(8)=m1 n1;
B2(8)=m1+n1;
B3(8)= (m2+n2);
B4(8)=m2 n2;

%(9) N_xphi
R(9)=4*D*r*k^4/(sqrt(gamma))^5*cos(k*x);
B1(9)= n1;
B2(9)=m1;
B3(9)=n2;
B4(9)= m2;

%(10) v
R(10)=4*D*r*k^3/(E*h*(sqrt(gamma))^7)*sin(k*x);
B1(10)=m1+n1*(1 gamma);
B2(10)=n1 m1*(1 gamma);
B3(10)= m2+n2*(1+gamma);
B4(10)= n2 m2*(1+gamma);

%(11) M_xphi
R(11)=2*D*k/r*cos(k*x);
B1(11)=alpha1;
```

```
B2(11)=beta1;
B3(11)=alpha1p;
B4(11)=beta1p;

%Variables
if SC<8
    A=a*B1(SC)*T1    a*B2(SC)*T2;
    B= b*B2(SC)*T1    b*B1(SC)*T2;
    C=c*B3(SC)*T3    c*B4(SC)*T4;
    D= d*B4(SC)*T3    d*B3(SC)*T4;
else
    A=a*B1(SC)*T5    a*B2(SC)*T6;
    B= b*B2(SC)*T5    b*B1(SC)*T6;
    C=c*B3(SC)*T7    c*B4(SC)*T8;
    D= d*B4(SC)*T7    d*B3(SC)*T8;
end
F=2*R(SC)*(A+B+C+D);

end
```

A.2 Edge Beam - Part Two

Part two of the code for shell design is presented below and discussed in Sec. 5.2.2. The edge beam code is required to configure a compatibility relation between the preliminary values of the shell developed by the above shell design code, and the values a an edge beam subjected to the ordinary flexural theory. The development of the compatibility relation allows for the computation of the final internal forces of the simply supported shell. The edge beam code also computed the required area of steel for the beam and shell. The code is presented as follows:

```
%Edge Beam
close all; fclose all; clear all; clc;
%%Inputs
b=1; %ft
d=2.25; %ft
L=66.5; %ft
r=26.6; %ft
h=0.25; %ft
phi_k=45*pi/180; %rad
phi=0*pi/180; %rad (measured from edge)
q=.080; %ksf
rho=.150; %kcf
w=b*d*rho; %klf
n=1;
k= n*pi/L;
x=L/2;
```

```
E=4.32e5;%ksf

%%N_x
N_x=99.03; %kip/ft (computed in Shell_Design)

%ASCE Manual 31 values from Table 2B
C1=96.10;          %(Vertical Edge Load   Delta v)
C2= 64.69;         %(Horizontal Edge Load   Delta v)
C3=2.500;          %(Shear Edge Load   Delta v)
%ASCE Manual 31 values from Table 2A
C4=19.64;          %(Vertical Edge Load   T_x)
C5=1.388;          %(Shear Edge Load   T_x)

%Correction Values
Np_phi=4/pi*q*r*cos(phi_k phi)*sin(k*x);
Np_xphi=4/pi*q*r*2/(r*k)*sin(phi_k phi)*cos(0);
VL=Np_phi*sin(phi_k);
HL=Np_phi*cos(phi_k);
SL=Np_xphi;

%Shell
NS=L^4/(r^3*h*E);
FS(1,1)=L^4/(r^3*h*E)*(q*r*(((2*r)/(pi*L))^2+2/pi^4+(r/L)^4*(cos(phi_k phi))^2)+C1*VL+C2*HL+C3*SL)*sin(k*x
    );
FS(2,1)=N_x/h;
S(1,1)=NS*C1*sin(k*x);
S(1,2)=NS*C3*sin(k*x);
S(2,1)=NS*E*r/L^2*C4*sin(k*x);
S(2,2)=NS*E*r/L^2*C5*sin(k*x);

%Beam
NB=L^4/(d^3*b*E);
FB(1,1)=NB* 4/pi*w*12/(pi*n)^4*sin(k*x);
FB(2,1)=NB*E*d/L^2*4/pi*w*6/(pi*n)^2*sin(k*x);
B(1,1)=NB*12/(pi*n)^4*sin(k*x);
B(1,2)=NB*d/L*6/(pi*n)^3*sin(k*x);
B(2,1)=NB*E*d/L^2*6/(pi*n)^2*sin(k*x);
B(2,2)=L/(b*d)*4/(pi*n)*sin(k*x);

%Compatibility
BS=S+B;
F=FS+FB;
X=BS\F;
Vb=X(1,1);
SB=X(2,1);

%%Final Internal Forces
%N_x
N_x=N_x+(Vb*C4)+(SB*C5);

%N_xphi
```

```
N_xphi=0;
C4=0;
C5=0.4;
N_xphi=N_xphi+Vb*C4+SB*C5;

%N_phi
N_phi=0;
C4=0.707;
C5=0;
N_phi=N_phi+Vb*C4+SB*C5;

%M_phi
M_phi=0;
C4=0;
C5=0;
N_xphi=N_xphi+Vb*C4+SB*C5;

Forces.N_x=N_x;
Forces.N_xphi=N_xphi;
Forces.N_phi=N_phi;
Forces.M_phi=M_phi;

%%Reinforcement
fs=20; %ksi
ds=2; %in
%Shell Reinforcement
N1=(N_x+N_phi)/2+sqrt(N_xphi^2+((N_x N_phi)/2)^2);
N2=(N_x+N_phi)/2 sqrt(N_xphi^2+((N_x N_phi)/2)^2);

As_shell=N1/fs;
As_bend=M_phi*12/(fs*7/8*ds);

%Beam Reinforcement
T=((N1+8.32)/2 8.32)*d;
As_beam=T/fs;

%Min Reinforcement
Amin1=0.0035*h*12*12;
Amin2=0.0018*h*12*12;
```